• Volume 5C, Number 1, December 1955

מוסד ויצמן לפרסומים במדעי הטבע והטכניקה בישראל · ירושלים
The Weizmann Science Press of Israel · Jerusalem

BULLETIN OF THE RESEARCH COUNCIL OF ISRAEL

Section C TECHNOLOGY

Bull. Res. Counc. of Israel. C. Techn.

Incorporating the *Scientific Publications* of the Technion — Israel Institute of Technology, Haifa

SYMPOSIUM ON MAGNESIUM COMPOUNDS

S. A. Abrahams / M. R. Bloch / O. Schaechter / A. S. Braunfeld / E. L. Clark / J. Aman A. Talmi / H. E. Heimann / J. Schnerb / S. Goldberg / A. V. I. Molleson / A. Markowicz

BULLETIN OF THE RESEARCH COUNCIL OF ISRAEL

יוצא לאור ע"י
מוסד ויצמן למדעים במדעי הטבע והטכניקה בישראל
המועצה המדעית לישראל • משרד החנוך והתרבות • האוניברסיטה העברית בירושלים
הטכניון — מכון טכנולוגי לישראל • מכון ויצמן למדע • מוסד ביאליק

Published by
THE WEIZMANN SCIENCE PRESS OF ISRAEL
Research Council of Israel • Ministry of Education and Culture
The Hebrew University of Jerusalem • Technion—Israel Institute of Technology
The Weizmann Institute of Science • Bialik Institute

Manuscripts should be addressed:
Executive Editor, The Weizmann Science Press of Israel, P.O.B. 801, Jerusalem
33, King George Ave., Jerusalem (Telephone 62844)

02/2557—2.56/1500 ד.מ. ירם

• Volume 5C, Number 1, December 1955

מוסד ויצמן לפרסומים במדעי הטבע והטכניקה בישראל · ירושלים

The Weizmann Science Press of Israel · Jerusalem

BULLETIN OF THE RESEARCH COUNCIL OF ISRAEL

Section C TECHNOLOGY

Bull. Res. Counc. of Israel. C. Techn.

Incorporating the *Scientific Publications* of the Technion — Israel Institute of Technology, Haifa

CONTENTS

SOLAR ENERGY COLLECTOR DESIGN *

WITH SPECIAL REFERENCE TO SELECTIVE RADIATION

H. TABOR

National Physical Laboratory of Israel, Jerusalem

ABSTRACT

The possibility of making solar energy collectors of high efficiency by use of selective black surfaces has prompted a re-statement of the problem of collector design. By means of two parameters, the overall transmission efficiency and the cut-off intensity, it is possible to determine the performance of a collector under various conditions of use. The concept of *retention efficiency* permits the construction of generalized yearly average efficiency curves from which the influence of a change in some design parameter is quickly seen.

Computations show that it should be possible to produce low pressure steam without optical concentration, and high pressure steam with a small degree of concentration.

INTRODUCTION

For over a century attempts have been made to harness the energy of solar radiation by its absorption by blackened bodies and its conversion to useful heat.

Due to the poor efficiency of collectors of this type at elevated temperatures, their use has been limited to the heating of water for domestic purposes or, by employing very accurate paraboloidal mirrors, for the production of relatively small quantities of heat at very high temperatures. The generation of steam for the operation of a modern turbine, while possible, to date does not appear to have been economically feasible. Even the water heaters are at the limit of economic feasibility, especially in areas where fuel is cheap.

The classical paper of Hottel and Woertz[1] which dealt with the design of flat-plate collectors, developed an interesting short-cut for dealing with systems employing multiple glass sheets. But the authors point out that their equation (13) is inaccurate for a collecting surface of low emissivity, such a case being "of interest only if such a surface could be found which were at the same time a substantially perfect absorber of sunlight". Drake[2] at the Wisconsin symposium in 1953 asserted that "there is no known surface having these properties".

However, it has recently been found[3] that, by the principle of selective radiation, it is possible to produce surfaces of low effective emissivity which are nevertheless good absorbers for solar energy. Surfaces have been developed which combine absorptivities of over 90% for solar radiation with emissivities of about 10% of that of a black body for heat radiation. Research is continuing with a view to increasing the absorptivity and reducing the emissivity still further.

* Contribution to the discussion in the Section on Thermal Processes at the First World Symposium on Applied Solar Energy, Arizona, November 1955.

Received September 7, 1955.

This progress has prompted a re-statement of the problem of collector design, and the present paper indicates methods of estimating the performance of solar energy collectors particularly when used to operate heat engines.

THE ENERGY BALANCE

If solar radiation is incident upon a receiving body from which useful heat may be extracted by, for example, the passage of a fluid through the body, the general equation of energy balance under equilibrium conditions is

$$\alpha\beta q_i = \alpha\beta P Q_i = q_0 = q_{l(T)} + q_{s(T)}\,, \tag{1}$$

where α —the absorption coefficient of the receiver for solar radiation

β —the transmission coefficient of any optical system interposed between the incoming solar radiation and the receiver

q_i — the incident solar energy rate per unit area of the *receiver*

P — the concentrating power defined as the ratio of the area of intercepted solar radiation to the area of the receiving surface

Q_i — the incident solar radiation intensity (energy rate per unit area)

q_0 —the solar energy rate reaching and absorbed by the receiver, per unit area of receiver

$q_{l(T)}$ —the rate of loss from the receiver by convection, conduction and radiation per unit area of receiver, at temperature T

$q_{s(T)}$ —the rate of useful energy extracted, per unit area of receiver, at temperature T

T —absolute temperature of the receiving surface.

$q_{l(T)}$ and hence $q_{s(T)}$ are both functions of T.

The fraction $N_{1(T)}$ of the incoming absorbed energy that is extracted as useful heat is

$$N_{1(T)} = q_{s(T)}/q_0 = 1 - q_{l(T)}/q_0. \tag{2}$$

N_1 may be called the *retention efficiency* of the system at temperature T.

The *collection efficiency* $\eta_{1(T)}$ at temperature T is

$$\eta_{1(T)} = q_{s(T)}/q_i = \frac{q_0 - q_{l(T)}}{q_i} = \alpha\beta\,[1 - q_{l(T)}/q_0] = \alpha\beta N_{1(T)}. \tag{3}$$

i.e. the collection efficiency is the product of the retention efficiency and the *overall transmission* efficiency ($\alpha\beta$).

The retention efficiency $N_{1(T)}$ may be written

$$N_{1(T)} = 1 - q_{l(T)}/q_0 = 1 - \left(\frac{q_{l(T)}}{\alpha\beta P}\right)\frac{1}{Q_i} = 1 - Q_x/Q_i \tag{2a}$$

The quantity $Q_x = q_{l(T)}/\alpha\beta P$ is termed the *cut-off* * solar intensity, since it is the

* Anderson, Hottel and Whillier[4] have termed a similar quantity — referring to horizontal intensities — the *critical* value The symbol Q_x should be regarded as a contraction for $Q_{x(T)}$ since, unlike Q_i, it is a function of T.

value of solar intensity Q_i for which the efficiency is zero, i.e. below which the receiver cannot reach the temperature T.

If the fluid being heated enters at temperature T_c and leaves at the output temperature T_b, it may readily be shown from equation (3) that the efficiency of collection is

$$\eta_{1h} = \frac{\alpha\beta\,(T_b p_b - T_c p_c)}{\int_{T_c}^{T_b} \frac{p_T\,dT}{N_{1(T)}}} = \frac{\alpha\beta\,(T_b p_b - T_c\, p_c)}{\int_{T_c}^{T_b} \frac{p_T\,dT}{1-q_{l(T)}/q_0}}, \tag{3a}$$

where η_{1h} is the efficiency of *heating*, being the ratio of the total heat extracted to the total incident solar energy, and p_b, p_c, p_T are the specific heats of the liquid at T_b, T_c, T. This equation applies only to a single phase, as, for example, the heating of water below the boiling point: in the case of water the specific heat is very nearly constant and (3a) may be written

$$\eta_{1h} = \frac{\alpha\beta\,(T_b - T_c)}{\int_{T_c}^{T_b} \frac{dT}{1-q_{l(T)}/q_0}} = \frac{\alpha\beta\,(T_b - T_c)}{\int_{T_c}^{T_b} \frac{dT}{N_{1(T)}}} = \alpha\beta N_{1h}\ , \tag{3b}$$

where N_{1h} represents the retention efficiency for heating. If boiling takes place, a large part of the receiver will be at nearly constant temperature T_b where T_b is the boiling point or, more correctly, a few degrees above the boiling point. For this part of the receiver the integrated collection efficiency is given directly by equation (3)

$$\eta_{1b} = \alpha\beta\,[1 - q_{l(T_b)}/q_0] = \alpha\beta\,[1 - Q_x/Q_i] = \alpha\beta N_{1b}\ , \tag{3c}$$

where N_{1b} represents the retention efficiency at constant temperature T_b. If superheating occurs, the efficiency for this section of the collector is given by an expression similar to (3a), i.e.

$$\eta_{1s} = \frac{\alpha\beta\,(T_0 p'_0 - T_b\, p'_b)}{\int_{T_b}^{T_0} \frac{p'_T\ dT}{1-q_{l(T)}/q_0}} = \alpha\beta N_{1s}\ * \tag{3d}$$

where T_0 is the final output temperature and p'_0, p'_b, p'_T are the specific heats of the vapour phase at temperatures T_0, T_b and T, and N_{1s} represents the retention efficiency for superheating.

* Integrals of the type of Equation (3d) and (3a) can only be solved graphically when $p_{(T)}$, $p'_{(T)}$ are taken from tables. The same applies to equation (3b) unless $N_{1(T)}$ is a simple function of T.

For a system which heats, boils and superheats a fluid it may readily be seen that the overall or *composite* efficiency of collection η_{1c} is given by

$$\eta_{1c} = \frac{h_w + h_{fg} + h_s}{\frac{h_w}{\eta_{1h}} + \frac{h_{fg}}{\eta_{1b}} + \frac{h_s}{\eta_{1s}}} \tag{3e}$$

where h_w — the added enthalpy to the liquid up to the boiling point
h_{fg} — heat of vaporization
h_s — added enthalpy in superheating the vapour.

h_w, h_{fg}, h_s are given by tables for any particular fluid and pressure.

If the heated fluid is used to operate an ideal Carnot heat engine, the efficiency η_2 of the engine is given by

$$\eta_2 = (T_0 - T_c)/T_0 \tag{4}$$

where T_0 is the output temperature of the collector, assuming for convenience that temperature T_c be used as the sink of the Carnot engine.

Hence the overall theoretical efficiency η of such a solar energy collector of efficiency η_1, operating an ideal Carnot engine, is

$$\eta = \eta_1 \cdot \eta_2 \tag{5}$$

and the design requirement is that the product $\eta_1 \eta_2$ shall be as large as possible.

For the case of the Carnot cycle, the efficiency η_1 must be calculated from Equation (3c), since all the heat is added at a constant output temperature T_0. Equations (3b), (3d) and (3e) are used when studying real cycles, and equations (3a) or (3b) for cases of heating in a single liquid phase.

As no engine can be made more efficient than the Carnot engine, it follows that all efforts to harness solar energy through the use of a heat engine must be concerned with the problem of obtaining simultaneously a high efficiency of collection and a high output temperature.

Examination of equation (2a) shows two approaches to this problem. The first is to make the concentrating power P large by means of lenses or mirrors. Much ingenuity has been applied to this problem in the past and it is hoped to deal with it in more detail in another paper, but the general conclusions are:

(a) the cost of the concentrating system rises with the concentrating power;
(b) systems with a concentrating power greater than 2—3 cannot be fixed but must be oriented to match the changing altitude of the sun;
(c) concentrating systems do not collect diffuse radiation from sky and clouds.

The second possibility for improving the collection efficiency is the reduction of the losses $q_{l(T)}$, and certain aspects of this problem are dealt with here.

ENERGY LOSSES IN THE COLLECTOR

The receiving surface loses energy by the three modes of heat transfer: convection, conduction and radiation.

Convection loss

The calculation of natural or free convection loss is fairly well established for bodies of regular shape and is adequately dealt with by McAdams[5], Fishenden and Saunders[6], Brown and Marco[7] and others. For the vast majority of cases dealt with in the present study the product of the Grasshoff and Prandtl numbers ($Gr \cdot Pr$) is between 10^3—10^9, so that the convection loss is of the form

$$q_c = C(ka^{1/4})\left(\frac{\Delta T}{L}\right)^{1/4}\Delta T \tag{6}$$

where C — a constant dependent on the system considered
k — conductivity of air at the mean temperature of the air film (BTU/hr·ft²·°F per ft)
a — modulus $= gy\varrho^2 c_p/\mu k$, a property of the air ($ft^{-3}\ °F^{-1}$)
L — characteristic dimension (ft)
ΔT — temperature difference between body and bulk air (°F)
g — acceleration due to gravity (4.17×10^8 ft/hr²)
y — coefficient of volumetric expansion of air ($°F^{-1}$)
ϱ — density of air (lb/ft^3)
c_p — specific heat of air at constant pressure (BTU/lb·°F)
μ — viscosity of air (lb/hr·ft = 2.42 viscosity in centipoise)
q_c — heat loss *per unit area* of surface.

For cylinders, the characteristic length is the diameter, for horizontal planes it is the length of the side, for vertical planes, the height. For L greater than 2 ft the value of L is taken as 2 ft.

As is seen from Table I, the product $ka^{1/4}$ is nearly constant for air, so that very often the convection loss is written as

$$q_c = A\left(\frac{\Delta T}{L}\right)^{1/4}\Delta T \tag{7}$$

or for $L > 2$ ft

$$q_c = B\Delta T^{5/4}. \tag{8}$$

TABLE I

Conductivity and modulus for air *

Mean T°F	60	80	100	150	200	250	300	350	400
k	.0148	.0153	.0158	.0172	.0182	.0192	.0204	.0216	.0227
$10^{-6}a$	1.7	1.4	1.2	0.83	0.58	0.42	0.31	0.23	0.18
$ka^{1/4}$	0.538	.525	.521	.518	.500	.488	.480	.472	.467

* Figures from Brown and Marco.

The product of the Grasshoff and Prandtl numbers is

$$(Gr \cdot Pr) = \frac{gy\Delta T L^3 \varrho^2 c_p}{\mu k} = a L^3 \Delta T,$$

the latter form being convenient for computation when a is tabulated.

The coefficient to be used in equation (6) depends upon the geometry of the system and there is, unfortunately, in many cases incomplete agreement between authorities. We consider here only four cases of free convection which are usually of interest in solar energy collector design:

1) a flat plate or other large body exposed in a large volume of air,
2) parallel plane surfaces a small distance apart,
3) horizontal cylinders,
4) concentric cylinders.

Case (1): Flat plates or other large bodies. The coefficient C in Equation (6) is given as 0.55 for vertical surfaces, 0.71 for horizontal surfaces facing upwards, 0.35 for horizontal surfaces facing downwards, and 0.45 for horizontal cylinders. Noting that the value of $ka^{1/4}$ in the usual working range is about 0.53, Fishenden and Saunders recommend using the value 0.30 for the coefficient B in Equation (8) for calculations on irregular bodies above about 1 ft in size.

(This case of natural convection does not occur often in solar energy collectors, since the heated bodies are usually enclosed by a glass cover, leading to cases (2) and (4). Where there is no cover, or one considers the cooling of the cover itself, the conditions are usually those of forced ventilation due to wind).

Case (2): Parallel plane surfaces (with closed edges). In this case the characteristic length L is taken as the spacing between the surfaces, assuming the surfaces to be large, and ΔT is now the temperature difference between the surfaces. For this purpose we write Equation (6) in its more primary form

$$Nu = \frac{q_c L}{k \Delta T} = C\,(Gr \cdot Pr)^n = C(aL^3 \Delta T)^n, \tag{6a}$$

where Nu is the Nusselt number, and n is the exponent taken as $1/4$ in the usual range. Note that in the present example the Nusselt number is the ratio between the heat transfer by convection q_c to the heat transfer by pure conduction alone $k \Delta T/L$. Fishenden and Saunders give a curve showing how the Nusselt number Nu is unity up to $(Gr \cdot Pr) = 10^3$ — i.e. for very small spaces L of the order of 1/50 ft or less convection is suppressed — while in the range $(Gr \cdot Pr) = 10^4 - 10^6$ Equation (6a) is approximately

$$Nu = \frac{q_c L}{k \Delta T} = 0.15\,(Gr \cdot Pr)^{1/4}$$

$$\text{or} \quad q_c = 0.15\,(ka^{1/4})\left(\frac{\Delta T}{L}\right)^{1/4} \Delta T \quad . \tag{9}$$

This is for vertical air spaces. Values of $(Gr \cdot Pr)$ larger than 10^6 usually mean that the gap between the surfaces has become very large and the transfer should be calculated in stages — from one surface to the air and from the air to the other surface —

assuming that the air takes up a mean temperature. At these high values of $(Gr \cdot Pr)$ the exponent n becomes $1/3$ and the coefficient for a single plate is 0.12 or for the two plates combined $= 0.12/2^{1.33} = 0.05$, remembering that the temperature difference for the calculation is half the difference between the plates and the heat transfer and is proportional to $\Delta T^{1.33}$,

$$\text{i.e.} \qquad Nu = \frac{q_c L}{k \Delta T} = 0.05 \, (a L^3 \Delta T)^{1/3}$$

$$\text{or} \qquad q_c = 0.05 \; k a^{1/3} \Delta T^{4/3},$$

i.e. q_c is no longer dependent on the size of the gap L. For this and other reasons the gap L is usually taken as about 1" and Equation (9) can be applied.*

For horizontal surfaces the coefficient is somewhat smaller. As pointed out by Hottel and Woertz, there is a range of values given by different experimenters for the value of the constant to be chosen for the case of a pair of surfaces tilted at say 30° to the horizontal (which is about the angle at which most fixed flat plate type solar energy collectors would be used) and they finally recommend the simplified form (for a gap of about 1")

$$q_c = 0.16 \, \Delta T^{5/4}, \tag{10}$$

ignoring the variation of $ka^{1/4}$. It should be noted that, if we take $ka^{1/4}$ as about 0.53 in the ambient temperature range, this may be written

$$q_c = 0.30 \, (ka^{1/4}) \, \Delta T^{5/4}, \tag{11}$$

which has the advantage over Equation (10) in that it may be applied over a larger temperature range.

Case (3): Horizontal cylinders. The coefficient C in Equation (6) is given as 0.45, thus

$$q_c = 0.45 \, (ka^{1/4}) \left(\frac{\Delta T}{D}\right)^{1/4} \Delta T, \tag{12}$$

where D is the diameter of the cylinder.

This case applies in solar energy collectors for those types employing a cylindrical parabolic mirror or a cylindrical lens, and in which the mirror is covered by a glass pane or the lens system is totally enclosed to prevent cooling of the receiver by the wind. Where such cooling can occur because the system is not closed — for example if the parabolic mirror is very large — it is customary to cover the receiver, which may be in the form of a cylinder, by a cylindrical glass envelope. This leads to case (4).

Case (4): Concentric cylinders. This case has been summarized by Fishenden and Saunders. By taking the diameter D_i of the inner cylinder as the characteristic dimension for computing $(Gr \cdot Pr)$, they have plotted log Nu against log $(Gr \cdot Pr)$ for various ratios

* See, for example, the curves of Rowley and Algren for conductance of air spaces quoted by Brown and Marco, Figure A-11.

of D_0/D_i, where D_0 is the inside diameter of the outer cylinder. Part of their curve is given in Figure 1a. The straight section can be represented approximately by the equation

$$Nu = \frac{q_c D_i}{k\Delta T} = 0.28\ (Gr{\cdot}Pr)^{1/4}$$

or

$$q_c = 0.28\ (ka^{1/4})\ \left(\frac{\Delta T}{D_i}\right)^{1/4} \Delta T. \tag{13}$$

The particular value of Figure 1a is in indicating a choice for the size of the outer cylinder in the case of a cylindrical receiver in a cylindrical glass envelope. If, for a given $(Gr{\cdot}Pr)$ value, D_0/D_i is chosen so that Nu is on the horizontal part of the curve, this means that there is no convection and the heat transfer is by conduction. Thus a very small ratio D_0/D_i should not be chosen. On the other hand, if a large D_0/D_i ratio is chosen, the outer cylinder has a large area and does not get so warm due to the flow of heat from the inner cylinder, as it would do were it smaller. As the aim is to get the inner cylinder as hot as possible with the minimum of heat loss, this means that the hotter the outer cylinder *for a fixed heat transfer*, the hotter the inner cylinder.

From this it appears that the best size for the outer cylinder is that which corresponds to the knee of the Nu-$(Gr{\cdot}Pr)$ curve. Thus Figure 1b shows the recommended ratio of the internal diameter of the glass envelope to the diameter of the cylindrical receiver for any working temperatures and expected temperature differences. In this case q_c is determined from Equation (13) with the coefficient increased about 10%. If the exact size is not available as a standard, the next nearest larger size of glass tube should be taken.*

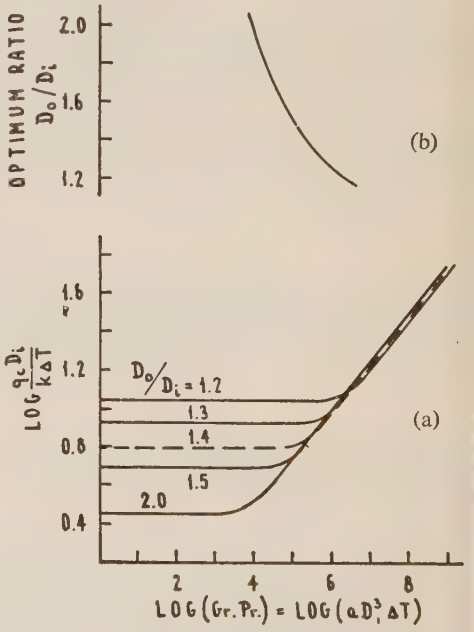

Figure 1
Convection loss between concentric cylinders.

Forced convection

The solar energy collector is generally subject to cooling due to wind. Therefore the outer surface of any glass envelope used will have a loss coefficient. In heating and ventilating practice it is customary to take the outside loss coefficient as 6 BTU/hr·ft² per °F temperature difference, which corresponds to a wind of 15 miles per hour. At 10 mph the figure is about 4 BTU, while under very still conditions it may fall to under 2 BTU. The figure includes convection and radiation loss under average

* Strictly speaking, every case should be calculated separately, as the optimum diameter ratio will depend on the form of cooling of the outer tube. Thus, if the outer tube is cooled so strongly that it hardly heats up, it should be made large, since making it small entails the risk of increased conduction loss. However, the recommendation of Figure 1b is probably a good starting point for most real designs.

conditions and is that applying to flat surfaces, but will be found to apply also to cylindrical surfaces if the diameter is more than about 6″. For more accurate computations which are sometimes necessary for the cylindrical case where the temperature difference between the cylinder and the air may be considerable, the cooling due to the wind should be computed from the formula of King and Knaus

$$q_c = 0.025 \frac{G^{0.58}(1 + 0.000576\,t)}{D^{0.42}} \Delta T \qquad (\text{BTU/hr}\cdot\text{ft}^2), \quad (14)$$

where t — average air temperature (°F)
G — mass velocity of the air (lb/hr·ft²).

To this should be added the radiation loss

$$q_r = 0.166 \times 10^{-8}(T_1 - T_a^4), \qquad (15)$$

where T_1 is the absolute temperature °R of the cylinder which is of glass and assumed to have an emissivity of about 0.96, the radiation taking place to an environment of absolute temperature T_a°R.*

Conduction loss

In general, this applies to the parts of the receiver not exposed to the solar radiation and in flat plate collectors may be termed the rear loss, q_{rear}. In general, by use of adequate insulation this term can be reduced to a very low fraction of the total loss, and may be computed from

$$q_{rear} = K_T/d \cdot \Delta T \qquad (\text{BTU/hr}\cdot\text{ft}^2), \quad (16)$$

where K_T — mean conductivity of the insulating material
d — thickness of the insulation (ft).

There is one special case of conduction loss which is sometimed more difficult to compute and which is of interest in high efficiency systems: i.e. the case of low pressure air gaps. The heat transfer from a body in air by convection depends upon the $(Gr \cdot Pr)$ product, i.e. depends upon the value of $gy\Delta TL^3\varrho^2 c_p/\mu k$.

Thus, reducing the air pressure i.e. the density ϱ reduces the $(Gr \cdot Pr)$ product so that a point is reached at which convection virtually ceases. (A vacuum of a few mm Hg will usually be sufficient). However, the *conductivity* of air is, in theory, independent of pressure down to very low pressures, so that a reduced pressure air environment can be regarded as a conducting medium of conductivity k where k is the conductivity of air at the mean temperature. This figure is so low that edge effects, which can be ignored when treating ordinary cases of insulation, must be considered in this case. As an example a thin rectangular receiver $L \times M$ ft is placed in a box $(L + 2\delta) \times (M + 2\delta) \times 2\delta$ ft, i.e. a uniform gap of δ all around. Using the equation of Langmuir** (when the plate thickness is less than $\delta/5$):

$$\text{Effective cooling area} = 2LM + 0.465 \times 4(L+M)\delta + 0.35\delta^2 =$$

$$= 2LM\left(1 + 0.93\delta\frac{L+M}{LM} + \frac{0.175\delta^2}{LM}\right). \qquad (17)$$

* When the environment is the open sky, meteorologists take the sky radiation as 0.7—0.9 T_a^4, depending upon the humidity and cloudiness. However, part of the glass tube will receive radiation from the ground or the concentrating mirror which, in general, will be at just above air-temperature, so the form of equation (15) is recommended.

** See Ref. 6, p. 35, or Ref. 4, p. 26.

Thus, if Equation (16) is used to calculate the heat conducted across the air gap, the effective cooling surface is increased by the terms in the bracket of Equation (17). As a typical example, for a plate 3ft × 6 ft and a 4″ air gap, the edge effect increases the conduction loss by 16%.

One other low-pressure air gap case is of interest, i.e. a cylindrical receiver in a cylindrical (glass) envelope, the air pressure being reduced to eliminate convection.

$$\text{Then} \quad q = \frac{2.73\ k}{\log_{10} D_0/D_i}\Delta T \qquad \text{(BTU/hr per ft of length)} \quad (18a)$$

$$= \frac{0.87k}{D_i \log_{10} D_0/D_i}\Delta T \qquad \text{(BTU/hr·ft}^2\text{ of inner cylinder).} \quad (18b)$$

Radiation loss

The radiation loss q_r per unit area of a body in a large enclosure is given by

$$q_r = E_0\sigma\,(T_0^4 - T_1^4), \qquad (19)$$

where E_0 — the emissivity of the body
T_0 — the absolute temperature of the body
T_1 — the absolute temperature of the enclosure
σ — Stephan-Boltzmann constant (0.173×10^{-8} BTU/hr·ft²·°R⁴)*.

When the body is surrounded by an envelope not much larger than the body, (19) becomes

$$q_r = \frac{1}{1/E_0 + 1/E_1 - 1}\,\sigma\,(T_0^4 - T_1^4)\ , \qquad (20)$$

where E_1 is the emissivity of the enclosure. The quantity $\dfrac{1}{1/E_0 + 1/E_1 - 1}$ may be termed the effective emissivity of the body *in the presence of the envelope* and is represented by E_e.

While normally the effective emissivity is nearly unity, since the enclosure is of glass giving $E_1 = 0.96$, and the receiving surface is painted black giving $E_0 = 0.95 - 0.98$, it is shown in ref. (1) that, by the principle of selective radiation, the effective emissivity can be greatly reduced. Two methods are described. In one, the black surface is selective in that it is an absorber only for wavelengths below 2 microns, i.e. in the solar radiation range, whereas it is a reflector (and hence a poor emitter) for wavelengths above 2 microns, i.e. for heat waves. In the second method the cover glass is so constructed that, while remaining transparent to solar radiation, it is a strong reflector (on its under-side) for heat waves, so that it has a low emissivity. Such a glass has been termed a *solartrap*. The computations in later sections of this paper show the very great reduction in losses that can be expected from the use of selective black surfaces or the solartrap and the effect upon the performance of solar energy machines.

Summarizing, the total loss, per unit area, of a receiver at temperature T in the presence of an envelope at temperature T_1 is given by

$$q_{l(T)} = q_c + q_r + q_{rear}$$
$$= C'\,(T - T_1)^{5/4} + E_e\sigma\,(T^4 - T_1^4) + \frac{k_T}{d}\,(T - T_1) \qquad (21)$$

* This is the value usually quoted. Hottel in the 1954 edition of McAdam's Heat Transmission gives $\sigma = 0.1713$.

for the case with convection loss, or

$$q_{l(T)}=C'' k(T-T_1)+E_e\sigma(T^4-T_1^4) \tag{22}$$

for the case with partial vacuum. In some cases a term in K_T must be added to Equation (22).

The constant $C' = 0.16$ or $0.3\ (ka)^{1/4}$ for the case of parallel flat plates; for the case of concentric cylinders $C' = 0.28 - 0.31\ ka^{1/4}/D_i^{1/4}$). In both cases, a check on the $(Gr{\cdot}Pr)$ product $= (aL^3\Delta T)$ or $(aD_i^3\Delta T)$ should be made.

As $q_{l(T)}$ is the loss per unit area of receiver at temperature T, the integrated effect of the losses from a receiver of which the various parts are at different temperatures must be determined as indicated in Equations (3a)—(3d). Taking, for example, Equation (3b), the integral $I=\int_{T_c}^{T_b}\frac{dT}{1-q_{l(T)}/q_0}$ may be determined graphically when the relationship between T and $q_{l(T)}$ has been computed for a series of values of $q_{l(T)}$ and T. In many cases a simplification occurs, for the $q_{l(T)} - T$ curve is found to be nearly linear.

Thus, if $q_{l(T)}$ varies linearly from zero at T_c to $q_{l(T_b)}$ at T_b, i.e.

$$q_{l(T)} = q_{l(T_b)}\frac{T-T_c}{(T_b-T_c)}, \tag{23}$$

then $$I = \int_{T_c}^{T_b}\frac{dT}{1-q_{l(T)}/q_0} = (T_b-T_c)\ \frac{q_0}{q_{l(T_b)}}\ \ln\left(\frac{1}{1-q_{l(T_b)}/q_0}\right)$$

which, from (1) and (2a), may be written

$$I=(T_b-T_c)\ \frac{Q_i}{Q_x}\ \ln\frac{1}{1-Q_x/Q_i} \tag{24}$$

and Equation (3b) becomes

$$\eta_{1h}=\frac{\alpha\beta\,(T_b-T_c)}{I} = \alpha\beta\frac{Q_x}{Q_i}\ \frac{1}{\ln\left(\frac{1}{1-Q_x/Q_i}\right)} \tag{25}$$

or the retention efficiency for heating N_{1h} is given by

$$N_{1h} = \frac{Q_x}{Q_i}\ \ln\left(\frac{1}{1-Q_x/Q_i}\right) \text{ or } \frac{-Q_x}{Q}\ \ln\left(\frac{1}{Q_x/Q_i}\right). \tag{26}$$

Q_x/Q_i may be called the cut-off ratio X, being defined as the ratio of the cut-off intensity Q_x to the actual intensity Q_i.

If, therefore, for any system, the cut-off value has been computed, the retention efficiency N_{1h} may be at once determined, for any particular incident insolation, from the following table.

TABLE II

$X=Q_x/Q_i$	.0	.1	.2	.3	.4	.5	.6	.7	.8	.9	.95	.98	1.0
N_{1h}	1.0	.95	.897	.843	.785	.723	.655	.543	.496	.391	.318	.25	0

As the losses invariably rise more rapidly than T, the actual efficiency of retention will always be slightly more than the values given in the table, since the losses at any point of the receiver will be less than those given by a straight line based upon the losses at the hot end.

Before considering specific computation examples, it is necessary to distinguish between efficiencies at any instant and average efficiencies over a period, particularly annual averages.

ANNUAL COLLECTION EFFICIENCIES

Consider a daily solar intensity curve (Figure 2a) as it falls upon a collector system. The intensity Q_i starts from zero at dawn, rises to a maximum (on a clear day) at noon and falls to zero at sundown. If the collector is controlled to collect at a constant output temperature T_0 when the losses from the receiver are $q_{l(T_0)}$ and the cut-off value $= Q_x = q_{l(T_0)}/\alpha\beta P$, then whenever Q_i is less than Q_x there is no collection.

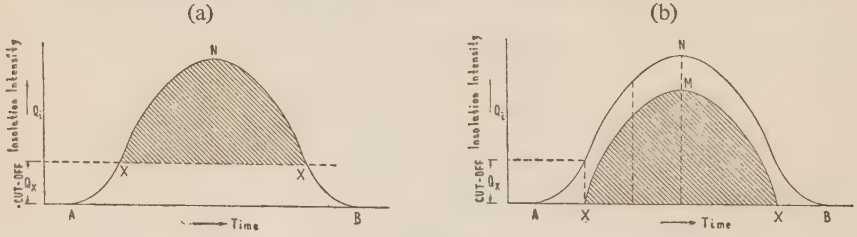

Figure 2
Graphical determination of collection efficiencies from daily radiation curve.

We first consider the case for a receiver used for boiling, or for any other case in which the whole receiver is substantially at the same temperature. The collection efficiency is given by Equation (3c)

$$\eta_{1b}=\alpha\beta\,(1-Q_x/Q_i)$$

or retention efficiency

$$N_{1b} = 1 - Q_x/Q_i \ . \tag{27}$$

From this it is at once clear that the average retention efficiency* during the day is the ratio of the area XNX between the solar intensity curve and the cut-off value Q_x to the total area under the solar intensity curve ANB (Figure 2a).

By taking actual measured solar intensity curves and drawing a series of cut-off lines XX at different heights, it is possible to construct a graph of retention efficiency against cut-off value, and by repeating this for a number of representative days of the year, a yearly graph can be obtained. This has been done in Figure 3**, where the

* Note that the time average of efficiency is $\int N_1\, Q_i d\tau / \int Q_i d\tau$ (taking only positive values) and not $\int N_1\, d\tau / \int d\tau$ which is the more usual definition of a time average.

** A bar over N_1 or η_1 signifies annual average values.

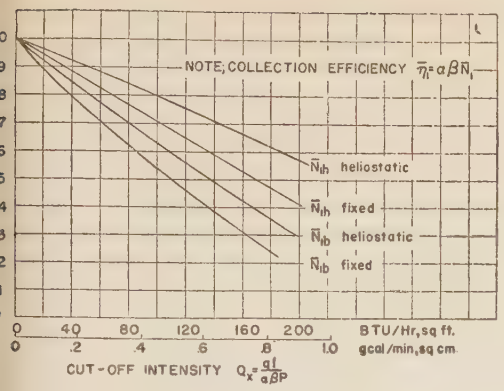

Figure 3

Annual efficiency as a function of cut-off intensity.

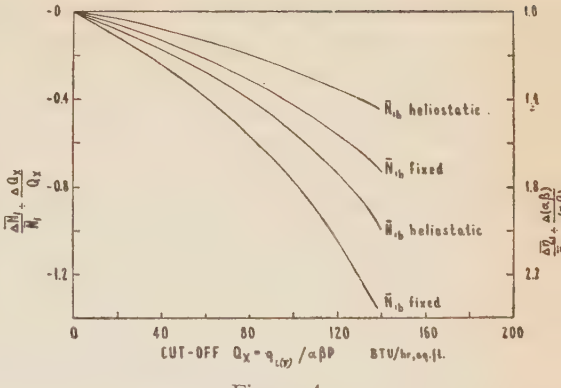

Figure 4

Fractional change in efficiency produced by small change in Q_x. Ordinates may be read as % change in $\bar{N}_1$ or $\bar{\eta}_1$ for 1% change in Q_x or $\alpha\beta$.

results, based on the solar intensity curve on a fixed tilted receiver and the solar intensity curve on a heliostatic receiver, are shown*. To obtain collection efficiencies it is necessary to multiply the retention efficiency by the overall transmission efficiency ($\alpha\beta$).

Figure 3 emphasizes the importance of keeping the overall transmission efficiency high, for, given a fixed loss $q_{l(T)}$, a reduction in the value of $\alpha\beta$ has two effects: it increases the cut-off value and therefore reduces the retention efficiency, and it reduces the collection efficiency as computed from the retention efficiency. This is illustrated in Figure 4, which shows the fractional change in collection efficiency η_1 for a small fractional change in $\alpha\beta$.

Because of the general nature of Figure 3, it indicates changes to be effected in a design in order to improve the efficiency, without, in many cases, having to re-compute the losses. Thus the effect of altering the concentrating power P is at once determined by its effect on the cut-off value Q_x.

The determination of annual average values of η_{1h} or η_{1s}, the efficiencies for heating or for superheating, is more difficult. Equation (3b) shows that

$$N_{1h} = \frac{T_b - T_c}{\int_{T_c}^{T_b} \frac{dT}{1 - q_{l(T)}/q_0}} = \frac{T_b - T_c}{\int_{T_c}^{T_b} \frac{dT}{1 - q_{l(T)}/\alpha\beta P Q_i}} . \qquad (28)$$

Unlike the computation for $\bar{N}_{1b}$, it is not possible to take the ratio of the areas XNX to ANX in Figure 2a, for the manner in which $q_{l(T)}$ varies with T must be known. Furthermore, even if this is known, the integral will depend on $\alpha\beta P$, thus not

* The representative days were the equinoxes and the solstices, on the (rather unfair) assumption that the rainy days are spread throughout the year. The error thus introduced is very small, particularly for low values of cut-off, because the retention efficiencies do not come out greatly different on different days, under the specific local conditions. Thus for $Q_x \sim 88.5$ BTU/hr. ft² (= 0.4 cal/cm²· min) $N_{1b} \sim 0.67$ on Dec. 21st, 0.67 on June 21st, and 0.68 on March 21st, for heliostatic mounting. Ashbell's[10] figures for solar radiation intensities in Jerusalem were used for the solar intensity curves and neither the diffuse (sky) radiation nor the reduction in direct radiation on "hamsin" days (which reduction can amount to 20% or more) are included. For flat plate collectors which utilize the diffuse radiation, the retention efficiencies will be greater than those shown. The reduction of efficiency for cloudy days is also not included; this would require that the yearly average be determined from 365 daily records, which was not possible at the time of writing. However, see section on Corrections to Figure 3.

permitting the construction of a generalized graph of the type of Figure 3. In order, therefore, to arrive at such a generalized graph which, if not highly accurate in the abolute sense, has at least the merit of giving an accurate picture of the effect of change of design parameters, the simplification of linear losses is introduced as in Equation (23) The daily average value of N_{1h} is determined by drawing the daily solar radiation intensity curve, choosing a value of Q_x, hence Q_x/Q_i is known for each point on the curve, multiplying the ordinates by the corresponding value of N_{1h} obtained from Table II, thus obtaining the curve XMX of Figure 2b, and then taking the ratio of area XMX to ANB. The results, averaged for the year as in the case of $\bar{N}_{1b}$, are also shown in Figure 3. The fixed tilt curve is the one to be used for solar water heaters.

Curves for N_{1s}, the retention efficiency for superheating, are not given as they cannot be generalized: in the first place the losses will be very remote from linear with temperature, secondly the range of integration varies from design to design. Fortunately, N_{1s} is hardly ever used in practice.

It is shown in Equation (3e) that the composite efficiency for a system which both heats and boils is given by

$$\eta_{1c} = \frac{h_w + h_{fg}}{h_w/\eta_{1h} + h_{fg}/\eta_{1b}} = \alpha\beta N_{1c} , \tag{29}$$

where N_{1c} is the composite retention efficiency, which may be written

$$N_{1c} = \frac{h_w + h_{fg}}{h_w/N_{1h} + h_{fg}/N_{1b}} . \tag{30}$$

The question arises: can yearly average values be substituted for N_{1h} and N_{1b} to yield a yearly average value for N_{1c}?

Theoretically this is not possible, because the composite of the averages is not the same as the average of the composites. However, a number of checks in the range of moderate steam pressures and reasonable retention efficiencies have shown that the error in using Equation (30) with yearly average values for N_{1h} and N_{1b}, instead of determining the yearly average value of Equation (30), is generally a fraction of 1%.

Thus we may write, for yearly averages

$$\bar{N}_{1c} = \frac{h_w + h_{fg}}{h_w/\bar{N}_{1h} + h_{fg}/\bar{N}_{1b}} = \frac{r + 1}{r/\bar{N}_{1h} + 1N_{1b}} \tag{31}$$

where $r = h_w/h_{fg}$,

also $\bar{\eta}_{1c} = \alpha\beta\, \bar{N}_{1c}$.

CORRECTIONS TO FIGURE 3

Apart from the limitations referred to in a previous footnote, there are a number of corrections which should be taken into account in using Figure 3. These are:

a) Solar intensity values at places other than Jerusalem, and effect of diffuse radiation and cloud;
b) effect of angle of incidence;
c) shading effect;
d) temperature drop in collector;
e) dirt on glass.

a) Solar intensity values. Figure 3 was based on solar intensity values in Jerusalem and excluded diffuse radiation, clouds, or the effect of hamsin, which may reduce the solar intensity without obscuring the sun. As it is the intensity rather than the shape of a daily solar radiation curve which varies from place to place and as this intensity Q_i is always used in the present calculations in the form of the ratio Q_x/Q_i, it follows that to use Figure 3 in a place with intensities other than in Jerusalem, it is sufficient to multiply the computed value of Q_x by the ratio $317/\overline{Q_{ipn}}$ where $\overline{Q_{ipn}}$ is the yearly mean value of normal incidence at noon (for clear days) in BTU/hr · ft², and 317 was the corresponding value used in the preparation of the curves of Figure 3.

Were the diffuse radiation in constant ratio to the direct radiation then a correction similar to that for solar intensity could be made here. This is not so as, in general, the diffuse radiation is proportionally greater in the mornings and evenings than at mid-day. This leads to a particular improvement in collection efficiency at low levels of Q_i. On the other hand, the effect of cloud is to reduce the efficiency of collection particularly at low levels of Q_i. In both cases, as low levels of Q_i contribute only a small part of the total annual insolation, the weight which changes of collection efficiency at low levels of Q_i exert on the average yearly efficiency is relatively small. The writer is unable to suggest a reliable short-cut to deal with these two problems and it is necessary to prepare $\overline{N}_1$—Q_x curves of the type of Figure 3 on the basis of actual measured intensities including cloud and including sky radiation for non-concentrating systems but without sky radiation for systems employing concentration. However, until new $\overline{N}_1 - Q_x$ curves are available, it is suggested that, to allow for cloud, the value of Q_x be multiplied, for flat plate collectors, by $(1+C)$ where C is half the fractional time of cloudy skies*. No correction for cloud is required for focusing heliostatic systems, provided that the total yearly insolation is measured with an integrating normal incidence pyroheliometer, since both the pyroheliometer and the focusing system will only respond to an unobscured sun. To allow for diffuse radiation, Q_x should be divided by $(1+S)$ for flat plate collectors where $S = 0.1$ for local conditions. This is based upon Prof. Ashbell's estimate that the diffuse radiation adds about 10% to the solar radiation on clear days, more on hamsin days, and that the greater percentage of diffuse radiation in the mornings and evenings (when it has the most beneficial effect) approximately cancels the fact that a tilted plate does not "see" the whole sky. No correction for diffuse radiation is required for focusing systems.

Thus the correction to Q_x in Figure 3 for flat plate collectors is

$$Q_x \text{ (corrected)} = Q_x \text{ (computed)} \; 317/\overline{Q_{ipn}} \; [(1+C)/(1+S)], \qquad (32)$$

where C represents the average reduction in intensity due to cloud — taken as half

* The sun is obscured for about 20—22% of sunshine hours in Jerusalem; an estimate shows that this results in about 10% reduction of total incident radiation.

the fractional time of cloudy skies — and S represents the average increase in intensity due to sky radiation. Under local conditions these two terms practically cancel out. For focusing systems the square bracket is not required. It must be stressed that Equation (32) is presented *faute de mieux* and may introduce an error of several percent in the value of Q_x.

b) Angle of incidence. The curves of Figure 3 were computed on the assumption that β, the transmission coefficient of the optical system, is a constant. For non-heliostatic mountings it is known that β falls off with increasing angles of incidence so that, in general, efficiencies of collection in the morning and the evening are less than they would be otherwise. The only correct method of allowing for this is to take the daily solar insolation curve (for the angle of the receiving plate being considered) and multiply the ordinates (insolation values) by a factor β_t/β_0, where β_0 is the transmission factor for the normal incidence and β_t the transmission factor for the angle of incidence corresponding to the time t. Such factors may be determined from the measurements given in the paper of Hottel and Woertz. The "corrected" curves of solar insolation are then treated as previoulsy described for determining $\overline{N}_{1h}$ and $\overline{N}_{1b}$. Such a procedure is suggested for very accurate studies of a particular design but it results in a certain loss of generalization.

An approximation permits the generalized graphs to be used. A few checks have indicated that the effect of angle of incidence is to reduce the collection or retention efficiency for flat plate collectors tilted at about 30—40° in latitudes of this range from 3 to 1% for each sheet of glass for the values of cut-off in the range $Q_x = 30$—150 BTU/hr·ft². It is suggested that about 2% reduction be taken as an average figure. As the usual black receiving surface suffers from a decrease in absorption with increasing angles of incidence, it is suggested that the collection or retention efficiency be reduced by a further 1% on this account, i.e.

$$\overline{N}_1 \text{ (corrected)} = (0.99 - 0.02\,n)\overline{N}_1 \quad \text{(from graph)} \tag{33}$$

where n is the number of sheets of glass. It is not recommended that this correction be used for $n > 2 - 3$.

c) Shading. This is very small for shallow flat plate collectors and can be still further reduced by painting the side walls white, while the use of aluminium foil on the sides will practically eliminate the shading error. Hottel and Woertz estimated about 4% due to shading for the case of a rather deep square collector (depth = 9.6% of side dimension — white painted) so that, as a first approximation, the reduction in collection or retention efficiency can be written as $40\,a/b\,\%$ where a/b is the depth-side ratio.

Shading can occur with heliostatic systems if multiple units are placed too close together and a check on any proposed design should be carried out. The $N_1 - Q_x$ curves of Figure 3 could be prepared to include such shading.

d) Temperature drop in receiver. For the case of flat plate collectors, where the

fluid flows in pipes attached to a plate, use can be made of the "plate-pipe efficiency factor" F of Hottel and Woertz:

$$F = \frac{2}{m} \frac{e^m - 1}{e^m + 1} \tag{35}$$

where

$$m = W\sqrt{q_l/\Delta T k' M} \tag{36}$$

W — distance between parallel pipes measured along collector plate (ft)
k' — thermal conductivity of collector plate (BTU/hr·ft², °F per ft)
M — thickness of collector plate (ft).

As F is the ratio of the energy collected to that which would be collected by a plate at uniform temperature, and as F, from Equations (35) and (36), is nearly independent of T, the factor F may be used directly as a correction factor to the average retention or collection efficiencies obtained from Figure 2. Its value should be of the order 0.97*.

For concentrating systems, where the energy falls directly on the tube containing the heated fluid, there is no plate-pipe efficiency factor. However, for all systems there is a difference in temperature δT between the temperature of the receiving surface and that of the heated fluid. If this temperature drop δT can be estimated or measured, the temperature $T + \delta T$ should be used for determining the cut-off intensity: i.e.

$$Q_x = q_{l(T+\delta T)} \ /\alpha\beta P \ .$$

e) Dirt on glass. Hottel and Woertz reported that their experiments for flat plate collectors gave maximum reduction in collection of 4.7% with about 1% as the average value. It is not yet known what is the effect of dirt on a glass cover or on the mirror of a focusing system, since the scattering of light in this case might be more serious than in a non-focusing system. The collection or retention efficiencies should thus be corrected by a factor $(1-D)$, where D is of the order 0.01.

Summarizing the corrections to be applied to Figure 3:

a) For flat plate collectors

$$Q_x \text{ (corrected)} = \frac{q_{l(T+\delta T)}}{\alpha\beta P} \cdot \frac{317}{\overline{Q}_{ipn}} \cdot \left(\frac{1+C}{1+S}\right), \tag{32a}$$

where $C \sim 0.10$, $S \sim 0.10$ under the local conditions;

$\overline{N}_1$ (corrected) $= (0.99 - 0.02\,n)\,(1 - 0.4\,a/b)\,F\,(1 - D)\,\overline{N}_1$ (from graph)** (34),

where n is the number of glass sheets, F is the plate pipe efficiency factor, $(1-D)$ is the dirt factor, a/b is the ratio of depth to side of box.

b) For focusing (heliostatic) collectors

$$Q_x \text{ (corrected)} = \frac{q_{l(T+\delta T)}}{\alpha\beta P} \cdot \frac{317}{\overline{Q}_{ipn}} \ , \tag{32b}$$

$$\overline{N}_1 \text{(corrected)} = (1-D)\,\overline{N}_1 \quad \text{(from graph)} \tag{34a}$$

In all cases, collection efficiency $\overline{\eta}_1 = (\alpha\beta) \times$ retention efficiency $\overline{N}_1$.

* This is the value given by Hottel and Woertz in their 1942 paper. However, Hottel[8] assumes a value 0.9 in a later paper. In the examples given later the present author has assumed $F = 0.97$, but where a flat plate collector is used to provide steam an additional temperature drop $\delta T = 10°F$ has been assumed.

** The $\overline{N}_1$ here can be any of the retention efficiencies, $\overline{N}_{1b}$, $\overline{N}_{1h}$ or the composite $\overline{N}_{1c}$.

Effect of heat capacity

There is one further correction which should be applied after the performance has been computed, i.e. the heat capacity loss.

For flat plate collectors Hottel and Woertz have suggested an approximate estimation of the effect of heat capacity — which results in a delay in reaching the collection temperature in the mornings. They suggest that the heat capacity per ft² of collector at equilibrium temperatures (calculated from the materials of construction and assuming linear temperature drop both ways from the plate) be divided by the temperature differences between the collector and the outside air to give a specific capacity m, and that in practice about $^2/_3\ m$ should be taken as the effective value (due to preheating by early morning radiation). The loss of collection each day is taken $^2/_3\ m\Delta T$ per ft². On days with heavy cloud, this loss, or part of it, might occur several times and this emphasizes the need for keeping m small by using low density insulation, and avoiding excess metal. In the careful design of Hottel and Woertz the capacity loss was 0.36 BTU/day · ft² per °F temperature difference or 34 BTU/day · ft² for the temperature difference of 94 °F between the temperature of the heat collector and that of the early morning outside air.

If Y is the total insolation per ft² during the year and $\overline{\eta}_1$ the mean yearly efficiency, then the actual useful energy obtained will be $Y\overline{\eta}_1 - 365 \times {}^2/_3\ m\Delta T$. Thus for well designed collectors used for water heating, under local conditions, the capacity loss is of the order of $0.017\ \Delta T/\overline{\eta}_{1h}\%$ or about 4% for $\overline{\eta}_{1h} \sim 0.3$—$0.4$ and $\Delta T \sim 90$ °F.

For focusing systems, it can readily be shown that the time taken to reach the temperature T (from cold) when subject to a constant insolation Q_i is given approximately by

$$t = \frac{-m\Delta T}{(\alpha\beta P)Q_x} \ln\left(1 - \frac{Q_x}{Q_i}\right) \text{ hours} \tag{37}$$

$$\simeq \frac{m\Delta T}{(\alpha\beta P)Q_i} \quad \text{if} \quad Q_x \ll Q_i\,. \tag{38}$$

where m is the specific capacity ("water equivalent") of 1 ft² of receiver. If the receiver is in the form of a thin walled tube filled with water then, for 1 ft² of receiver surface, length $L = 1/\pi D$ and the volume $= D/4$ ft³, i.e. ignoring the specific heat of the tube, the specific capacity is $62.4/4 \cdot D$ BTU per °F taking 1 ft³ water $= 62.4$ lb. Thus for Example 4 in the next section $D = {}^1/_2$ ft giving $m = 7.8$. This shows that for $\Delta T = 250$°F, $\alpha\beta P = 4.67$ and Q_i about 200 BTU per hr · ft², the time to reach the collection temperature is about 2 hours and for larger models would be proportionately larger. This is a serious loss and can be reduced by increasing the concentrating power P or by making the receiver as a cylindrical annulus or a small tube with radial fins to increase the collection diameter. The latter method can probably reduce m by a factor of 10, thus bringing the time delay down to a few minutes and the capacity loss to a few per-cent.

The whole question of heat capacity loss needs careful examination, since this term can easily cause great disappointment in an actual collector. In particular, for days in which the sun is periodically obscured by clouds, the output of a collector may be very low indeed in relation to the actual integrated solar insolation for that day.

TYPICAL EXAMPLES

Using the formulae given in the earlier sections, it is possible to construct a Q_x—T curve for any given design. The usual method is to assume a loss q_l and determine the temperature rise for each stage from the outside inwards. Thus for a flat plate collector with two cover glasses first the temperature of the outer glass is determined from the outside loss coefficient; then the temperature drop across the first gap using the Equation

$$q_{l(T)} = 0.30\,(ka^{1/4})\,\Delta T^{5/4} + 0.160\left[\left(\frac{T_1}{100}\right)^4 - \left(\frac{T_2}{100}\right)^4\right] \text{(BTU/hr·ft}^2\text{)}, \quad (39)$$

the first term being the convection loss (Equation (11) and the second the radiation loss, taking the emissivity of each sheet of glass as 0.96.

This gives the temperature of the second sheet of glass, whence, by a formula similar to that of Equation (39) but modified for the emissivity of the receiving surface, the temperature of the receiver can be determined. Equations of the type of (39) can be quickly solved graphically if a family of curves of $0.160[(T_1/100)^4 - (T_2/100)^4]$ (for different values of T_2) are plotted as positive ordinates, against ΔT (T_1—T_2 in this case) as abscissa. On the same graph $0.30ka^{1/4}\Delta T^{5/4}$* is plotted as a negative ordinate against ΔT as abscissa. In this way, the sum of the positive and negative ordinates give $q_{l(T)}$ against ΔT so that, with the aid of a pair of dividers, the value of ΔT is rapidly determined. When T_0, the temperature of the receiver, is known, the rear loss q_{rear} can be computed and this, added to $q_{l(T)}$, gives the total $q_{l(T)}$. [If the glass absorbs energy it is possible to add this into the step by step procedure, but this presents the difficulty that the incoming intensity must be known in order to know the percentage absorbed. Except in the case of systems of very high concentrating power, where the energy absorbed by a glass cover tube** might contribute considerably to its temperature rise, it appears to be not worthwhile to include this item in the calculations.]

Once the $Q_x - T$ curve has been obtained, the performance is given by Figure 3 (adding the corrections described) and composite efficiencies are determined with the aid of Equation (31). Where peak efficiency is required rather than annual average values, the retention efficiencies can be determined directly from Equations (3a, b, c, d) and (26).

For studying the possibilities of producing power with a solar collector and heat engine the product of the Carnot cycle efficiency (Equation (4)) and the collection efficiency can be plotted against T to determine the optimum operating temperature. [In this case the *boiling* efficiency η_{1b} or $\bar{\eta}_{1b}$ must be used, since in a Carnot cycle it is assumed that all the heat is provided at the source temperature T_0]. Such curves indicate the best possible result that could be obtained from a given collector: in practice the power output would be between 0.3—0.6 that of the theoretical Carnot cycle. An alternative procedure, more attractive to steam engineers, is to determine the composite efficiency of the collector as a steam "boiler" and then apply this to steam engines of known thermal efficiency***.

* The changes in $ka^{1/4}$ with T_2 will be so small that a family of curves is hardly justified.

** This tube would probably be of pyrex type glass which has an extremely small absorptivity to sunlight.

*** This will be illustrated in a later paper.

The following cases have been considered particularly with the purpose of seeing the effect of the use of selective black surfaces. In all cases, the absorption coefficient α is taken as 0.95; the outside loss coefficient as 6 BTU/hr·ft²·°F and the ambient temperature 70°F (21°C) (a considerable change in these two parameters has only a small effect on the results). In all cases except Examples (5a) and (6a), the glass covers are assumed to be "water white", i.e. with a transmission of 91% for sunlight, but in Examples (5a) and (6a) "window" glass with a transmission of 86—87% has been assumed, since this is approximately the type of glass often used in commercial solar water heaters. Also for these two examples the rear insulation is taken as 2" glass wool instead of 4" as for the other cases*. For the case of the cylindrical parabola Equations (3) and (4), the mirror is assumed to be 10 ft (3 metres) wide and the receiver a tube 6" (15. cm) diam. with a 8" O.D. 7½" I.D. surrounding glass tube. The concentrating power is $10/0.5\pi = 6.37$, which is quite small. The aperture — solar image ratio, assuming that the solar image is only 4" wide to avoid glancing incidence, is 30 : 1. This should be readily achievable in practice, since a perfect cylindrical parabola of 180° total aperture would have a 200 : 1 aperture—image ratio, taking the angular diameter of the sun as 1/100 radian.

In the corrections to Figure 3, the plate-tube efficiency F is taken as 0.97 for the flat plate collectors but for all the examples used in Figure (7b) for steam generation an extra 10°F temperature drop between steam and receiver surface has been allowed. D, the dirt factor, is taken as 0.01. No allowance has been made for heat capacity loss and this must be taken into account after the general performance has been determined.

TABLE III

Example No.	*Type*	*Emissivity (E)*	β	*P*	*Convection loss*
1	Flat plate one glass cover	—0.95	0.91	1	normal
1a	—do.—	—0.95	0.91	1	eliminated
2	—do.—	—0.1	0.91	1	normal
2a	—do.—	—0.1	0.91	1	eliminated
2b	—do.—	—0.05	0.91	1	eliminated
3	Parabola tubular glass cover	—0.95	0.773**	6.37	normal
4	—do.—	—0.10	0.773**	6.37	normal
5	Flat plate two glass covers	—0.95	0.827	1	normal
5a	—do.—	—0.95	0.750	1	normal
6	—do.—	—0.10	0.827	1	normal
6a	—do.—	—0.10	0.750	1	normal

* In examples 1a, 2a, 2b, the "conduction" loss across the convectionless air gaps is taken as 0.06 BTU/hr· ft²·°F. (corresponding to about 4" of stagnant air).

** Reflection coefficient of mirror = 0.85, transmission of glass cover = 0.91.

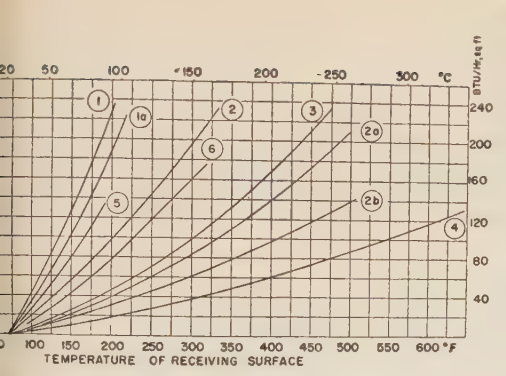

Figure 5

-off intensity Q_x as a function of receiving surface temperature.

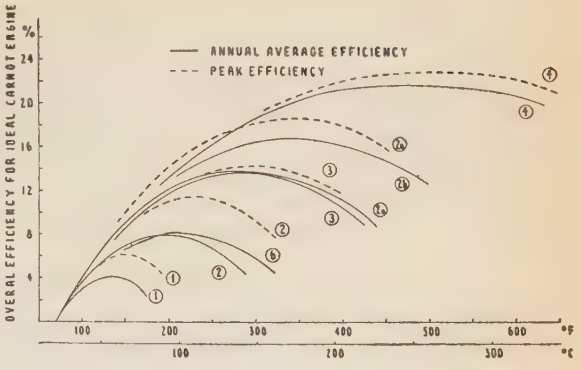

Figure 6

Theoretical overall efficiency of ideal Carnot engines operated by solar energy collectors.

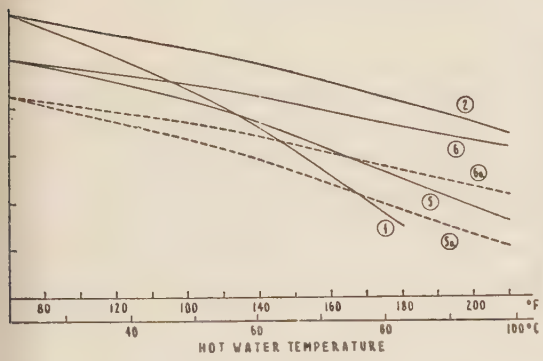

(a)

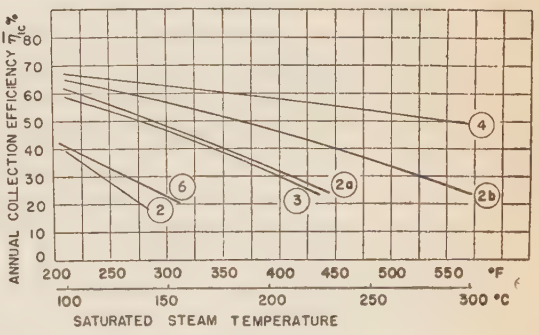

(b)

Figure 7

a) Efficiencies of flat plate collectors used as water heaters.
b) Collection efficiency for solar steam boilers.

The flat plate systems are assumed set at a fixed tilt to the horizontal (approximately equal to the latitude). The parabolic system is assumed to be heliostatically mounted.

The results of the computations are shown in Figures 5, 6, 7a, and 7b. Several points stand out very clearly:

(a) The effect of the selective black is considerable in all cases.

(b) While the use of partial vacuum to eliminate convection loss results in only a slight improvement for a normal black, it is very significant when used with a selective black (compare Example 1 with 1a and 2 with 2a).

(c) As a water heater, a flat plate collector using 1 cover glass and selective black (Example 2) shows at 150°F an annual collection efficiency of 67% as compared with 51% for a collector with normal black and one cover glass (Example 2) or 54% with

two cover glasses (Example 5). For a "commercial" design (glass transmittance 0.86 and 2" of rear insulation) the results become: 61% for the selective black, single glass; 45% for the normal black, single glass; 46% for the normal black with two sheets of glass. These are the results for a region with the exceptionally high mean peak normal solar incidence $\overline{Q_{ipn}}$ of 317 BTU/hr·ft² (1.435 gcal/cm²·min). In a region where $\overline{Q_{ipn}}$ is, say, 288 BTU/hr·ft² (1.30 gcal/cm²·min), the results for the "commercial" design would be: selective black, single glass 59.5%; normal black, single glass, 42.2%; normal black with two sheets of glass 42.5%.

(d) As seen from (c) above and from Figure 7a, the improvement in using a second sheet of glass is very small and will be negative at low collection temperatures. Thus curves (1) and (5) in Figure 7a cross over at about 138°F, while for the commercial design the cross over would be about 10° higher. It is thus seen that from the point of view of annual efficiency the second sheet of glass in commercial solar water heaters is of little value, though it may be shown to help on cloudy days. The use of a second sheet of glass with a selective black is definitely disadvantageous (see curves 2 and 6 in Figure 7a), since the cross-over point is above the boiling point of water. However, as a steam generator the second sheet of glass may be advantageous, as is seen from curves 2 and 6 in Figure 7b.

(e) The production of steam at moderate pressures, which is out of the question for flat plate collectors using normal black surfaces, becomes possible when a selective black is used. Thus curves 2 and 6 in Figure 7b show that low pressure steam can be produced with a collection efficiency of about 30%, while if the convection can be eliminated double this efficiency or much higher pressures are possible. It is of considerable interest to note that a flat plate collector with one glass and selective black $E=0.1$ and no convection will give a slightly better performance than a normal black used with a concentrating system $P = 6.37$. The production of process steam by means of a fixed solar energy collector would thus appear to be feasible. For the cooling of houses in sunny climates by means of an absorption refrigerator requiring a "boiler" temperature of, say, 240°F, such a solar energy collector looks very promising, particularly as the collection efficiency in sunny weather will be higher than the annual efficiency.

(f) In Figure 6, which shows the computed performance of solar energy collectors used to operate theoretical Carnot engines, the difference between the peak performance (Q_i = 300 BTU/hr·ft² *) — dotted line — and the yearly average — full line — is small for Examples 3 and 4 because of the heliostatic mounting: but for flat plate collectors the difference is considerable. (This constitutes a warning against computing overall efficiencies on the basis of peak sunshine!).

(g) Figure 3 shows that a heliostatic mounting gives a considerably better average collection efficiency than a fixed mounting, the improvement depending upon the value of Q_x but being of the order of 10—15% in the usual range of Q_x values. When it is remembered that a heliostatic flat plate will receive some 50% more sunshine than a stationary one, the overall improvement — of the order of 70% total output — may justify the cost of the moving mechanism, though far more ground area is required.

* Plus 10% diffuse radiation for the flat plate collectors.

For non-focusing collectors, the rotating mechanism does not have to be very accurately timed.

(h) From a study of Figure 7b it is possible to determine the performance of a solar energy collector operating a steam engine or turbine. It will be shown that, if fuel fired superheating is permissible, it is possible to reach overall conversion efficiencies of 16% using the parabola of Example 4 together with a large moderate pressure turbine, or about 11% using the flat plate collector of Example 2a.

CONCLUSIONS

A satisfactory selective black of emissivity $E = 0.1$ will provide a flat plate collector of high efficiency for water heating and of moderate efficiency for a low pressure steam generator or an absorption refrigerating unit. If the elimination of convection loss by reduced pressure is practically possible, the flat plate collector may eliminate the need for a focusing system for many applications. The advantage of the non-focusing system is particularly great in cloudy areas: it requires no rotation to follow the sun, though if this were added the yearly collection would be increased about 70%.

REFERENCES

1. Hottel, H. C. and Woertz, B. B., 1942, The performance of flat plate solar heat collectors, *Trans. A.S.M.E.*, **64**, 91—104.
2. Drake, E. J., *Notes on Solar Power and other uses of solar energy*, Ref. (9), p. 97.
3. Tabor, H., 1955, Selective radiation, *Bull. Res. Counc. of Israel*, **5A**, 119—134.
4. Anderson, L. B., Hottel, H. C. and Willier, A., Publication No. 36, Solar Energy Conversion Research Project, M. I. T. report in Ref. (9), p. 47.
5. McAdams, W. H., *Heat Transmission*, McGraw-Hill, 2nd or 3rd Ed.
6. Fishenden, M. and Saunders, O. A., 1950, *An Introduction to Heat Transfer*, Oxford University Press.
7. Brown, A. I. and Marco, S. M., 1951, *Introduction to Heat Transfer*, McGraw-Hill.
8. Hottel, H. C., *Power Generation with Solar Energy*, Publication No. 37, Solar Energy Conversion Research Project, M. I. T., reported in Ref. 9, p. 85.
9. 1955, Solar Energy Research; edited by F. Daniels & J. A. Duffie, University of Wisconsin Press.
10. Ashbel, D., 1942, *Solar Radiation and Soil Temperature* (in Hebrew), Hebrew University Press.

MEASUREMENTS OF FRICTION BETWEEN SINGLE FIBRES BEFORE AND AFTER AN OXIDATIVE TREATMENT

E. Alexander

Department of Physics, The Hebrew University of Jerusalem

M. Lewin and Miriam Shiloh

Institute for Fibres and Forest Products Research, Ministry of Agriculture, Jerusalem

ABSTRACT

In the course of an investigation on the oxidation of wool fibres, it was necessary to determine the influence of such treatments on the surface structure of the fibres. The coefficients of friction of wool fibres and human hair were measured before and after treatment with bromate solutions.

The method of measurement consists in detecting the slide movement of two twisted fibres, which are stretched under different constant loads. This movement, or disturbance of the equilibrium state, happens when the number of twist-turns is decreased to a critical value, where the coefficient of friction can be calculated.

All the friction coefficients increase after the treatment, but no significant change was found in the Directional-Frictional-Effect.

It seems that in order to get better reproducibility of similar measurements it is necessary to take crimp of wool fibres into consideration.

In the course of a general investigation on the oxidation of wool fibres by bromic acid or mixtures of bromate and hydrochloric acid, it was attempted to determine the effect of these treatments on the physical properties of the fibres.

In the following, full results of several series of measurements of the friction between single wool and hair fibres, before and after chemical treatment, including statistical considerations, are reported.

Significant differences of friction coefficients before and after treatments were found. However, difficulties were encountered in assessing the influence of the treatment on the wool fibres which find expression n the *Directional Frictional Effect*, δ, (D.F.E.)[1,2].

Whereas several measurements of the D.F.E. of single wool fibres before and after chemical treatment have been recorded in the literature[3,4,5], not enough data on the statistical significance of these experiments were found.

Measurements were carried out using a modification of the Gralén Method[6], as described by van der Vegt[8] and also by Hood[7]. (See Experimental 1).

By this method, the coefficient of friction is measured by means of changing the number of turns of two twisted fibres (as well as the angle β between the fibres) under constant load (0.5 g) until slip occurs.

Received June 13, 1955.

EXPERIMENTAL

1. *Apparatus and method of measurement*

Both the apparatus and its application are similar to those used by van der Vegt[8].

In this method two fibres are stretched by means of a pulley and weights P_1 each (0.5 g). The fibres are then twisted together and a second load P_2 (0.5 g) applied to one of them. The fibres are fastened on the frame shown in Figure 1. The vertical axis of this frame can be rotated and the number of turns n is read on a counter. The original number of turns is chosen high enough to allow for the application of this additional load without slip. The measurements consist in untwisting the fibres until slip occurs. At this state, the number of turns n is read, and the angle β between the fibres measured.

The static coefficient of friction μ is given by[6,8]:

$$\mu = \ln \frac{(P_1 + P_2)}{P_2} \Big/ \pi n \beta \tag{1}$$

The first and further slips could be detected with accuracy by magnifying the movements of the pulley A (see Figures 3 and 4) by optical projection. The arrangement of the apparatus is shown in Figure 2. A lamp illuminates one of the holes drilled near the circumference of the pulley A. This is magnified by a lens and projected on a white screen, where a dark straight line is drawn, so that the movements of the pulley are easily detected.

Because of crimp, the angle β was measured with a special cross-haired eye-piece graduated for angular measurements and attached to a small microscope ($\times$ 60).

Microscopic inspection of the twisted fibres showed clearly that crimp was far from being eliminated under the loads applied, and that the fibres were not twisted homogeneously (Figure 5), but inhomogeneously (Figure 6).

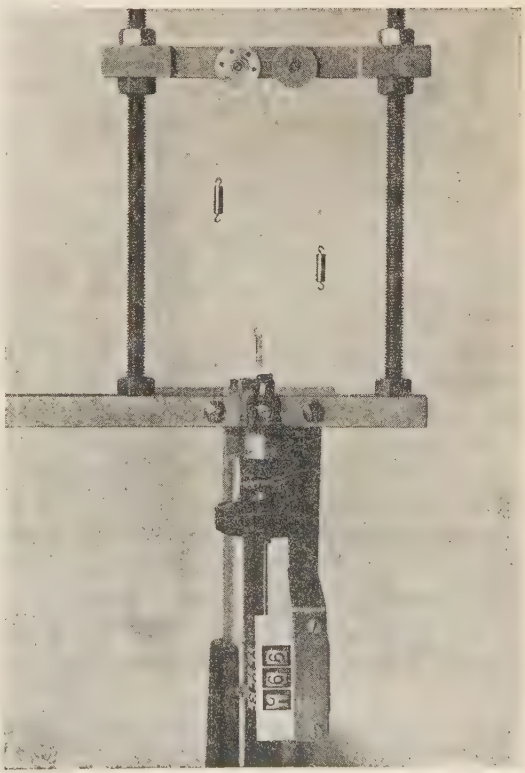

Figure 1

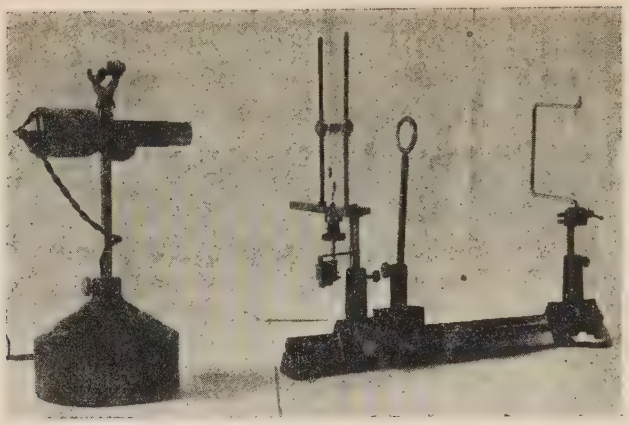

Figure 2

This phenomenon is especially pronounced in wool fibres. It reduces not only the accuracy of the results owing to inhomogeneous normal pressure as explained below, but also the accuracy of the direct measurements of the angle β.

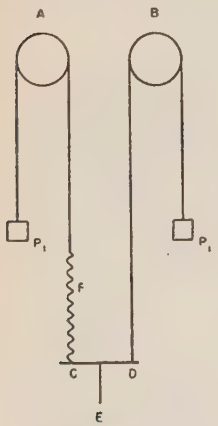

Figure 3

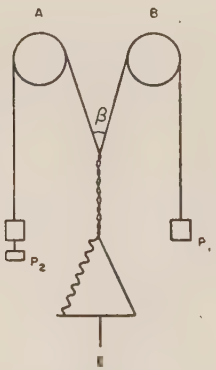

Figure 4

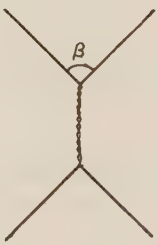

Figure 5

Figure 6

2. *Chemical treatment*

Knitted wool purified by scouring in a solution of soap and ammonia and thoroughly rinsing in distilled water was used in the present experiments. Scottish Black-faced fibres of diameter 10—20 μ and length 10—15 cm and human hair of similar dimensions were purified by the same procedure. After performing measurements of friction, the labelled fibres were sewn to the knitted wool squares and treated with the following solution: 0.0125 M/l $KBrO_3$, 0.097 N HCl, 0.15 N NaCl, and Tergitol 7 wetting agent 0.12 g/l. The temperature was maintained at $25° \pm 1°C$ at a liquor to wool ratio of 26 : 1.

The treatment was interrupted after 135 minutes, when the amount of bromate reduced was equal to 0.0125 M bromate per 100 g dry wool.

In this treatment, as will be shown in subsequent publications, a part of the disulphide linkages is oxidized and wool is rendered non-felting in severe handmilling tests.

The wool fibres and hairs were submitted after air drying to further friction measurements.

All measurements were performed in an air-conditioned room of 65% R.H. and 20°C.

Several hundred friction measurements of wool fibres and human hair were performed before and after the oxidizing chemical treatment. The results of the measurements (each figure being a mean of 20 measurements) are given in Tables I and II.

It can be seen from Tables I and II that:

(1) The friction coefficients increase significantly after chemical treatment in the case of wool fibres as well as in the case of human hair. The with-scale coefficients of the wool fibres were about 30% higher after chemical treatment, and the anti-scale coefficients show about 15% increase. For human hair both coefficients increase by ~50%.

(2) No significant change was found in the D.F.E. after the chemical treatment.

(3) The D.F.E. were generally more pronounced in wool fibres than in human hair.

The accuracy of the measurements can be determined as follows:

a) Differences between friction coefficients of different pairs of fibres reached 50%.

b) Coefficient of variation calculated for each pair of fibres equals 10—15% for the same mounting.

METHODICAL CONSIDERATIONS

The figures obtained show much lower accuracy and reproducibility than those mentioned in ref. 6 and 8.

Unavoidable disturbances produced while attaching and detaching the small weights cannot fully explain this fact.

One of the main reasons for the poor reproducibility would appear to be the presence of crimp in the fibres. Especially at low values of tension, crimp causes the twisted fibres to assume a non-ideal helical shape (see Experimental 1). Inhomogeneous normal pressures are, therefore, formed along the contact region of crimped fibres. It is well known that friction coefficients of fibres are generally dependent on normal pressure. Therefore, local high pressures result in higher apparent average friction coefficients in measurements with the Gralén method. Changes in crimp between different pairs of fibres can be relatively high, resulting in high differences of apparent friction values. The measurements of Hood[7] giving a steep rise in friction coefficients for low tensions can also be understood in the light of these considerations of crimp influence.

Another reason for the scattering of the friction values would seem to be the varying diameters of the fibres, which are not accounted for in the Gralén theory[6,8], which assumes uniform diameters.

Differences in shape and distribution of the scales should also enhance the scattering of the friction measurements of wool and hair.

The various sources of error will have a different bearing on friction measurements of one pair of fibres than on measurements on several pairs of fibres.

TABLE I

Measurements of friction coefficients of human hair

	before chemical treatment							*after chemical treatment*									
	with-scale			*anti-scale*			δ_{21} =	*with-scale*			*anti-scale*			δ_{43} =			
Pair No.	n_1	β_1	μ_1	n_2	β_2	μ_2	$=\mu_2-\mu_1$	n_3	β_3	μ_3	n_4	β_4	μ_4	$=\mu_4-\mu_3$	$\mu_3-\mu_1$	$\mu_4-\mu_2$	$\delta_{21}-\delta_{43}$
A_1A_2	3.28	7.30	0.3085	2.80	8.20	0.3220	0.0135	2.63	7.30	0.3850	2.51	7.04	0.4195	0.0345	0.0765	0.0975	—0.0210
B_1B_2	4.60	9.52	0.1685	3.67	9.10	0.2215	0.0530	3.23	7.80	0.2935	2.62	6.21	0.4546	0.1611	0.1250	0.2331	—0.1081
C_1C_2	4.30	9.73	0.1766	3.65	6.88	0.2938	0.1172	3.21	11.03	0.2085	2.95	7.21	0.3470	0.1385	0.0319	0.0532	—0.0213
D_1D_2	4.61	12.00	0.1333	4.45	10.10	0.1643	0.0310	3.44	7.18	0.2988	3.26	7.25	0.3127	0.0139	0.1655	0.1484	0.0171
E_1E_2	5.25	9.20	0.1535	3.30	10.70	0.2089	0.0554	3.20	6.83	0.3378	2.92	7.19	0.3521	0.0143	0.1843	0.1432	0.0411
F_1F_2	4.90	12.00	0.1255	4.00	12.80	0.1444	0.0189	2.67	6.30	0.4398	2.54	6.32	0.4612	0.0214	0.3143	0.3168	—0.0025
G_1G_2	5.70	9.58	0.1352	3.65	11.20	0.1805	0.0453	3.13	6.59	0.3589	2.60	7.12	0.4000	0.0411	0.2231	0.2195	0.0036
H_1H_2	4.20	16.30	0.1077	3.80	6.50	0.2900	0.1823	3.48	6.18	0.3431	3.06	5.86	0.4120	0.0689	0.2354	0.1220	0.1134
I_1I_2	3.50	7.20	0.2939	3.10	7.80	0.3060	0.0121	3.45	8.04	0.2668	3.01	8.90	0.2763	0.0095	—0.0271	—0.0297	0.0026
J_1J_2	3.63	6.13	0.3320	2.80	7.33	0.3600	0.0280	3.19	7.50	0.3090	2.80	6.65	0.3966	0.0876	—0.0230	0.0366	—0.0596
mean			0.1935			0.2491	0.0556			0.3241			0.3832	0.0591	0.1306	0.1341	—0.0035
error			0.0266			0.0236	0.0171			0.0202			0.0194	0.0171	0.0363	0.0328	0.0185

TABLE II

Measurements of coefficients of friction of wool fibres

(*Degreased "Scottish Blackface", diameter* 10—20 μ, *length* 10—15 *cm*)

	before chemical treatment							*after chemical treatment*									
	with-scale			*anti-scale*			δ_{21} =	*with-scale*			*anti-scale*			δ_{43} =			
Pair No.	n_1	β_1	μ_1	n_2	β_2	μ_2	$=\mu_2-\mu_1$	n_3	β_3	μ_3	n_4	β_4	μ_4	$=\mu_4-\mu_3$	$\mu_3-\mu_1$	$\mu_4-\mu_2$	$\delta_{21}-\delta_{43}$
K_1K_2	5.10	6.30	0.2300	4.40	6.63	0.2540	0.0240	4.36	6.66	0.2540	3.90	6.90	0.2742	0.0202	0.0240	0.0202	0.0038
L_1L_2	3.32	6.00	0.3715	3.17	5.50	0.4230	0.0515	3.40	5.96	0.3648	2.97	5.44	0.4590	0.0942	—0.0067	0.0360	—0.0427
M_1M_2	4.33	7.82	0.2180	2.52	5.56	0.5280	0.3100	3.44	5.86	0.3665	2.70	5.39	0.5080	0.1415	0.1485	—0.0200	0.1685
N_1N_2	4.21	6.80	0.2775	3.00	5.20	0.4740	0.1965	2.88	5.96	0.4300	2.54	4.55	0.6400	0.2100	0.1525	0.1660	—0.0135
O_1O_2	3.60	7.32	0.2805	2.76	6.27	0.4207	0.1402	3.43	6.53	0.3299	2.72	6.32	0.4295	0.0996	0.0494	0.0088	0.0406
P_1P_2	4.10	6.27	0.2865	2.50	5.60	0.5265	0.2400	2.68	5.64	0.4883	2.60	5.20	0.5466	0.0583	0.2018	0.0201	0.1817
Q_1Q_2	4.21	7.96	0.2145	2.82	6.76	0.3870	0.1725	3.96	7.01	0.2660	2.78	6.18	0.4297	0.1637	0.0515	0.0427	0.0088
R_1R_2	4.25	7.8	0.2227	3.24	6.53	0.3485	0.1258	3.37	6.25	0.3500	2.75	5.65	0.4758	0.1258	0.1273	0.1273	±0.0000
S_1S_2	3.83	5.55	0.3479	3.10	5.63	0.4235	0.0756	3.64	5.74	0.3540	2.99	5.40	0.4578	0.1038	0.0061	0.0343	—0.0282
T_1T_2	3.78	7.44	0.2627	2.96	7.58	0.3302	0.0675	3.27	6.18	0.3655	2.97	5.27	0.4716	0.1061	0.1028	0.1414	—0.0386
mean			0.2712			0.4115	0.1404			0.3569			0.4692	0.1123	0.0857	0.0547	0.0281
error			0.0171			0.0274	0.0286			0.0219			0.0294	0.0168	0.0224	0.0209	0.0257

Crimp generally remains constant for different measurements of the same pair of fibres as long as the same region is used in all the measurements. As the diameter of the fibre will generally not change appreciably along the twisted part of one pair of fibres, its contribution to the coefficient of variation may also be neglected. Thus the shape and the distribution of scales on the fibre will be mainly responsible for the scattering of the friction values measured on one pair of fibres, resulting in 10—15% coefficient of variation found.

In measurements on a single pair of fibres not having the surface scale structure, a rather low coefficient of variation should therefore be expected in case of complete elimination of crimp.

In comparing values of friction coefficients obtained on *several* pairs of wool fibres (variation of 50%), the crimp and diameter of the fibres turn out to have a much more pronounced influence. The load necessary to eliminate the crimp completely varies from fibre to fibre, and sometimes it is in the range of the breaking load. It is, therefore, not enough to compare the friction coefficients obtained on several fibres of the same wool, or of wools of different origins. It would be necessary to work under the same *crimp* values; measurements of *Effective Crimp Diameter* as defined in a previous paper[9] would seem to be essential for that purpose. In this way the variation introduced owing to the crimp may be reduced and the sum of the influences of the diameter and scale shape and distribution evaluated. The influence of the diameter could not be separated from the influence of the scales in the case of wool fibres. It could, however, be determined for fibres not having the scale structure.

On the other hand, it would seem desirable to measure the influence of the crimp on the friction coefficient, and not only the influence of the load[6,7,10].

Further studies and measurements are now under way for estimating the correlation between crimp, diameter, and surface structure, and the friction coefficients.

An oxidizing anti-felting treatment would seem to influence both the crimp and the scaled surface structure, but would not influence the diameter of the fibres. It is necessary, therefore, to apply the above considerations when evaluating the changes in friction due to oxidizing treatments.

On the other hand, the changes in crimp itself should also be considered a factor in the modification of the felting properties of wool fibres.

REFERENCES

1. Mercer, E. H. J., 1945, *Council. Sci. Ind. Research*, **18**, 188.
2. Lindberg, J., 1948, *Text. Res. J.*, **18**, 470—4.
3. Frishman, D., Smith, A. L. and Harris, M., 1948, *ibid.*, **18**, 475—80.
4. Lindberg. J. and Gralen, N., 1949, *ibid.*, **19**, 183—201.
5. Lindberg, J., 1953, *ibid.*, **23**, 225—36.
6. Lindberg, J. and Gralen, N., 1948, *ibid.*, **18**, 287—301.
7. Hood, B. G., 1953, *ibid.*, **23**, 495—505.
8. Van der Vegt, A. K., Communication No. 1, Central Laboratories, T.N.O., Delft, Holland.
9. Lewin, M., Shiloh M. and Alexander, E., 1954, *Bull. Res. Counc. of Israel*, **4**, 75—77.
10. Langston, H. H. and Rainey, W. T., Jr., 1954, *Text. Res. J.*, **24**, 643—653.

WEIGHT ESTIMATE OF THE PAPYRUS CULMS GROWING IN THE HULA MARSHES

M. Zohari, G. Orshan

Department of Botany, The Hebrew University of Jerusalem

H. V. Muhsam

Department of Statistics, The Hebrew University of Jerusalem

M. Lewin

Institute for Fibres and Forest Products Research, Ministry of Agriculture, Jerusalem

ABSTRACT

1. The area occupied by papyrus stalks, as shown by aerial photographs, was 13,029 dunams.

2. An estimate was made of the total weight of papyrus stalks in the Hula. For this purpose, the number of stalks was determined, and the weight was taken of individual stalks in 40 plots along peat section No. 19, which runs through the area between the western border of the marsh and the Jordan river.

3. The total weight of green stalks growing in the marshes was estimated to be 98,761 $\pm$ 8,280 tons, and that of dry stalks was estimated at 44,896 tons.

4. The area of clearings in the region of peat section No. 19 does not reach 3 per cent of the total area. In regions of different densities it may, perhaps, reach up to 10 per cent of the total area. Hence it may be necessary to lower the above estimates accordingly.

5. The papyrus reproduces every year. It may be assumed that the weight of the existing green stalks expresses approximately also the annual reproduction; a not negligible number of dry stalks may also be expected to be found already a year after harvesting.

INTRODUCTION

An estimate of the total weight of papyrus stalks growing in the marshes of the Hula area and their rate of regrowth after being cut was made to determine the possibility of using papyrus for industrial purposes. The estimate had to be of a reasonable degree of accuracy, without involving time-consuming or expensive procedures of investigation.

To estimate the weight of papyrus stalks the area on which the papyrus grows had to be measured and then the average weight of the stalks per unit area determined by counting the number of stalks per unit area and estimating the average weight of a stalk.

This harvesting of certain plots for the first survey afforded, a year later, an opportunity of carrying out a number of observations on the annual reproduction of papyrus after harvesting.

Received June 15, 1955.

AREA COVERED BY PAPYRUS

The areas on which the papyrus grows were estimated by means of aerial photographs on which they are easily distinguished. Within these areas, a variety of shades was distinguished on the photographs, probably indicating differences in the density of the stalks.

Accordingly, five zones of different density were marked on the map (see Figure 1 and Table I). The total area covered by papyrus was estimated to be 13,000 dunams (1 d = 1000 m^2).

AVERAGE WEIGHT OF PAPYRUS CULMS PER UNIT AREA

The straightforward method of estimating the average weight of stalks per unit area, by harvesting a number of plots of given size representative of the entire marsh area and weighing the stalks growing on each of them, was found to be unpracticable.

A preliminary test was carried out in March 1953, on a square plot of 100 m^2 situated near peat section No. 19, at a distance of approximately 100 m from the edge of the marsh.

The square was divided into rectangular strips 10 m long and 1 m wide. One of the rectangles was subdivided into ten squares of 1 m^2 each. Table II shows the weight of stalks in each of these squares.

The papyrus was cut at water level and weighed. In this case, as in all the later tests, the weight of the fresh and green stalks was determined separately from that of the dry ones.

The weight of the green papyrus from the square of 100 m^2 was 794 kg, while the weight of the dry papyrus stood at 634 kg. A comparison of these figures with those obtained for the squares of 1 m^2 (see Table II) shows a reasonably good correlation with respect to the fresh papyrus; this, however, is not the case for the dry plants.

The differences in the weight of papyrus harvested from plots of 1 m^2 are very high, and plots of this size are, therefore, obviously too small a sampling unit for the determination of the weight of papyrus per unit area. An area of 10 m^2 would be a much more suitable unit, at least as far as fresh plants are concerned. This method of weighing total yields of unit areas, however, would be far too expensive, mainly because of the difficulty in moving large and heavy scales to considerable distances within the marsh area. It was therefore thought preferable to divide the procedure into two steps, namely, to estimate first the average number of stalks per unit area and then the average weight of a stalk.

Determination of the density of stalks

The density of stalks was determined from mid-June to mid-July 1953 in 41 plots chosen along peat section No. 19, which cuts across the marsh from its western edge to the river Jordan. Out of these, eleven plots were 10 m^2 (5 × 2 m), ten were 15 m^2 (5×3 m), ten 20 m^2 (5×4 m) and ten 25 m^2 (5×5 m). Plots of various sizes were used in

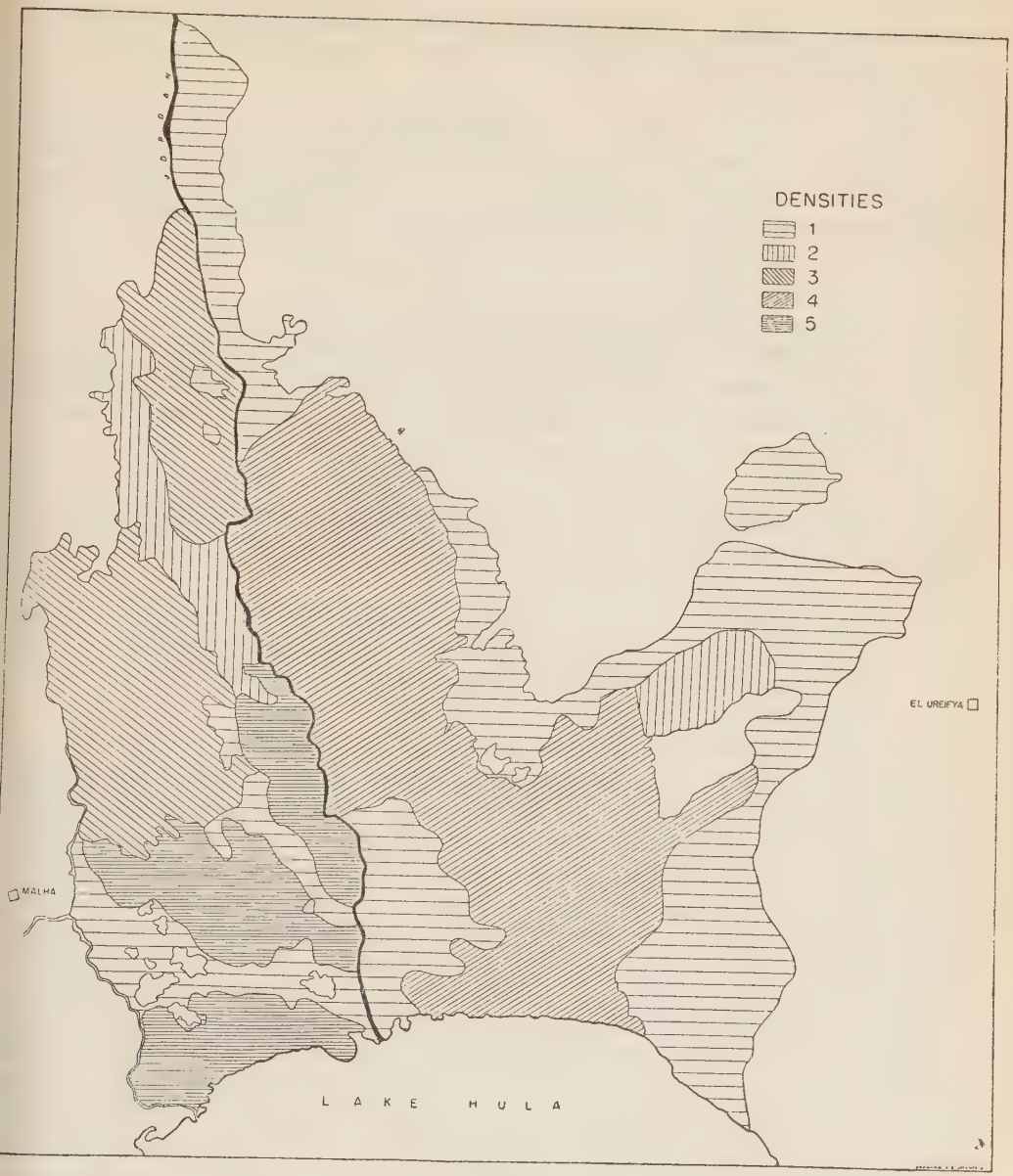

Figure 1

order to determine the most economic plot size for subsequent work, should additional information be required.

The cross section appearing in Figure 2 indicates schematically the position of the various plots along the section and the exact dates of stalk counting. The easiest way of counting the stalks was to cut them first and to count them afterwards. Green and dry stalks were counted separately.

The results of countings in all the plots are shown in Tables III—VI, while Table VII presents the average number of stalks per dunam, estimated on the basis of data from plots of different size.

The variations in the number of dry stalks are much higher than the variations in the number of fresh plants. Taking this fact into account, and also the assumption that, if regularly cut, much fewer dry stalks, if any, would appear at subsequent harvests, the statistical analysis of the results was carried out for the green stalks only.

The average number of green stalks per dunam was found to be 16,826, and of dry stalks 33,775.

A slight increase in the density of green stalks (by 1 stalk per 10 m^2 from one plot to the next one) with increasing distance from the Jordan was noted, but, as the standard error of this increase equals 1.25, it cannot be considered statistically significant.

It was also shown that in the examined area there were no spots or zones comprising 2—4 plots in which the density of stalks was higher or lower than in others.

The latter observation does not tally with the information gleaned from the aerial photographs. Although peat section No. 19 runs through areas of two different shades and touches an area of a third shade, the counts do not indicate zones of different densities of stalks.

The different shades on the photographs, therefore, most probably indicate other fluctuations in the overall density of stalks, such as for instance differences in the number or size of clearings. Such clearings, from about 2—3 m^2 up to 100 m^2 or even 200 m^2, are found, in fact, all over the area.

In selecting the plots for counting stalks, such clearings were intentionally avoided.

On the other hand, it can be inferred from the most cursory inspection of the area that the importance of these clearings cannot be very great. It was, therefore, thought sufficient for the present purpose to estimate very roughly the total area of these clearings on the basis of the fact that only 5 such clearings are encountered by section 19, which is a straight path 5 m wide and 2 km long. If each clearing were a circle of a diameter of exactly d metres, the probability (p) of any clearing being hit by the path would be the proportion of the area of the path broadened by d metres to the total area of the marsh or $p = 2\ (5 + d)\ /\ 13{,}000$. If there are N such clearings in the area, the expected number (n) of clearings encountered by the path will be $n = Np$. The only observed value of n was, as already mentioned, 5. Thus, if a suitable assumption has been made regarding the diameter (d) of the clearings, the total number (N) of these clearings can be estimated. An upper confidence limit for N can be obtained by using the normal approximation, i.e. by assuming $(n - Np)\ /\ \sqrt{Np\ (1-p)}$ to be normally distributed with zero mean and unit standard deviation. At the 95% level, using a one-sided confidence limit, this limit (N^*) is a root of the equation

$$(n - N^*p)\ /\ \sqrt{N^*p\ (1-p)} = 1.64, \text{ namely}$$

$$N^* = (1.64^2 + 2n)\ /\ 2 + \sqrt{(1.64^2 + 2n)^2\ /\ 4 - n^2)}\ /\ p,$$

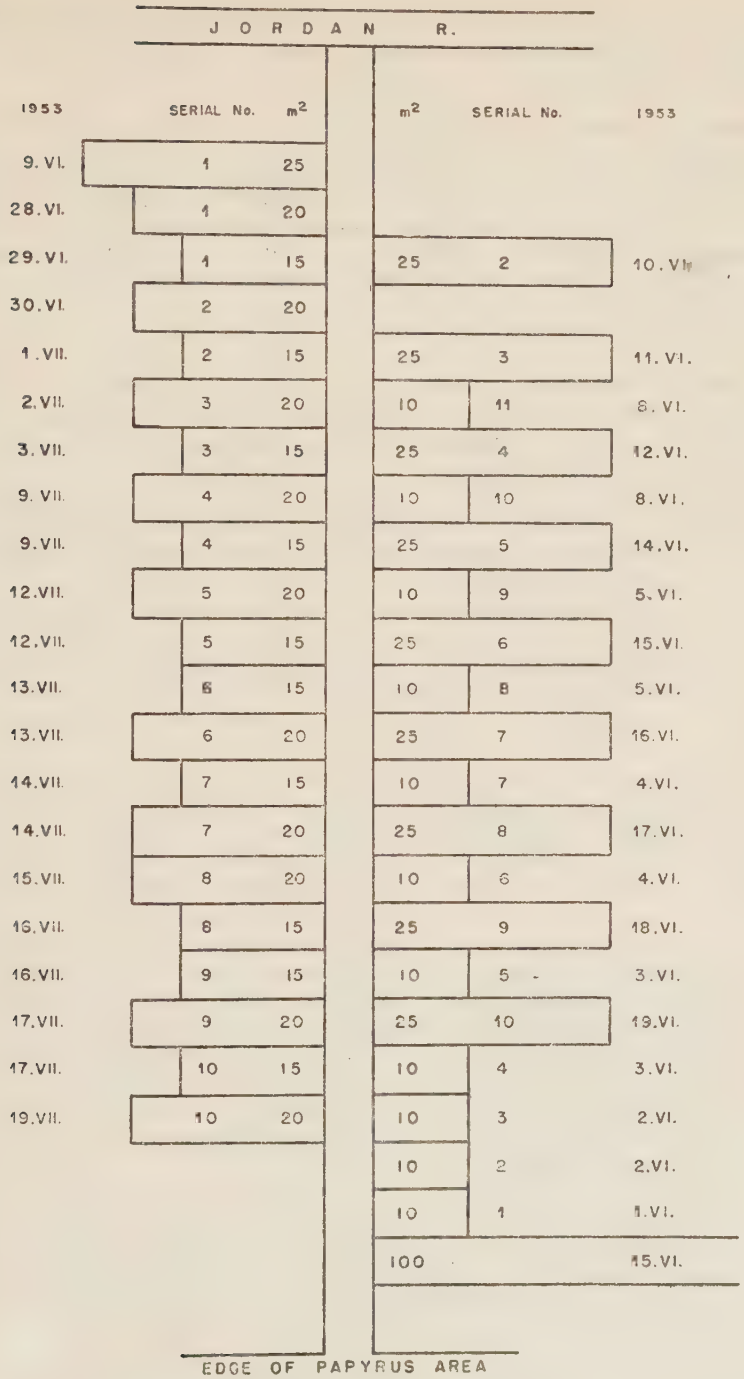
J O R D A N R.
1953
SERIAL No.
m²
m²
SERIAL No.
1953
9. VI. 1 25
28. VI. 1 20
29. VI. 1 15 25 2 10. VI.
30. VI. 2 20
1. VII. 2 15 25 3 11. VI.
2. VII. 3 20 10 11 8. VI.
3. VII. 3 15 25 4 12. VI.
9. VII. 4 20 10 10 8. VI.
9. VII. 4 15 25 5 14. VI.
12. VII. 5 20 10 9 5. VI.
12. VII. 5 15 25 6 15. VI.
13. VII. 6 15 10 8 5. VI.
13. VII. 6 20 25 7 16. VI.
14. VII. 7 15 10 7 4. VI.
14. VII. 7 20 25 8 17. VI.
15. VII. 8 20 10 6 4. VI.
16. VII. 8 15 25 9 18. VI.
16. VII. 9 15 10 5 3. VI.
17. VII. 9 20 25 10 19. VI.
17. VII. 10 15 10 4 3. VI.
19. VII. 10 20 10 3 2. VI.
10 2 2. VI.
10 1 1. VI.
100 15. VI.
EDGE OF PAPYRUS AREA

Figure 2

where $(1-p)$ has been put equal to 1. The estimated numbers of clearings and their total areas as obtained by assuming various values of the average diameter (d) of a clearing are as follows:

Assumed value of d	4	5	7	10
Estimate of N	3610	3250	2710	2170
Upper confidence limit of N	7350	6630	5530	4430
Total area of clearings (dunams) accepting:				
Estimate of N	45	64	104	170
Upper confidence limit of N	92	130	213	348

It might be mentioned that, with the Poisson approximation, the upper confidence limit of N becomes somewhat smaller.

Thus, the available information, though in fact poor, does not give place to any suspicion that the total area of these clearings might reach even as little as 3 per cent of the total area occupied by papyrus.

Disregarding clearings, the number of fresh papyrus stalks in the marsh would be 16,826 stalks per dunam x 13,000 dunam = 219 million, and the percentage standard error of this estimate is 5.9%. The number of dry stalks should come to 436 million.

Determination of the average weight of stalks

In 40 out of the 41 plots in which the number of papyrus stalks had been determined, 5 fresh and 5 dry stalks were weighed immediately after cutting. The results are presented in Tables VIII—XI. Moreover, 9 groups of 30 fresh stalks each, cut next to the plot of 100 m² of peat section No. 19, were also weighed. Results are given in Table XII.

Here, again, results were analysed in detail only as regards the fresh papyrus stalks. The data from the weighings from 40 plots were homogeneous, whereas results of weighings of groups of 30 stalks differed from them. The average weight of the 200 fresh stalks, cut in 40 different plots, was found to be 558.4 g, the estimated standard deviation being 232 g. The average weight of the stalk in 9 groups of 30 stalks each was 393 g, with estimated standard deviation of 303 g. There is, therefore, a difference of 165 g, and, since the standard error of this difference is 26 g, such a difference would appear to be significant.

This difference may simply have been caused by the growth of stalks in the course of time, i.e. from May to June—July. Another possible explanation may be the worker's bias in picking individual stalks for weighing; he might in fact have chosen, from time to time, intentionally or unintentionally, a particularly "beautiful" stalk for weighing, thus raising the average.

The average weight of all stalks examined comes to 456.4 g. The standard error of this mean weight, estimated on the basis of 200 weighings of separate stalks, is 18.4 g or 2.6%. It should be noted that the weight of stalks rose from plot to plot on the

average by 4.92 g as we moved away from the Jordan. Since the standard error of this value is 3, this increase is not significant from the statistical point of view.

The analysis shows that there were no zones or large spots containing 2—4 neighbouring plots in which the average weight of a stalk differed from that in other zones; just as no such difference existed with regard to the density of the stalks.

The curve of distribution of stalks by weight had two maxima, one around 400 g, the other around 800 g, while stalks of a weight of 500—600 g were relatively rare. There is no evidence to decide whether this is the natural composition of the stalk population or whether it is typical only for the season at which the investigation was carried out, or again whether it is rather a result of the above mentioned suspected bias of the worker who picked stalks for weighing. Be that as it may, this circumstance made a proper estimation of sampling errors difficult.

THE TOTAL WEIGHT OF PAPYRUS STALKS GROWING IN THE HULA MARSHES

In the previous paragraph, data were presented for the number of papyrus stalks per unit area and in the whole marsh area, and for the average weight of each papyrus stalk. These data permit to estimate the total weight of papyrus growing in the Hula.

As shown above, the number of fresh stalks in the Hula reaches 219 million, and the number of dry stalks 436 million. The average weight of the fresh stalk is 456 g and of the dry stalk 103 g.

Accordingly, the total weight of the stalks throughout the Hula marshes amounts to 98,761 tons of fresh stalks, and 44,896 tons of dry stalks. The estimate of the standard error for the total weight of fresh stalks is 8,280 tons or 8.4% of the total weight.

REPRODUCTION

One year after the first survey, in the summer of 1954, stalks were counted and weighed in three of the plots harvested in 1953. The other plots had been affected by a fire, so that they could not be used for this purpose.

The results are listed in detail in Table XIII.

The plots where papyrus stalks were counted both in 1953 and in 1954 showed at the first harvest an average density approximately identical with the average density for the region as a whole. However, the stalks growing there had been considerably heavier than the average (see Table XIV). This last difference resulted from the presence of a number of stalks of a heavier type (between 700 and 800 g) in these plots; stalks of this type did not occur at all in the second test. It is quite probable that, so short a time after a harvest, no such heavy stalks would have grown. It should, however, be considered possible that the number of stalks was too small to warrant the inclusion of any of the relatively rare heavier stalks.

The density of 23,270 green stalks per dunam at the time of the second harvest is surprisingly high; it is higher than both the average density in the selfsame plots during the first harvest and the average density of the whole area. Only in two plots out of 41 examined during the first investigation, the density was greater than the *average* density of the three plots examined in 1954, — hence there can be no doubt that the difference is statistically significant.

Even more surprising is the figure of 17,300 dry stalks per dunam. True, this number is considerably smaller than the number of dry stalks counted at the first harvest: then the number of dry stalks was about twice as great as that of green stalks, whereas the corresponding ratio at the second harvest was only 1: 0.35.

The number of observations carried out in this second investigation was too small to enable us to make an estimate of sampling errors of the weight of the stalks and their density. If, however, the figures obtained are accepted at their face value, the weight of the green stalks likely to grow within a year after each harvest is estimated to reach 117,000 tons, and the weight of the dry stalks for the same period 23,000 tons.

DISCUSSION

The questions which are still left to be answered in connection with these estimates of the existing papyrus and its expected reproduction are as follows:

a) In how far is peat section No. 19 representative of the whole marsh area?

b) Has the working method, employed in estimating the total weight of papyrus defects which were not taken into account?

In order to check if the area near peat section No. 19 is representative of the total area, a parallel test should be carried out near another section, and results regarding the density of stalks, the weight of stalks and the size and frequency of clearings should be compared. In choosing the second peat section, the density areas indicated on the map might be taken into account.

It has, however, already been pointed out that neither the density nor the weight of stalks harvested from different plots showed statistically significant fluctuations. Thus, no results which would completely reverse the present conclusions can be expected from the examination of the area near another section. The problem of differences in shade within the papyrus area noticed on the aerial photographs, and the assumedly connected problem of the frequency and the size of clearings, need further investigation. But here, again, no surprising results can be feared, if it is assumed that disregarding the clearings may have caused an error in the estimated number or total weight of stalks up to, say, 10 per cent.

Regarding the second question, a suspected bias of the worker in selecting stalks for weighing, and the smallness of the sample used in estimating the density of stalks a year after a first harvest, certainly impair the reliability of some of our conclusions.

TABLE I

Papyrus areas in the Hula

Degree of density	Area (dunams)
1	1,553
2	4,058
3	2,072
4	0,817
5	4,529
Total	13,029

(1 is the highest degree of density, 5 the lowest)

TABLE II

Weight of papyrus stalks in a rectangular plot of 10 m^2, divided into 10 plots of 1 m^2 each

No. of plot	Weight of fresh stalks (kg)	Weight of dry stalks (kg)
1	0.375	10.000
2	2.000	0.675
3	1.000	0.450
4	13.750	1.000
5	12.000	2.500
6	9.500	3.000
7	5.750	0.325
8	1.000	0.500
9	12.000	4.500
10	10.750	4.250
Total	68.125	27.200

TABLE III

Number of fresh and dry stalks from plots of 15 m^2 (5 × 3 m) in peat section No. 19

No. of plot	Number of fresh stalks	Number of dry stalks
B/1	203	550
2	270	490
3	170	470
4	322	600
5	250	320
6	290	500
7	315	620
8	230	395
9	380	520
10	175	300

TABLE IV

Number of fresh and dry stalks in 11 plots of 10 m^2 (2 x 5 m) in peat section No. 19

No. of plot	Number of fresh stalks	Number of dry stalks
A/1	213	590
2	120	368
3	153	478
4	174	494
5	160	380
6	136	345
7	152	397
8	170	500
9	180	285
10	204	620
11	189	355

TABLE V

Number of fresh and dry stalks in 10 plots of 20 m^2 (4 x 5 m) in peat section No. 19

No. of plot	Number of fresh stalks	Number of dry stalks
C/1	250	510
2	211	226
3	210	500
4	350	520
5	340	760
6	400	800
7	370	635
8	390	500
9	380	520
10	330	680

TABLE VI

Number of fresh and dry stalks in 10 plots of 25 m^2 (5 × 5m) in peat section No. 19

No. of plot	Number of fresh stalks	Number of dry stalks
D/ 1	235	515
2	390	970
3	397	540
4	552	910
5	350	738
6	393	560
7	378	810
8	452	890
9	722	1230
10	370	670
Average	423.9	783.3

TABLE VII

Estimate of the average number of stalks on a 1 dunam area for plots of different size

Area of plot (m^2)	fresh stalks	dry stalks
10	16827	43745
15	17367	31767
20	16155	28255
25	16956	31332

TABLE VIII

Weight of separate papyrus stalks in plots of 10 m^2 (5 × 2 *m*) *in peat section No.* 19

1		2		3		4		5		6		7		8		9		10	
(*a*)	(*b*)	(*a*)	(*b*)	(*a*)	(*b*)	(*a*)	(*b*)	(*a*)	(*b*)	(*a*)	(*b*)	(*a*)	(*b*)	(*a*)	(*b*)	(*a*)	(*b*)	(*a*)	(*b*)
235	125	675	155	500	80	760	120	550	100	400	100	815	90	950	90	400	125	700	100
375	65	500	110	320	60	280	165	460	95	380	110	510	110	290	60	740	110	720	65
950	100	775	170	420	110	510	90	425	60	500	80	730	140	880	115	765	110	280	80
550	110	450	100	670	140	480	170	500	150	580	85	480	65	990	100	390	65	390	55
780	95	620	125	460	125	380	150	290	145	480	170	360	145	360	185	300	100	300	95

(*a*) Fresh stalks, (*b*) dry stalks.

TABLE IX

Weight of separate papyrus stalks in plots of 15 m^2 (3 × 5 *m*) *in peat section No.* 19

1		2		3		4		5		6		7		8		9		10	
(*a*)	(*b*)	(*a*)	(*b*)	(*a*)	(*b*)	(*a*)	(*b*)	(*a*)	(*b*)	(*a*)	(*b*)	(*a*)	(*b*)	(*a*)	(*b*)	(*a*)	(*b*)	(*a*)	(*b*)
290	110	390	80	210	100	550	170	700	75	250	155	480	120	725	110	675	150	950	165
655	165	300	110	190	90	800	80	650	140	180	120	450	100	650	100	825	90	925	90
600	90	395	145	670	145	500	140	800	110	200	65	200	90	550	170	800	75	875	65
330	100	765	100	640	110	170	100	880	110	400	140	650	75	750	165	825	100	175	110
870	55	600	85	300	65	320	65	580	125	450	80	700	170	780	140	970	140	200	120

(*a*) Fresh stalks, (*b*) dry stalks.

TABLE X

Weight of separate papyrus stalks in plots of 20 m^2 (4 × 5 *m*) *in peat section No.* 19

1		2		3		4		5		6		7		8		9		10	
(*a*)	(*b*)	(*a*)	(*b*)	(*a*)	(*b*)	(*a*)	(*b*)	(*a*)	(*b*)	(*a*)	(*b*)	(*a*)	(*b*)	(*a*)	(*b*)	(*a*)	(*a*)	(*a*)	(*b*)
990	100	760	140	480	90	780	110	550	155	550	120	450	120	475	65	325	100	475	170
760	130	760	90	600	55	500	165	500	115	550	110	560	90	225	155	350	140	775	90
390	90	290	100	710	165	350	75	450	170	780	70	620	110	925	170	775	110	450	100
450	55	500	60	390	120	300	100	480	100	250	90	280	80	375	100	450	120	750	80
340	110	600	85	810	50	650	110	550	85	400	150	490	165	950	85	850	150	970	165

(*a*) Fresh stalks, (*b*) dry stalks.

TABLE XI

Weight of separate papyrus stalks in plots of 25 m^2 (5 × 5 *m*) *in peat section No.* 19

1		2		3		4		5		6		7		8		9		10	
(*a*)	(*b*)	(*a*)	(*b*)	(*a*)	(*b*)	(*a*)	(*b*)	(*a*)	(*b*)	(*a*)	(*b*)	(*a*)	(*b*)	(*a*)	(*b*)	(*a*)	(*b*)	(*a*)	(*b*)
790	100	610	160	400	40	480	40	800	140	640	40	240	65	710	150	615	50	370	125
700	145	610	110	360	40	500	130	390	40	400	80	255	90	560	110	775	165	300	80
290	90	490	90	300	40	500	120	290	100	340	125	310	55	500	90	440	100	355	75
480	90	390	95	690	110	510	60	940	125	270	80	790	100	500	40	400	125	870	130
400	60	600	60	990	145	290	95	550	50	950	75	700	125	870	70	460	80	490	45

(*a*) Fresh stalks, (*b*) dry stalks.

TABLE XII

Weight of fresh papyrus in bundles

No. of bundle	No. of stalks	kg
1	30	9.800
2	30	9.750
3	30	13.500
4	30	12.500
5	30	10.000
6	30	11.000
7	30	13.300
8	30	14.400
9	30	11.900

TABLE XIII

No. of stalks and their weight during the second investigation

Serial No.		Plot		
			A/1	A/2
Size		10 × 10 *m*	5 × 2 *m*	5 × 2 *m*
No. of green stalks		2291	213	256
No. of dry stalks		1815	146	192
Weight of green stalks (g)	1	350	380	480
	2	300	350	350
	3	360	310	310
	4	420	300	290
	5	580	510	510
Weight of dry stalks (g)	1	50	150	160
	2	75	100	90
	3	100	125	110
	4	80	120	100
	5	100	80	80

TABLE XIV

Comparison between first and second harvest in 3 plots

Serial No.		Plot			Average in plots investigated in 1954	General average
			A/1	A/2		
Date of first investigation		March 1953	1.6.1953	2.6.1953		
No. of green stalks per m²	1953	—	21.3	12.0	16.7	16.8
	1954	22.91	21.3	25.6	23.27	—
No. of dry stalks per m²	1953	—	59.0	36.8	47.9	33.5
	1954	18.15	14.6	19.2	17.3	—
Average weight of green stalks (g)	1953	393	578	604	523.0	456.41
	1954	402	370	388	386.7	—
Average weight of dry stalks (g)	1953	—	89	132	110.5	103
	1954	81	115	108	101.3	—

THE MODULI OF AN ELASTIC SOLID REINFORCED BY RIGID PARTICLES

Z. HASHIN

Div. of Mechanics, Technion — Israel Institute of Technology, Haifa

INTRODUCTION

It is common practice to improve the mechanical properties of elastic solid materials by reinforcing them through the introduction of particles of greater rigidity. Thus mortar is prepared by adding sand particles to a cement binder, rubber is reinforced by fillers consisting of small dustlike particles which may be assumed to be infinitely rigid in comparison with rubber. In the following we shall call the cement or rubber, etc., the *medium*, the particles the *filler*, and the material produced by the dispersion of the filler in the medium the *system*.

Let the medium be of known elasticity, i.e. let the bulk modulus $\varkappa$ and the shear modulus G be known, and therefore also the Young-modulus E and the Poisson ratio ν throughout the formulae

$$E = \frac{9\varkappa G}{3\varkappa + G} \tag{0.1}$$

$$\nu = \frac{3\varkappa - G}{2(3\varkappa + G)}$$

and the volume concentration c_v of the filler, be known. What then are the elastic moduli of the system (denoted by an asterisk, e.g. $\varkappa^*$)? This problem can be approached either experimentally or theoretically. The present paper is a first attempt at a theoretical solution. In order to overcome the mathematical difficulties the following simplifying assumptions have been made:

a) the medium is an ideal elastic, isotropic and homogeneous material,

b) the filler consists of spherical and perfectly rigid particles,

c) there is perfect adhesion between the filler and the medium,

d) the volume concentration of the filler is so small that interaction effects between its particles may be neglected.

A problem similar to the one under consideration was the subject of a paper by Einstein[1,2] in which the viscosity η of a solution is related to the viscosity of the medium η^* and the volume concentration of the solute. Einstein's formula for a dilute solution in which the particles are also assumed to be rigid spheres is

$$\eta^* = \eta(1 + 2.5\, c_v). \tag{0.2}$$

It was found experimentally that the formula is valid for concentrations up to 3%.

Received August 18, 1955.

Our present problem is one degree more complicated through the fact that we have to deal with two material constants ($\varkappa$ and G or E and ν), while in the above case the shear viscosity η only was taken into consideration. By the well known analogy between the behaviour of an incompressible elastic medium and a viscous fluid in steady slow motion (i.e. when non-linear terms in the Navier-Stokes equation may be neglected) our equations must yield Einstein's viscosity equation when $\nu = \frac{1}{2}$ and G is replaced by η. This will provide a check on our calculations.

There is no serious drawback in assuming a spherical shape of the particles, as it will be shown that the stress distribution in their immediate vicinity is not of interest in this problem. It may well be assumed that at some distance from a particle, the shape of which does not seriously depart from that of a sphere, the stress distribution will not be altered much by introducing an equivalent spherical particle. (*)

Assumption (*d*) is much more restrictive, as it will not permit application of results to volume concentrations higher than 2—3 percent.

Results found should accordingly be regarded as defining a limit case of more general formulae which do not imply small concentrations and neglect interaction. As far as known to the author, such formulae have not been derived up to now theoretically.

In Section I, the effect of one rigid spherical inclusion in an infinite medium is determined. This problem has already been solved for the case of uniform tension by a different method by J. N. Goodier[3], using spherical coordinates. The development in Section I is based on a general method by Lord Kelvin[4], an account of which is given by Love[5] (Chap. XI).

The determination of the elastic constants in Section II is based on Einstein's method. It was not, however, assumed that the particles are of equal size. A dimensional argument that the particle size is immaterial may be found in Reiner[6] (p. 60).

I. ONE RIGID SPHERICAL INCLUSION IN AN INFINITE ELASTIC MEDIUM

In the following an infinite elastic medium is considered, subjected to a state of stress which is homogeneous at infinity. In this medium a rigid spherical inclusion is placed, and the disturbance of the state of stress brought about by the inclusion is calculated. Let the principal axes of stress be the directions of a Cartesian system of coordinates x_i with origin at the centre of the inclusion (Figure 1). Then the problem in terms of the elastic displacements u_i is reduced to solving the following equations:

$$(\lambda + G)\frac{\partial \Delta}{\partial x_i} + G\nabla^2 u_i = 0, \tag{1.1}$$

where λ and G are two moduli of elasticity, and

$$\Delta = \frac{\partial u_\alpha}{\partial x_\alpha}. \tag{1.2}$$

(*) It should be noted that this assumption cannot be made with respect to Einstein's problem because of the rotation of the particles, which, when these are not spheres, introduces an additional complication. In the deformation of an elastic solid the rotation will not materially affect conditions.

Subject to the boundary conditions

$$r \to \infty,\ u_i = \varepsilon_{(0)i\ i} = {}_{(0)i} \qquad (1.3)$$

$$r = a,\ u_i = 0$$

where $r^2 = x_\alpha x_\alpha$. (*)

For convenience, the displacements u_i will be split according to

$$u_i = u_{(0)i} + u'_i \ , \qquad (1.4)$$

where $u_{(0)i} = \varepsilon_{(0)i} x_i$ throughout the medium and

$$u_i = -u_{(0)i} = \varepsilon_{(0)i}\ x_i \text{ for } r = a \qquad (1.5)$$

$$u'_i = 0 \qquad \text{for } r = \infty .$$

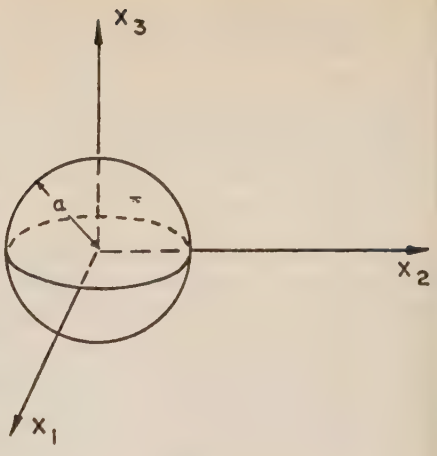

Figure 1

Owing to the linearity of the equations (1.1), (1.2), superposition of u'_i and $u_{(0)i}$ will give the desired solution satisfying boundary conditions (1.3).

The problem of solving equations (1.1), (1.2) within a spherical region when the u_i assume given values on the boundary has been solved by Lord Kelvin (compare Love, l.c.[5]), the solution being

$$u_i = \Sigma \left(\frac{r}{a}\right)^n Y_{n_i} + \Sigma M_n (a^2 - r^2) \frac{\partial \psi_{n-1}}{\partial x_i} \qquad (1.6)$$

where the Y_n denote spherical surface harmonics of degree n, and

$$M_n = \frac{1}{2} \frac{\lambda + G}{(n-1)\lambda + (3n-2)G} \qquad (1.7)$$

$$\psi_{n-1} = \frac{\partial}{\partial x_\alpha} \left\{ \left(\frac{r}{a}\right)^n Y_{n_\alpha} \right\} \qquad (1.8)$$

The functions Y_n are obtained by expension of the values of the u_i for $r = a$ in a series of spherical surface harmonics

$$u_{i_{(r=a)}} = Y_{n_i} \ . \qquad (1.9)$$

The solution may be inverted to satisfy equations (1.1), (1.2) in an infinite region outside a sphere by substitution of $-n-1$ for n in Eq. (1.6), (1.8), except for Y_n(**). Thus a solution will be obtained in which the u_i vanish at $r \to \infty$ due to the negative degree of the spherical solid harmonics involved, and assume given values on the surface of a sphere, the centre of which is the origin of the coordinate system.

(*) A Greek index appearing twice in the same expression denotes summation with respect to 1,2,3.

(**) This follows from the theory of spherical harmonics. $V_n = r^n Y_n$, being a spherical solid harmonic of positive integral degree, $V_{,n-1} = Y_n / (r^{n+1})$ will be a spherical solid harmonic of negative integral degree, compare MacRobert[7].

The general solution is accordingly

$$u'_i = \sum \left(\frac{a}{r}\right)^{n+1} Y_{n_i} + \sum M_{-n-1} \, (a^2 - r^2) \frac{\partial \psi_{-n-2}}{\partial x_i} \tag{1.10}$$

$$M_{-n-1} = -\frac{1}{2} \frac{\lambda + G}{(n+2)\lambda + (3n+5)G} \tag{1.11}$$

$$\psi_{-n-2} = \frac{\partial}{\partial x_\alpha} \left\{ \left(\frac{a}{r}\right)^{n+1} Y_{n_\alpha} \right\} \tag{1.12}$$

A solution satisfying the boundary conditions (1.5) may now be constructed with the aid of (1.10) — (1.12) as follows: —

Eq. (1.5) may be written

$$u'_i = -\varepsilon_{(0)i} r \frac{x_i}{r} = -\varepsilon_{(0)i} a \frac{x_i}{r} \qquad (r = a).$$

As the x_i are solid harmonics of the first degree, x_i/r will be surface harmonics associated with them. Accordingly Eq. (1.9) now reads

$$u'_{i\,(r=a)} = -\varepsilon_{(0)i} a \frac{x_i}{r} = Y_{1i} \tag{1.13}$$

$$\psi_{-n-2} = \psi_{-3} = \frac{\partial}{\partial x_\alpha} \left\{ -\left(\frac{a}{r}\right)^3 \varepsilon_{(0)\alpha} x_\alpha \right\}$$

$$\psi_{-3} = \frac{3a^3}{r^5}(\varepsilon_{(0)\alpha} x_\alpha^2) - \frac{a^3}{r^3} \Delta_{(0)} \tag{1.14}$$

$$\Delta_{(0)} = \varepsilon_{(0)1} + \varepsilon_{(0)2} + \varepsilon_{(0)3} \, .$$

Introducing ψ_- into Eq. (1.10), we get

$$u'_i = -\frac{a^3}{r^3} \varepsilon_{(0)i} x_i - \frac{1}{4(4-5\nu)} (a^2 - r^2) \left\{ \frac{15a^3 x_i}{r^7} (\varepsilon_{(0)\alpha} x_\alpha^2) + \frac{6\varepsilon_{(0)i} a^3 x_i}{r^5} + 3a^3 \frac{\Delta_{(0)} x_i}{r^5} \right\}$$

and finally, in accordance with (1.4),

$$u_i = \varepsilon_{(0)i} x_i - \varepsilon_{0)i} \frac{a^3}{r^3} x_i - \frac{1}{4(4-5\nu)} (a^2 - r^2) \left\{ -\frac{15a^3 x}{r^7} (\varepsilon_{(0)\alpha} x_\alpha^2) + \right.$$

$$\left. + \frac{6\varepsilon_{(0)i} a^3 x_i}{r^5} + \frac{3a^3 x_i}{r^5} \Delta_{(0)} \right\} \tag{1.15}$$

$$\Delta = \frac{\partial u_\alpha}{\partial x_\alpha} = \Delta_{(0)} \left(1 - \frac{a^3}{r^3}\right) + \frac{3a^3}{r^5} (\varepsilon_{(0)\alpha} x_\alpha^2) + \frac{1}{4(4-5\nu)} \frac{3a^3}{r^5} \cdot$$

$$\cdot \left\{ \Delta_{(0)} - \frac{3}{r^2} (\varepsilon_{(0)\alpha} x_\alpha^2) \right\} \cdot \tag{1.16}$$

II. CALCULATION OF THE ELASTIC CONSTANTS OF THE SYSTEM

We shall now investigate the effect of the presence of a large number of small rigid spheres which are dispersed at random in the elastic medium. In view of the rigidity of the dispersed spheres, which can be considered as a degeneration of elasticity, it

may be assumed that the system will also be elastic. Secondly, in view of the random distribution of the spheres, it may be assumed that the system is isotropic, with directions of the principal axes of stress and strain under the action of some stress system identical with those which would arise if the filler were absent. We shall now proceed with the determination of the bulk modulus $\varkappa^*$, the modulus of shear G^*, Poisson's ratio ν^*, and Youngs 'modulus E^* of the system.

II.1. *The bulk modulus* $\varkappa^*$

We consider the case of uniform isotropic tension. This may be described kinematically by the strains:

$$\varepsilon_{(0)i} = \varepsilon_{(0)} = \text{const.} \tag{2.1}$$

The displacements (1.15) now become

$$u_i = \varepsilon_{(0)} x_i \left(1 - \frac{a^3}{r^3}\right) \tag{2.2}$$

and the dilatation (1.16)

$$\Delta = \Delta_{(0)} = 3\varepsilon_{(0)} . \tag{2.3}$$

Bearing in mind that x_i are the components of the vector $\mathbf{r}$, the radial displacement u_r is

$$u_r = \varepsilon_{(0)} r \left(1 - \frac{a^3}{r^3}\right). \tag{2.4}$$

Furthermore,

$$u_\theta = u_\varphi = 0 \qquad \text{by symmetry.} \tag{2.5}$$

This could also have been derived directly from integration of the equations of equilibrium for the case of radial symmetry — compare Love[5] (p. 142). The radial stress is

$$p_{rr} = (\lambda + 2G) \frac{du_r}{dr} + 2\lambda \frac{u_r}{r}, \tag{2.6}$$

which becomes, using (2.4),

$$p_{rr} = \varepsilon_{(0)} \left(3\varkappa + 4G \frac{a^3}{r^3}\right), \tag{2.7}$$

where we have used the relation

$$3\lambda + 2G = 3\varkappa.$$

We shall now cut an imaginary sphere of radius r out of the medium, concentric with the rigid sphere of radius a, which will be called the composite sphere.

The strain energy stored in it by the action of isotropic tension is given by the surface integral

$$W = \int \frac{1}{2} u_r p_{rr} dS$$

taken over the spherical surface with radius r. We get

$$W = \frac{1}{2} u_r(r) p_{rr}(r) \, 4\pi r^2$$

$$W = \frac{3}{2}\,\varepsilon_{(0)}^2\,\left(1 - \frac{a^3}{r^3}\right)\,(3\varkappa v + 4G\varphi), \tag{2.8}$$

where

$$v = \frac{4}{3}\pi r^3 \quad \varphi = \frac{4}{3}\pi a^3. \tag{2.9}$$

In the absence of the rigid sphere

$$W = W_{(0)} = \frac{9}{2}\,\varepsilon_{(0)}^2\,\varkappa v. \tag{2.10}$$

Denoting the change in strain energy owing to the presence of the rigid sphere by ΔW, we write

$$W = W_{(0)} + \Delta W, \tag{2.11}$$

where

$$\begin{aligned} W &= \frac{3}{2}\,\varepsilon_{(0)}^2\,\left\{\left(1 - \frac{a^3}{r^3}\right) 4G\varphi - 3\varkappa\,\frac{a^3}{r^3}v\right\} \\ \Delta W &= \frac{9}{2}\,\varepsilon_{(0)}^2\,\varkappa\varphi\left\{\left(1 - \frac{a^3}{r^3}\right)\,\frac{4G}{3\varkappa} - 1\right\}. \end{aligned} \tag{2.12}$$

The strains produced by the action of some stresses in the system will be different from those in the medium in the absence of filler.

Let $\varepsilon_{(0)i}$ be the principal strains produced in the medium in the absence of filler, and $\varepsilon_{(0)i}^*$ the principal strains produced in the system. We now introduce a Cartesian system x_i into the system, the axes of which are in the direction of the principal axes of stress and strain. At an arbitrary point A with coordinates x_i the elastic displacements would have been

$$u_i = \varepsilon_{(0)i} x_i \tag{2.13}$$

in the absence of filler.

Let there now be m spheres dispersed in the medium and the centre of each given by the coordinates $x_i^{(m)}$ (see Figure 2).

The additional displacement produced by one sphere is given by u_i' defined by (1.4).

Taking into account that the volume concentration is very small, we shall assume that the effect of all spheres at the point x_i is simply additive, and write accordingly

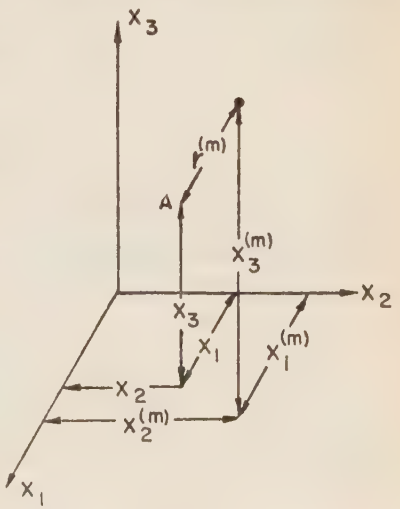

Figure 2

$$u_i = u_{(0)i} + \sum_1^m u_i'^{(m)}, \tag{2.14}$$

then

$$\varepsilon_i^* = \frac{\partial u_i}{\partial x_i}, \tag{2.15}$$

or, after carrying out the differentiation,

$$\varepsilon_i^* = \varepsilon_{(0)i} + \sum_1^m \frac{\partial u_i'}{\partial x_i} \quad . \tag{2.16}$$

As the distance $r^{(m)}$ between the centre of an arbitrary sphere and the point x_i is given by

$$r^{(m)^2} = (x - x_\alpha^{(m)})\ (x - x_\alpha^{(m)}) \quad , \tag{2.17}$$

we shall introduce new coordinates

$$y_i^{(m)} = x_i - x_i^{(m)} \quad . \tag{2.18}$$

Accordingly,

$$\varepsilon_i^* = \varepsilon_{(0)i} + \sum_1^m \frac{\partial u_i'^{(m)}}{\partial y_i^{(m)}} \quad .$$

Choosing now the point of reference as the origin of our coordinates, i.e. $x_i = 0$, (2.18) becomes

$$y_i^{(m)} = -x_i^{(m)} \tag{2.19}$$

and (2.19)

$$\varepsilon_i^* = \varepsilon_{(0)i} - \sum_1^m \frac{\partial u_i'^{(m)}}{\partial x_i^{(m)}} \qquad (x_i = 0) \quad . \tag{2.20}$$

We shall assume that the number of spheres per unit volume is n, and their size distribution is the same throughout the dispersed system.

Let the frequency distribution function of sizes be $f(a)$, where

$$\int_{a_1}^{a_2} f(a)da = 1 \quad ,$$

with a_1—radius of smallest sphere, and a_2—radius of largest sphere. The number of spheres of radius a per volume element dT will accordingly be $n\,dT \cdot f(a)da$.

Owing to the large number of spheres, summation in (2.20) may be replaced by volume integration. Accordingly,

$$\varepsilon_i^* = \varepsilon_{(0)i} - n \int_{(T)} \int_{a_1}^{a_2} \frac{\partial u_i'}{\partial x_i} f(a)dT\,da, \tag{2.21}$$

where the index m has been omitted. From (2.2) (2.18) and (2.19) we get

$$u_i'^{(m)} = \varepsilon_{(0)} x_i^{(m)} \frac{a^3}{r^{(m)3}}, \qquad (x_i = 0)$$

or, omitting the index m,

$$u_i' = \varepsilon_{(0)} x_i \frac{a^3}{r^3} \, . \tag{2.22}$$

Let

$$u_i' = a^3 \bar{u}_i' \, . \tag{2.23}$$

Then (2.21) becomes

$$\varepsilon_i^* = \varepsilon_{(0)i} \int_{(T)} \frac{\partial \bar{u}_i'}{\partial x_i} dT \int a^3 f(a) da \,. \tag{2.24}$$

Now the number of all spherical particles within a large sphere of radius R and volume V is given by

$$m = nV \tag{2.25}$$

and their volume by

$$\Phi = m \int \frac{4}{3} \pi a^3 f(a) da. \tag{2.26}$$

As the $\bar{u}_i'$ may be regarded as vectors in the direction of the x_i, we have

$$\text{div } \bar{\mathbf{u}}_i' = \frac{\partial \bar{u}_i'}{\partial x_i} \text{ (no sum on } i\text{)}.$$

By Gauss' theorem

$$\int_{(T)} \text{div } \bar{\mathbf{u}}_i' \, dT = \int_{(T)} \frac{\partial \bar{u}_i'}{\partial x_i} \, dT = \int_{(S)} \bar{u}_i' \cos(\bar{u}_i', r) \cdot dS = \int_{(S)} \bar{u}_i' \frac{x_i}{r} \, dS. \tag{2.27}$$

Denoting the volume concentration of spheres in the medium by

$$c_v = \frac{\Phi}{V}, \tag{2.28}$$

and using (2.25), (2.26) and (2.27), formula (2.24) assumes the form

$$\varepsilon_i^* = \varepsilon_{(0)i} - \frac{c_v}{4\pi/3} \int_{(S)} \bar{u}_i' \frac{x_i}{r} \, dS. \tag{2.29}$$

From (2.23) and (2.24)

$$\varepsilon_i^* = \varepsilon_{(0)i} - \frac{c_v \, \varepsilon_{(0)i}}{4\pi/3} \int \frac{x_i^2}{r^4} \, dS.$$

The integral evaluated over the surface (S) of a sphere of radius (R) yields $4\pi/3$. Therefore, taking into account (1), we get

$$\varepsilon_i^* = \varepsilon^* = \varepsilon_{(0)}(1 - c_v). \tag{2.30}$$

Assuming now that the dispersed system is isotropic and homogeneous, and denoting its bulk modulus by $\varkappa^*$, the strain energy stored in the large sphere will be, in view of (2.10),

$$W^*(R) = \frac{9}{2} \varepsilon^{*2} \varkappa^* V. \tag{2.31}$$

This may also be written

$$W^*(R) = W^{(0)} + \sum^m \Delta W,$$

or, using (2.12),

$$W^*(R) = \frac{9}{2} \varepsilon_{(0)}^2 \varkappa V + \frac{9}{2} \varepsilon_{(0)}^2 \varkappa \sum_1^m \left\{ \left(1 - \frac{a_m^3}{r_m^3}\right) \frac{4G}{3\varkappa} - 1 \right\} \varphi_m \,.$$

As the volume concentration is small, powers of a/r higher than 3rd will be neglected. Taking into account $\sum_1^m \varphi_m = \Phi$ and (2.28),

$$W^*(R) = \frac{9}{2}\,\varepsilon_{(0)}^2\,\varkappa V\left\{1 + \left(\frac{4G}{3\varkappa} - 1\right) c_v\right\}. \tag{2.32}$$

Now

$$\frac{4G}{3\varkappa} = 2 \cdot \frac{1-2\nu}{1+\nu}.$$

Equating (2.31) to (2.32) and using (2.30), we finally get

$$\frac{\varkappa^*}{\varkappa} = 1 + 3\,\frac{1-\nu}{1+\nu}\,c_v, \tag{2.33}$$

where only first powers of c_v have been retained.

II. 2. *The shear modulus G**

In order to calculate the coefficient of shear G^*, we shall choose a state of pure shear at a large distance from a single sphere. This may be described kinematically by

$$\varepsilon_{(0)1} = \varepsilon_{(0)}, \quad \varepsilon_{(0)2} = -\varepsilon_{(0)}, \quad \varepsilon_{(0)3} = 0 \qquad \Delta_{(0)} = 0. \tag{2.34}$$

Substituting in (2.15) we get

$$u_1 = \varepsilon_{(0)}\left(1 - \frac{a^3}{r^3}\right) x_1 - \frac{1}{4(4-5\nu)}\left\{\frac{15\varepsilon_{(0)}a^3x_1}{r^5}(x_1^2 - x_2^2) + \frac{6\varepsilon_{(0)}a^3x_1}{r^3}\right\}$$

$$u_2 = \varepsilon_{(0)}\left(1 - \frac{a^3}{r^3}\right) x_1 - \frac{1}{4(4-5\nu)}\left\{\frac{15\varepsilon_{(0)}a^3x_2}{r^5}(x_1^2 - x_2^2) + \frac{6\varepsilon_{(0)}a^3x_2}{r^3}\right\} \tag{2.35}$$

$$u_3 = -\frac{1}{4(4-5\nu)}\left\{\frac{15\varepsilon_{(0)}a^3x_3}{r^5}(x_1^2 - x_2^2)\right\} =$$

$$= \frac{15}{2}\,\frac{1-2\nu}{4-5\nu}\,\varepsilon_{(0)}\,\frac{a^3}{r^5}(x_1^2 - x_2^2). \tag{2.36}$$

As the elastic displacements will only be needed to calculate strain energies, only the values on the surface of the composite sphere are of interest. The volume concentration is assumed so small that, when taking as the radius of the composite sphere half the mean distance between the centres of the inclusions, $(a/r)^5$ may be neglected in comparison with $(a/r)^3$. Accordingly, in displacements (2.35) and dilatation (2.36) only the powers $(a/r)^3$ have been retained. The stresses may be calculated from (2.35) and (2.36) by using the stress-strain relations

$$p_{ij} = \lambda\Delta\delta_{ij} + 2Ge_{ij} \qquad \begin{cases}\delta_{ij} = 1 & i = j\\ \delta_{ij} = 0 & i \neq j\end{cases} \tag{2.37}$$

Accordingly,

$$p_{11} = \frac{15}{2}\lambda\frac{1-2\nu}{4-5\nu}\varepsilon_{(0)}\frac{a^3}{r^5}(x_1^2-x_2^2) + G\varepsilon_{(0)}\left\{1-\frac{a^3}{r^3}+\frac{3a^3x_1^2}{r^5}-\right.$$

$$\left.-\frac{1}{4(4-5\nu)}\left[\frac{15a^3}{r^5}(x_1^2-x_2^2) - \frac{75a^3}{r^7}(x_1^2-x_2^2)+\frac{48a^3x_1^2}{r^5}-\frac{6a^3}{r^3}\right]\right\}$$

$$p_{22} = \frac{15}{2}\lambda\frac{1-2\nu}{4-5\nu}\varepsilon_{(0)}\frac{a^3}{r^5}(x_1^2-x_2^2) - G\varepsilon_{(0)}\left\{1-\frac{a^3}{r^3}+\frac{3a^3x_2^2}{r^5}-\right.$$

$$\left.-\frac{1}{4(4-5\nu)}\left[-\frac{15a^3}{r^5}(x_1^2-x_2^2)+\frac{75a^3}{r^5}x_2^2(x_1^2-x_2^2)+\frac{48a^3}{r^5}x_2^2-\frac{6a^3}{r^3}\right]\right\}$$

$$p_{33} = \frac{15}{2}\lambda\frac{1-2\nu}{4-5\nu}\varepsilon_{(0)}\frac{a^3}{r^5}(x_1^2-x_2^2) - \frac{1}{4(4-5\nu)}G\varepsilon_{(0)}\left[-\frac{75a^3}{r^7}x_1^3\cdot(x_1^2-x_2^2)+\right.$$

$$\left.+\frac{15a^3}{r^5}(x_1^2-x_2^2)\right] \tag{2.38}$$

$$p_{13} = G\varepsilon_{(0)}\left\{\frac{3a^3x_3x_1}{r^5}+\frac{1}{4(4-5\nu)}+\left[\frac{150a^3x_1x_3}{r^7}(x_1^2-x_2^2)-\frac{48a^3x_1x_3}{r^5}\right]\right\}$$

$$p_{12} = \frac{150}{4(4-5\nu)}G\varepsilon_{(0)}\frac{a^3}{r^7}x_1x_2(x_1^2-x_2^2).$$

The stress vectors acting on the surface of the composite sphere may be calculated from

$$\overset{n}{X}_i = \overset{r}{X}_i = P_i\cos(r,\alpha) = P_{i\alpha}\frac{x_\alpha}{r}, \tag{2.39}$$

where $\mathbf{n} = \mathbf{r}$ is the outward normal to the spherical surface. The elastic strain energy stored in the composite sphere is next calculated from

$$W = \frac{1}{2}\int_{(S)}\overset{r}{X}_i\,u_i\,dS. \tag{2.40}$$

In exactly the same way as for the isotropic case described in II.1, it is found that

$$W_{(0)}(R) = 2\varepsilon_{(0)}^2GV. \tag{2.41}$$

When a large sphere of radius R is cut out of the dispersed system, it is found that

$$W^*(R) = 2\varepsilon_{(0)}^2GV\left(1+\frac{1}{2}\frac{5\nu-1}{4-5\nu}c_\nu\right), \tag{2.42}$$

where we have made use of the following surface integrals when calculating the energy by (2.40):

$$\int_{S)} dS = 4\pi R^2$$

$$\int_{(S)} x_i \, dS = \frac{4}{3}\pi R^4 \qquad \int_{(S)} x_i^2 x_j^2 \, dS = \frac{4}{15}\pi R^6$$

$$\int_{(S)} x_i^4 \, dS = \frac{4}{5}\pi R^6 \qquad \int_{(S)} x_i^2 x_j^4 \, dS = \frac{4}{35}\pi R^8$$

$$\int_{(S)} x_i^6 \, dS = \frac{4}{7}\pi R^8 \qquad \int_{(S)} x_i^2 x_j^2 x_k^2 = \frac{4}{105}\pi R^8 \qquad i \neq j \neq k.$$

Assuming the dispersed system to be isotropic and homogeneous, the shear modulus being G^*, we have

$$W^*(R) = 2\varepsilon^{*2} G^* V. \tag{2.43}$$

By the method of II.1, it is also found that

$$\begin{aligned} \varepsilon_1^* &= \varepsilon_{(0)}(1 - c_v) \\ \varepsilon_2^* &= -\varepsilon_{(0)}(1 - c_v) \\ \varepsilon_3^* &= 0 \end{aligned} \tag{2.44}$$

Equating (2.43) to (2.42), and using (2.44), we finally get

$$\frac{G^*}{G} = 1 + \frac{15}{2} \frac{1 - \nu}{4 - 5\nu} c_v \quad , \tag{2.45}$$

where again only first powers of c_v have been retained. For the case $\nu = \frac{1}{2}$ we get from (2.45)

$$\frac{G^*}{G} = 1 + 2.5\, c_v , \tag{2.46}$$

which is analogous to Eq. (0.2), and provides the mathematical check on our calculations.

II. 3. *Poisson's ratio ν^* and Young's modulus E^**

As an isotropic homogeneous elastic material has only two independent elastic constants, having determined $\varkappa^*$ and G^* we may now calculate the remaining elastic constants. Of these only Poisson's ratio ν^* and Young's modulus E^* will be determined. They are given in terms of $\varkappa^*$ and G^* by

$$\nu^* = \frac{3\varkappa^* - 2G^*}{2(3\varkappa^* + G^*)} \tag{2.47}$$

$$E^* = \frac{9\varkappa^* G^*}{3\varkappa^* + G^*} \tag{2.48}$$

Carrying out the calculations, using (2.33) and (2.45), and retaining only first powers of c_v, we get

$$\nu^* = \nu + 3\,\frac{(1-\nu)\,(1-5\nu)\,(1-2\nu)}{2\,(4-5\nu)}\,c_\nu \tag{2.49}$$

$$\frac{E^*}{E} = 1 + 3\,\frac{(1-\nu)\,(5\nu^2-\nu+3)}{(1+\nu)\,(4-5\nu)}\,c_\nu\,. \tag{2.50}$$

As in the theory of structural viscosity (compare Reiner[6], Chap. IV), we shall introduce the term relative elastic modulus defined by:

$$M_{rel} = \frac{M^*}{M}, \tag{2.51}$$

where M denotes a modulus of elasticity which has the dimensions of stress. The specific elastic modulus is defined by

$$M_{spec} = M_{rel} - 1. \tag{2.52}$$

The intrinsic elastic modulus is defined by

$$M_i = \frac{M_{spec}}{c_\nu}\,. \tag{2.53}$$

Formulae (2.33), (2.46), (2.50) may accordingly be written in the more convenient form

$$\varkappa_i = 3\,\frac{1-\nu}{1+\nu} \tag{2.54}$$

$$G_i = \frac{15}{2}\,\frac{1-\nu}{4-5\nu} \tag{2.55}$$

$$E_i = 3\,\frac{1-\nu}{1+\nu}\;\frac{5\nu^2-\nu+3}{4-5\nu}\,. \tag{2.56}$$

Graphs of the intrinsic moduli as functions of the Poisson ratio ν of the binder and also a graph of

$$\frac{\nu^*-\nu}{c_\nu} = \frac{3}{2}\,\frac{(1-\nu)\,(1-2\nu)\,(1-5\nu)}{4-5\nu} \tag{2.57}$$

are attached (see Figures 3—6).

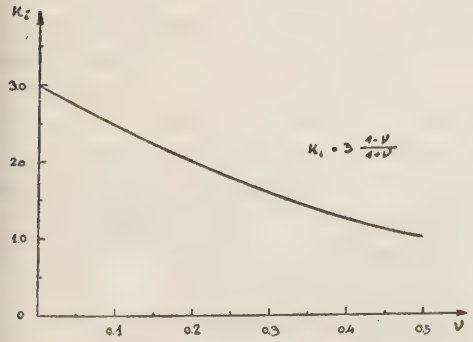

Figure 3

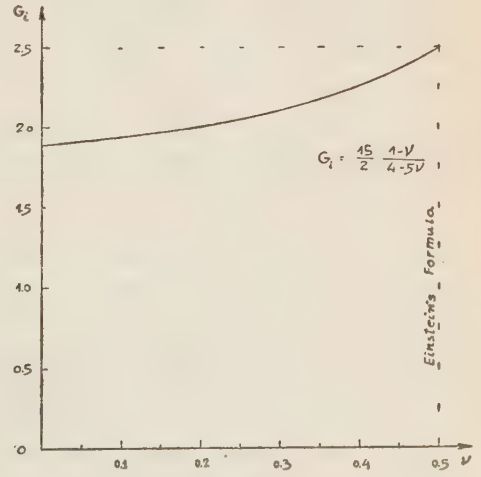

Figure 4

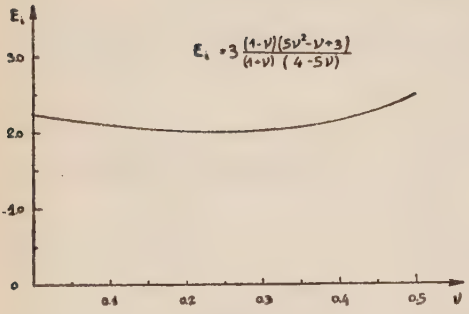

Figure 5

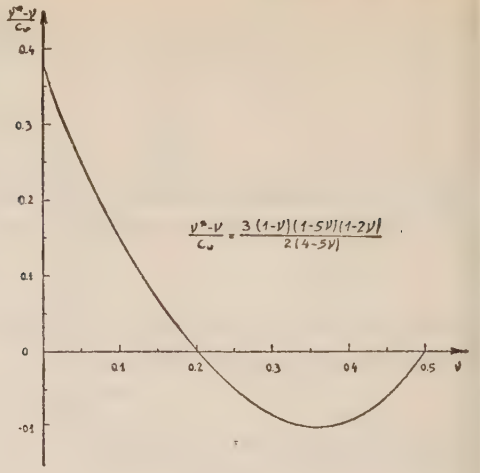

Figure 6

III. DISCUSSION

That the elastic moduli of a material are increased by reinforcing it with rigid particles is confirmed by the foregoing results, as it has been shown that in general

$$M^* = M(1 + M_i c_v), \tag{3.1}$$

where M_i is defined by (2.51)—(2.53). It has been shown that M_i is a function of ν of the binder. For the three cases of moduli having the dimensions of stress, i. e. $\varkappa$, G, E, this function is always positive for $0 \leq \nu \leq 0.5$.

It is found that $\varkappa_i$ uniformly decreases, G_i uniformly increases when ν increases. The behaviour of $\varkappa_i$ and G_i is much simpler than that of $(\nu^* - \nu)/c_v$ or E_i. This may well be understood from the fact that $\varkappa$ and G are the "natural" elastic constants of a material, the first being determined by the case of isotropic stress, i.e. volume change without distortion, the second by pure or simple shear, i.e. distortion without volume change. In contradistinction, the coefficients ν and E are determined from the experiment of *simple* tension or compression which is a much more complex phenomenon, giving rise to both volume change and distortion (compare Reiner[6], Chap. X).

From Figure 6 it can be seen that, when $\nu = 0.5$, $\nu^* = 0.5$, i.e. that an incompressible material remains incompressible after adding rigid particles. This should be expected, as incompressibility means that under any stresses acting the volume dilatation vanishes. As the particles added are rigid, the material obviously remains incompressible.

In the other extremity, when $\nu = 0$, $\nu^* = 0.375\, c_v$. This can be understood by considering simple compression of a prismatic bar of an elastic material. When $\nu = 0$, there will be no lateral expansion of the cross section. This means that only displacements in the direction of the generatrix will exist. This state will be disturbed by the introduction of rigid particles. The material will be forced by compression into the spaces between the particles, and lateral displacements will be produced which are measured as an expansion of the cross section, i.e. a Poisson ratio.

As a curious result it is found that for $\nu = 0.2$, $\nu^* = 0.2$ as well.

The greatest decrease in ν produced by the filler is found for $\nu = 0.36$.

Two different ways may be indicated for continuing theoretical research. The first is based, as before, on the assumption that c_v is infinitesimally small, and concerns particles of different rheological materials or different shapes.

The problem of determining the material coefficients of a dispersion of spheres of a material having other rheological properties than the binder has been determined for small c_v in the following cases:

1. Rigid spheres in viscous fluid — Einstein[1,2].
2. Elastic spheres in viscous fluid — Froehlich and Sack[8].
3. Spherical holes in elastic solid — MacKenzie[9].

For the case of cement mortar, it is of interest to consider the case of elastic particles, and of holes filled with water in an elastic binder.

The problem of particles other than spherical has been solved for the case of dispersions of rigid ellipsoids, rods, dumbbells etc., in a viscous fluid.

The second and more difficult problem is the consideration of finite volume concentration, which is of great technical importance.

The concentration of sand particles in mortar, for instance, reaches values of 50—60%.

It is expected that, for increasing c_v, the material constant of the system will increase (or decrease) much more than according to the linear law expressed by (3.1).

In general, for the case of a binder having some rheological equation, and containing a filler of a rheological different material, Eq. (3.1) may be written for any c_v

$$M^* = M \cdot f(c_v), \tag{3.2}$$

where $f(c_v)$ may be expressed as a power series as follows:

$$f(c_v) = 1 + M_i c_v + M_i' c_v^2 + M_i'' c_v^3 + \ldots \tag{3.3}$$

where M_i is the intrinsic constant defined by (3.1).

It is expected that, for increasing c_v, the graph of $f(c_v)$ will curve upward for a filler stronger than the binder and downward for a weaker one.

The analogous case of finite concentration of rigid spheres in a viscous fluid has been a subject of research for the past 50 years. Up to now no purely theoretical solution valid for the range 0—100% for c_v has been found.

ACKNOWLEDGMENT

The author wishes to express his sincere thanks to Prof. M. Reiner for his kind help in the preparation of this paper.

REFERENCES

1. Einstein, A., 1906, *Ann. Phys.*, **19**, 289.
2. Einstein, A., 1911, *ibid.*, **34**, 591.
3. Goodier, J. N., 1933, *J. appl. Mech.*, **55**, A-39.
4. Thomson and Tait, 1879—1883, *Natural Philosophy*, Pt. II, Cambridge.
5. Love, A. E. H., 1927, *A Treatise on the Mathematical Theory of Elasticity*, 4th ed., Cambridge.
6. Reiner, M., 1949, *Deformation and Flow*, London.
7. MacRobert, T. M., 1944, *Spherical Harmonics*, New York.
8. Froehlich, H. and Sack, R., 1946, *Proc. roy. Soc.*, A **185.**
9. MacKenzie, J. K., 1950, *Proc. phys. Soc. Lond.*, B **63**, 361 B, 2—11.

COMPOSITION OF BITTER ORANGES GROWN IN ISRAEL

A. Ephraim and J. J. Monselise

Laboratories of ASSIS Ltd., Ramat Gan

ABSTRACT

Physical and chemical examination of bitter oranges grown in Israel yielded the following results:

(1) Specific gravity of the fruit varies in the range 0.726 to 0.875.
(2) Juice content: *v/w* ranges between 26.7 and 39.8%.
(3) T.S.S. of mature fruit is 11 to 13 Bx°.
(4) Total sugars of the juice amount to 6—7%.
(5) Difference between T.S.S. and total sugar is about 5.
(6) T.S.S./acidity ratio is 2.68—3.66.
(7) Ratio of total to reduced sugars is 1.4.
(8) Acidity of juices ranges between 3.7 and 4.2% (as anhydrous citric acid).
(9) Ascorbic acid content ranges between 30 and 40 mg/100 ml juice.
(10) Oil content (by steam distillation) for small fruit is 7.86 and for large fruit 6.45 kg/ton.
(11) Aldehyde content is 1.0% (as citral).

Bitter oranges picked from groves of the Petah Tiqva district in the middle of the citrus season (February 10—15, 1955) were analyzed 24—48 hours after picking for the qualities enumerated in the Abstract above, and also for specific gravity, invert sugar content, refractive index and angle of rotation of the peel oil.

The analysis of the fruit was carried out in such a way as to determine the differences in composition and properties of 1) large (ca. 150 g) and small (ca. 100 g) fruit and 2) mature (reddish peel) and incompletely ripened (yellow peel) fruit.

ANALYTICAL METHODS

Specific gravity of the fruit was determined by measuring the volume of the displaced water, and the T.S.S. of the juice by an Abbé refractometer (reading not being corrected for acidity). The acidity of the juice was determined by titration against 0.1 N NaOH (phenolphthalein) and the results reported as anhydrous citric acid. For measuring *p*H of the juice, a Beckmann line-operated *p*H-meter was used (glass electrode). The determination of ascorbic acid content of the juice was carried out by titration with 2,6-dichlorophenolindophenol, standardized against pure ascorbic acid. The purity of the ascorbic acid was checked by iodometric titration. Total sugars and the invert sugar content of the juice were determined by the Lane Eynon method.

The essential oil content of the peel was determined by steam distillation of the minced peels, previously soaked in brine, according to a modification of Wilson's

Received October 6, 1955. Bull. Res. Counc. of Israel, Vol. 5C, 1955.

method[1,2]. Acidity and aldehyde content of the essential oil were determined potentiometrically according to Monselise and Gueron[3], and the angle of rotation of the essential oil $[\alpha]_D^{20}$ was determined in a 10 cm tube.

TABLE I

Sample No.	*T.S.S.*	*Total sugars*	*Invert sugar*	*Total sugars / Invert sugar*	*T.S.S. / Total sugars*
1	11.0	6.24	4.44	1.40	4.8
2	13.1	7.28	5.44	1.34	5.8
3	12.2	7.14	5.28	1.35	5.1
4	12.5	7.05	5.16	1.36	5.5

RESULTS

Differences in composition and properties between large and small fruit

The specific gravity of the small fruit (0.821—0.875) was higher than that of the large fruit (0.726—0.807) (see samples 1—20). This was confirmed by analyzing a second series of fruits (see samples 20—30).

Thickness of peel of the small fruit was 2—4 mm while in the large fruit it was 4—6 mm.

Juice content in the small fruit was found to be ca. 32%, whereas in the large fruit it was ca. 30%.

As to the properties of the juice, no substantial differences were observed between that of the large and of the small fruits.

Differences in composition and properties of mature and incompletely ripened fruit

The differences observed indicate that it is justified to judge the maturity of fruit according to peel colour.

T.S.S. of mature fruit was found to be higher (up to 12.4) than that of the yellow fruit (up to 10.8).

T.S.S./acid ratio was found to be higher (3.2) in mature fruit than in the yellow fruit (2.8).

No other differences were observed.

Work is proceeding, particularly on pectin content, buffer effect in juice, ash content and analysis, oil analysis.

REFERENCES

1. Braverman, J. S. and Carmi, A., 1937, The composition of Palestine oranges, *Hadar*, **10**, 147—152.
2. Braverman, J. S. and Monselise, J. J., 1940, Studies on citrus oils of Palestine, *ibid.*, **13**, 225—226.
3. Monselise, J. J. and Gueron, I., 1952, Méthode potentiométrique rapide pour la détermination des aldéhydes et de l'acidité dans les huiles essentielles d'agrumes, *Industr. agric.*, **69**, 9—10; 703—704.

TABLE II

	Sample No.	Weight (g)	Volume (ml)	Sp. grav. (20°C)	Juice						Peel oil (Steam distilled)					
					% Juice v/w	T.S.S.	Acidity (% citric a.)	T.S.S./acid	pH	Ascorbic acid (mg/100g)	Content (g/kg)	Aldehyde (% citral)	Acidity (mg KOH/g)	Refractive index (20°)	D20 (°)	Sp. grav. (20°C)
Big mature fruit	1	157	197	.796	26.8	11.9	3.77	3.16		38.2						
	2	172	217	.792	26.7	13.0	3.97	3.28		39.6						
	3	176	218	.807	32.4	13.0	4.39	2.96		35.4						
	4	171	233	.733	28.1	11.3	3.77	3.00		35.0						
	5	174	225	.773	27.0	11.2	3.06	3.66		46.9						
	6	163	209	.779	30.6	11.4	3.79	3.01	2.73	34.6	6.45					
	7	160	210	.761	30.0	12.0	4.21	2.85		35.7						
	8	152	197	.771	30.9	11.9	4.48	2.66		34.8						
	9	150	192	.781	34.6	11.1	3.92	2.83		29.1						
	10	160	205	.785	31.1	12.0	4.11	2.92		34.8						
	Average	—	—	.777	29.8	11.8	3.95	3.03	2.73	36.4		1.04	0.33	1.472	+90.4	.845
Small mature fruit	11	92	112	.821	29.4	11.8										
	12	91	106	.858	29.8	11.3	3.74	3.05	2.75	35.5						
	13	100	121	.826	33.0	11.2										
	14	113	132	.856	39.8	13.1										
	15	64	75	.853	34.2	13.0	4.17	3.13	2.68	36.9	7.86					
	16	79	92	.858	31.8	12.0										
	17	96	112	.857	31.4	12.0										
	18	75	88	.852	27.9	11.2	4.10	2.82	2.72	35.0						
	19	86	102	.843	34.7	11.3										
	20	64	75	.853	28.2	11.5										
	Average	—	—	.847	32.0	11.8	4.00	3.00	2.72	35.8						
Big mature fruit	21	229	315	.726	27.2	11.3										
	22	199	267	.745	29.6	11.9										
	23	220	300	.733	30.9	11.9										
	24	192	262	.732	30.8	11.9										
	25	197	270	.729	32.4	11.3										
	Average	—	—	.735	30.3	11.7										
Small mature fruit	26	85	100	.850	30.6	12.2										
	27	112	132	.848	32.5	11.9										
	28	105	120	.875	30.5	11.9										
	29	106	122	.868	32.1	12.0										
	30	101	118	.855	32.7	11.6										
	Average	—	—	.859	31.6	11.9										
Mature fruit	31	181	222	.815	35.9											
	32	158	203	.778	35.1	12.0	3.86	3.11	2.75	33.4						
	33	143	170	.841	37.7											
	34	125	147	.850	31.2											
	35	124	153	.810	30.6						6.95					
	36	122	148	.824	35.2											
	37	114	134	.850	37.7	12.8	3.90	3.28	2.75	34.3						
	38	104	122	.852	29.8											
	39	111	132	.840	31.5											
	40	94	114	.824	29.8											
	Average	—	—	.828	33.4	12.4	3.88	3.19	2.75	33.8		1.03	0.33	1.472	+90.4	.845
Not completely mature fruit	41	198	238	.831	34.8											
	42	181	218	.830	34.8	10.5	3.91	2.68	2.73	32.2						
	43	172	202	.851	38.9											
	44	156	182	.857	34.6				2.78	34.8						
	45	147	175	.840	33.3	10.9	3.71	2.94			6.01					
	46	150	174	.862	38.0											
	47	130	152	.855	30.4											
	48	151	181	.834	32.4	11.0	3.93	2.80	2.73	34.3						
	49	100	122	.819	27.0											
	50	98	117	.837	29.6											
	Average	—	—	.841	33.4	10.8	3.85	2.80	2.74	33.6						

THE PERFORMANCE OF RECIPROCATING AIR-COMPRESSORS

J. F. Ury

Fac. of Mechanical Engineering, Technion — Israel Institute of Technology, Haifa

ABSTRACT

In this paper empirical formulae are derived which permit a precalculation, with a fair degree of accuracy, of the performance of given compressor-stages under varying working conditions. This is done by studying the deviations from an ideal polytropic process which occur in actual compressor-stages. A lower limit of the pressure-difference per stage is found, however, below which this method, based on thermodynamic considerations alone, is not applicable.

INTRODUCTION

An air-compressor has to deliver air at elevated pressure. During compression heat is generated, which increases the temperature of the air. This increase, which cannot be suppressed completely even by the most effective water-cooling, forms in nearly all practical cases a highly disadvantageous and undesirable secondary effect, as it increases the power required to drive the compressor, but does not contribute anything to the achievement of the purpose for which the compressed air is intended.

We have, therefore, to compare the actual work of compression with the minimum work by which the pressure could be raised from the initial value p_e to the final value p_2^*, i.e. with the isothermal compression between these pressures at the ambient temperature T_{em}. This is the temperature which the air would have, if it were to pass through the cylinder without undergoing compression. It is dependent on the temperature T_e of the air entering the cylinder in question, and on the temperature T_e of the cooling water entering the jacket surrounding it. It cannot, however, be predicted with certainty to what extent each of these two factors would be effective.

In a generalized form it will be:

$$T_{em} = \frac{T_e + \tau T_e}{1 + \tau} \tag{1}$$

where τ is a coefficient to be determined by experiment.

The German code for testing reciprocating air-compressors compares the actual work with the isothermal work at a temperature which is the arithmetic mean between the temperatures of air and water, i.e. $\tau = 1$ in formula (1). In other codes, e.g. ASME, the temperature of the air alone is taken for comparison, i.e. $\tau = 0$. In this paper the middle course was adopted, namely $\tau = \frac{1}{2}$.

This gives

$$T_{em} = \frac{2T_e + T_e'}{3} \tag{1a}$$

Received October 25, 1955.

With the isothermal work at this temperature we have to compare the actual (indicated) work of the stage in question, in order to determine its efficiency. In this expression, as stated above, T_e is the temperature of the air entering a certain stage. In the higher stages this temperature may be considerably above the room temperature at which the air enters the first stage, but the incapability of the intercooler to restore the initial temperature, although decreasing the efficiency of the compressor as a whole, should not influence our judgment of the performance of the stage in question alone.

THE TEMPERATURE INCREASE

As stated above, the compression is accompanied by an increase of the air temperature from T_e to T_4, which is measured in the air-stream after passing the discharge valve, and this increase, in turn, affects the amount of air delivered and the power required to compress it.

The aim of this paper is, therefore, to find out whether, and in which manner, the temperature increase, $\Delta T = T_4 - T_{em}$, the weight of air delivered at each cycle, g_v, and the indicated work, L_{ind}, can be represented as functions of the speed n (rpm) and of the pressure-ratio $\Pi = p_2^*/p_e$, and thereby their values predicted for various working conditions of a given compressor.

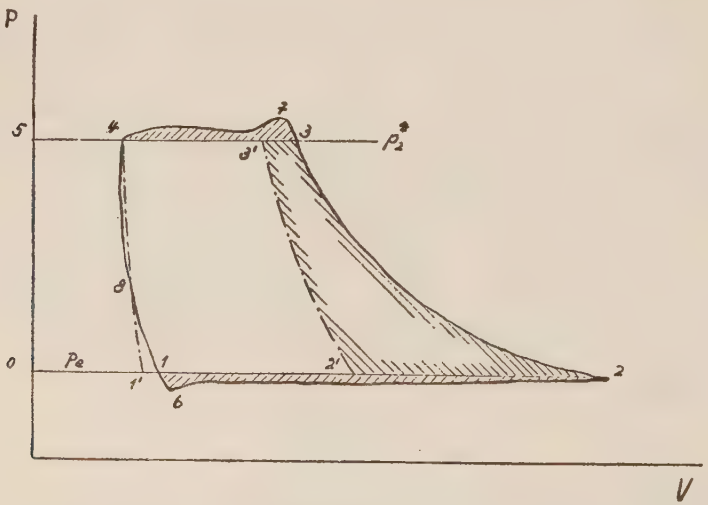

Figure 1

Of course such laws can only be determined by experiments which should cover speeds and pressures over as wide a range as possible. The equipment at the disposal of the Laboratory of Mechanical Engineering at the Israel Institute of Technology does not, however, permit tests of the required scope. It was, therefore, necessary to use reports of tests referred to in literature[1] and ascertain the extent of applicability of the laws derived from these wider-scope tests to other types of compressor-stages, with which more restricted ranges of experiments could be carried out in that laboratory.

The tests referred to above were carried out with the second stage of a two-stage air compressor of conventional design, at different pressures, speeds, and also cooling-

water temperatures. Thus they will give a very comprehensive picture of the effect which the variation of each of these factors will have on the performance of a compressor.

First, the process of compression shall be considered, as represented in the diagrams P—V (pressure-volume) and T—S (temperature-entropy).

The indicator diagram with its area (see Figure 1) $F = (1—6—2—3—7—4—1)$ gives, with the use of proper scales of pressure and volume, the work of compression per cycle (say in mkg), and, divided by the weight of air delivered per cycle — the indicated work per kg air

$$L_{ind} = \frac{F}{g_v} \tag{2}$$

This work can be regarded as the sum of the amounts of work of two separate reciprocating machines without clearance:

a) An ideal compressor, the indicator diagram of which is the area $F_2 = (0—1—6—2—3—7—4—5)$. It compresses the total amount of air $g_0 + g_v$, where g_0 denotes the weight of air remaining in the clearance space of the real compressor; the indicated work per kg of air compressed is, therefore,

$$L_{c\ ind} = \frac{F_2}{g_0 + g_v} \tag{3}$$

Actually, an error is introduced in this idealized consideration by the fact that the part of the work represented by the diagram areas below 0—1—2 and above 3—4—5

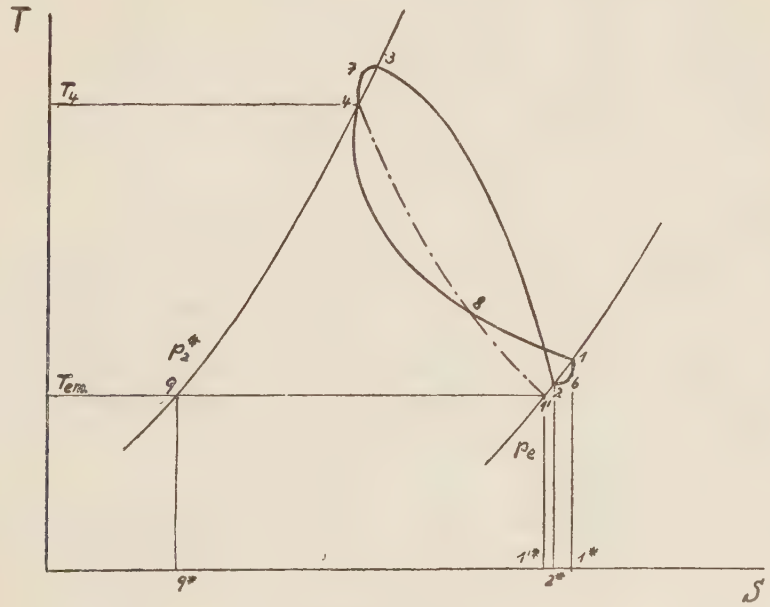

Figure 2

is not put into this whole amount $g_0 + g_v$, but into an amount which varies gradually between that value and g_0. These areas are, however, generally so small in comparison with the total area, that the error can be considered negligible.

b) An ideal compressed-air motor which, by expansion of the amount g_0 along the line 4—1 does the indicated work represented by the area $F_1 = (5—4—1—0)$ and the work per kg of driving air

$$L_{e\ ind} = \frac{F_1}{g_0} \tag{3a}$$

$L_{c\ ind}$ and $L_{e\ ind}$ may also be represented in the $T—S$ diagram (Figure 2). They are

$L_{c\ ind} = (9^*—9—4—7—3—2—6—1—1'—1'^*)$ and

$L_{e\ ind} = (1'^*—1'—1—8—4—9—9^*)$

which may be compared with the polytropic work for processes along the polytropic between the points 1′ (point of intersection of p_e and T_{em}) and 4

$$L_{pol} = \frac{p_e V_e}{G} \frac{k}{k-1} \left[\left(\frac{p_2^*}{p_e} \right)^{\frac{k-1}{k}} - 1 \right] \tag{4}$$

where G is the weight of air (in kg), V_e its volume (m^3) at pressure p_e (kg/m^2), and k the exponent of the polytropic. By substituting

$$\Pi = \frac{p_2^*}{p_e}, \qquad \theta = \frac{T_4}{T_{em}}, \qquad \frac{k}{k-1} = \frac{\log \Pi}{\log \theta}, \qquad \Delta T = T_4 - T_{em},$$

and by using the ideal gas law $PV = GRT$, another form is obtained:

$$L_{pol} = R \frac{\log \Pi}{\log \theta} \cdot \Delta T \tag{4a}$$

with the gas constant $R = 29.27$ for air at moderate pressures.

The real processes of compression and expansion cannot follow an exact polytropic curve, because in such a case the heat removed from the cylinder at each instant would be proportional only to the work done at the same time, whereas in fact this heat transfer must also be dependent on the temperature difference between the wall and the air at each moment. But since the polytropic gives a well-defined ideal limit for the work of compression or expansion between any two given points, it provides a very suitable basis for comparison with different real processes.

The first task will therefore be to calculate, for the different tests, the values of T_{em}, Π, θ, and

$$k = \frac{\log \Pi}{\log \Pi - \log \theta} \tag{5}$$

and, if possible, express k as function of the speed n. the pressure ratio Π, and the initial ambient temperature T_{em}. This done, the temperature T_4 of the delivered air can be predicted for every set of values.

TABLE I

a) $T_e' \sim 282°K$, $\Pi \sim 4.3$, n varying between 63 and 163 rpm

Test No.	1	2	3	4	5	
(n)	163.2	140.2	121.5	91.42	62.91	rpm
(p_2^*)	18.98	18.98	18.98	18.98	18.98	ata
(p_e)	4.45	4.40	4.40	4.40	4.40	ata
(Π)	4.27	4.31	4.31	4.31	4.31	
$\log \Pi$	0.6299	0.6349	0.6349	0.6349	0.6349	
(T_4)	420.2	414.0	408.0	397.0	382.3	°K
(T_e)	295.3	292.4	290.7	288.0	285.8	°K
(T_e')	281.8	281.8	281.8	281.8	281.8	°K
(T_{em})	290.8	288.9	287.7	285.9	284.5	°K
θ	1.445	1.433	1.418	1.389	1.344	
$\log \theta$	0.1599	0.1562	0.1518	0.1426	0.1283	
k	1.339	1.328	1.315	1.290	1.252	

b) $T_e' \sim 282$ °K, $\Pi \sim 3.6$, n varying between 62 and 174 rpm

Test No.	6	7	8	9	10	
(n)	174.0	140.0	121.5	89.0	62.3	rpm
(p_2^*)	14.98	14.98	14.98	14.98	14.98	ata
(p_e)	4.33	4.15	4.13	4.16	4.30	ata
(Π)	3.45	3.61	3.62	3.60	3.48	
$\log \Pi$	0.5390	0.5575	0.5596	0.5564	0.5420	
(T_4)	403.4	395.5	390.6	379.3	367.5	°K
(T_e)	296.0	291.8	289.8	287.1	285.4	°K
(T_e')	281.8	281.7	281.7	281.7	281.7	°K
(T_{em})	291.3	288.4	287.1	285.2	284.2	°K
θ	1.385	1.372	1.361	1.330	1.293	
$\log \theta$	0.1414	0.1372	0.1337	0.1238	0.1117	
k	1.356	1.328	1.314	1.287	1.259	

TABLE II

a) $T_e' \sim 282$ °K, $\Pi \sim 2.78$, n varying between 62 and 173 rpm

Test No.	11	12	13	14	15	
(n)	173.1	137.8	116.2	92.5	62.4	rpm
(p_2^*)	10.98	10.98	10.98	10.98	10.98	ata
(p_e)	4.00	3.97	3.95	3.95	3.90	ata
(Π)	2.75	2.77	2.78	2.78	2.82	
$\log \Pi$	0.4385	0.4418	0.4440	0.4440	0.4495	
(T_4)	375.6	369.0	364.5	358.7	349.5	°K
(T_e)	296.5	292.4	290.2	287.8	285.8	°K
(T_e')	281.9	281.9	281.9	281.9	281.8	°K
(T_{em})	291.6	288.9	287.4	285.8	284.5	°K
θ	1.288	1.277	1.268	1.255	1.229	
$\log \theta$	0.1099	0.1062	0.1032	0.0986	0.0894	
k	1.336	1.318	1.302	1.288	1.248	

b) $T'_e \sim 282$ °K, $\Pi \sim 2.25$, n varying between 62 and 183 rpm

Test No.	16	17	18	19	20	
(n)	183.2	149.4	117.0	91.2	62.2	rpm
(p_2^*)	8.49	8.49	8.49	8.49	8.49	ata
(p_e)	3.88	3.79	3.75	3.77	3.73	ata
(Π)	2.19	2.24	2.26	2.25	2.28	
log Π	0.3401	0.3503	0.3549	0.3526	0.3572	
(T_4)	356.5	351.0	345.6	340.0	333.3	°K
(T_e)	297.2	293.4	290.2	288.0	286.1	°K
(T'_e)	281.9	281.9	281.9	282.0	282.0	°K
T_{em}	292.1	289.6	287.4	286.0	284.7	°K
θ	1.221	1.212	1.203	1.189	1.171	
log θ	0.0866	0.0835	0.0801	0.0751	0.0684	
k	1.342	1.310	1.291	1.271	1.238	

TABLE III

a) $T'_e \sim 283$ °K, $\Pi \sim 1.65$, n varying between 62 and 165 rpm

Test No.	21	22	23	24	25	
(n)	164.6	140.7	118.6	92.5	61.85	rpm
(p_2^*)	5.97	5.97	5.97	5.97	5.97	ata
(p_e)	3.67	3.62	3.60	3.57	3.52	ata
(Π)	1.627	1.648	1.658	1.672	1.696	
log Π	0.2113	0.2170	0.2197	0.2233	0.2294	
(T_4)	331.3	329.5	326.5	321.5	316.0	°K
(T_e)	292.6	291.1	289.7	287.0	285.6	°K
(T'_e)	282.8	282.8	282.8	282.8	282.8	°K
T_{em}	289.3	288.3	287.4	285.6	284.7	°K
θ	1.145	1.143	1.136	1.126	1.114	
log θ	0.0588	0.0581	0.0554	0.0514	0.0467	
k	1.388	1.369	1.338	1.300	1.256	

b) T'_e varying between 282 and 313 °K, $\Pi \sim 4.3$, $n \sim 163$ rpm

Test No.	26	27	28	29	1	
(n)	163.0	162.4	162.4	163.5	163.2	rpm
(p_2^*)	18.96	18.96	18.96	18.96	18.98	ata
(p_e)	4.40	4.40	4.40	4.40	4.45	ata
(Π)	4.31	4.31	4.31	4.31	4.27	
log Π	0.6344	0.6344	0.6344	0.6344	0.6299	
(T_4)	441.0	433.3	430.3	428.4	420.2	°K
(T_e)	293.5	294.0	293.7	293.7	295.3	°K
(T'_e)	313.0	303.2	296.4	293.2	281.8	°K
T_{em}	300.0	297.1	294.6	293.5	290.8	°K
θ	1.470	1.458	1.461	1.460	1.445	
log θ	0.1673	0.1639	0.1646	0.1643	0.1599	
k	1.358	1.350	1.350	1.350	1.339	

In Tables 1—3 the items in brackets are quoted from Kollmann's paper, the rest calculated from the equations given above.

The values of k are plotted in Figure 3, with n as abscissae. It is seen that all points are situated so that a continuous line can be drawn through them with little deviation. Only the values for tests No. 21—25, especially for those at higher speeds, are somewhat above this line. An explanation for this deviation may be as follows: the discharge

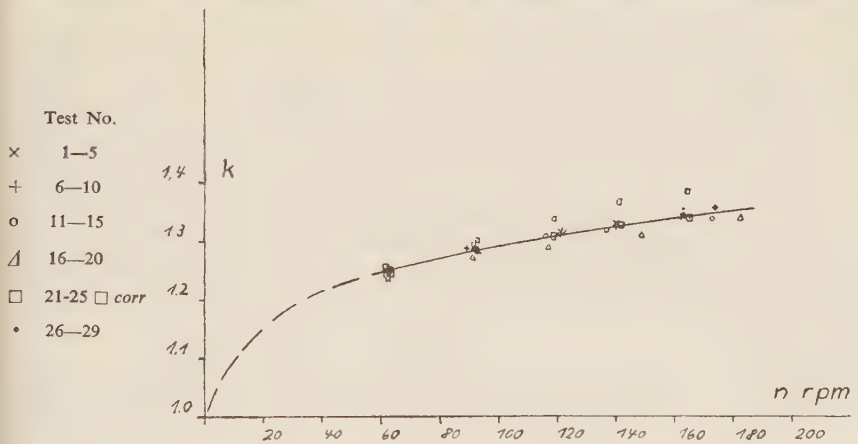

Figure 3

of the compressed air from the cylinder induces strong vibrations of the discharge valves, and under favourable conditions these vibrations may continue beyond the dead centre of the piston. Kollmann noticed this phenomenon in the course of his tests with the low-pressure cylinder, and brought it out by means of out-of-phase diagrams. It can be assumed that these after-vibrations ensue if a sufficient pressure-difference is not built up on the valves rapidly enough, i.e. if the pressure-difference $p_2^* - p_e$ falls below some critical value. In the report published by Kollmann on the low-pressure cylinder tests this value amounts to 2.7 at., whereas in the tests No. 21—25 it drops as low as 2.3 at. One may therefore assume in this case, too, that some air flowed back into the cylinder during the after-vibrations of the discharge valve, and thus increased the weight of air undergoing reexpansion. The amount of this increase will be dealt with later; here, it suffices to state that it counteracts, or even cancels out entirely, the effect of the cooling-water on the temperature of the incoming air. We may, therefore, expect a closer approximation by putting in this case $T_{em} \sim T_e$, and with this assumption the values of k are calculated once more for tests No. 21—25 in Table IV and also plotted in the diagram (Figure 3). It is seen that now they fall exactly on the line drawn through the other points.

TABLE IV

Test No.	21	22	23	24	25	
(n)	164.6	140.7	118.6	92.5	61.85	rpm
$\theta_{corr.}$	1.132	1.132	1.127	1.120	1.110	
$\log \theta_{corr.}$	0.0539	0.0539	0.0519	0.0493	0.0453	
k	1.342	1.331	1.310	1.283	1.247	

Hence, k can be assumed a function of the speed n alone, all effects of T_{em} apart from those caused by the variation of n being negligibly small.

(It is interesting to note that according to Kollmann the exponent k is, on the contrary, dependent only on the pressure-ratio Π, and not at all on the speed — if taken for the actual compression alone, as given by the temperatures T_2 and T_3 at its beginning and end respectively. But since these are only momentary temperatures inside the cylinder during the working cycle and cannot be measured normally, this relation is of little practical value.)

From Figure 3 it follows that k increases with the increase of speed. The line drawn through the points determined in the tests is very nearly straight, and a relation could be formulated accordingly. This, however, seems unsatisfactory, since k should approach a value of 1 when the heat transfer is increased infinitely with n approaching zero, and, on the other hand, some finite maximum value when the heat transfer is reduced to zero by an infinite increase in speed. Hence, in order to formulate the relation between n and k a quantity should be found which would be constant for each polytropic and increase from zero to infinity for k increasing from 1 to $\varkappa$. Such a property is displayed by the reciprocal of the subtangent to the polytropic curve. The equation of the polytropic in the T—S diagram is

$$S = S_1 + c_v \frac{k-\varkappa}{k-1} \ln T \tag{6}$$

and with the assumption that within the narrow range in question the specific heat c_v can be regarded as constant

$$-\frac{dT}{dS} = \frac{T}{c_v} \frac{k-1}{\varkappa-k} \tag{7}$$

The subtangent is

$$\frac{T}{-dT/dS} = c_v \frac{\varkappa-k}{k-1} \tag{7a}$$

and its reciprocal

$$\frac{1}{c_v} \frac{k-1}{\varkappa-k} \tag{7b}$$

The simplest form of the required relation would accordingly be

$$n = \frac{C'}{c_v} \left(\frac{k-1}{\varkappa-k}\right)^{\alpha} = C \left(\frac{k-1}{\varkappa-k}\right)^{\alpha} \tag{8}$$

since c_v was assumed constant. If C and α are constants, the graph (Table V)

$$\log \frac{k-1}{\varkappa-k} = f(\log n)$$

should be a straight line.

However, when plotted it was found that the values follow a straight line only fo speeds up to 100 rpm approximately, while for higher speeds the line curves distinctl upwards (see Figure 4). This can be understood by taking into account the fact tha k is actually increased not only by the decreased heat transfer at higher speeds, bu

also by the additional heat generated by internal and external friction, which is increased many times under these conditions. The upper limit of the exponent k will therefore be higher than $\varkappa = 1.4$, and in accordance with the values found for uncooled turbo-compressors may be assumed to be $\varkappa^* = 1.6$. The subtangent has consequently

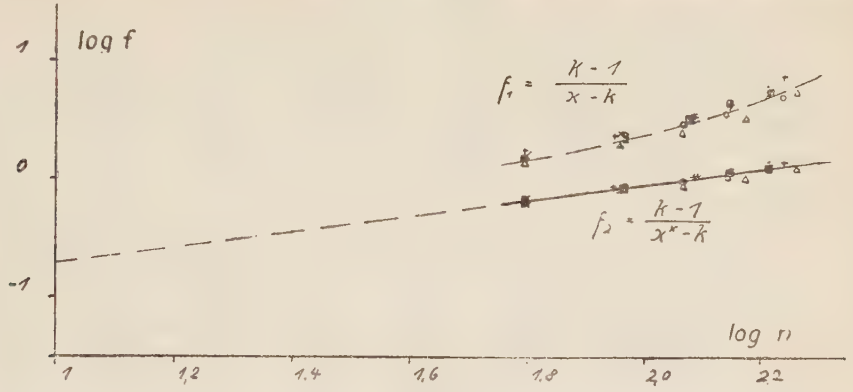

Figure 4

to be increased by a constant so that the value would be zero (or the reciprocal infinitely large) not for the adiabatic with $\varkappa = 1.4$, but only for a polytropic with $\varkappa^* = 1.6$. This is equivalent to

$$n = C\left(\frac{k-1}{\varkappa^* - k}\right)^{\alpha}. \tag{8a}$$

The function (Table V)

$$\log \frac{k-1}{k^* - \varkappa} = f(\log n)$$

was also plotted in Figure 4. This time a straight line was obtained, and from it the constants were determined as follows:

$$\log C = 2.05 \qquad C = 112.2 \qquad \alpha = 1.50$$

From equation (8a) follows:

$$n = C\left(\frac{k-1}{\varkappa^* - k}\right)^{\alpha} = C\,\frac{\log \Pi / (\log \Pi - \log \theta) - 1}{1.6 - \log \Pi / (\log \Pi - \log \theta)} = \frac{C}{0.6 \log \Pi / \log \theta - 1.6}$$

and on substituting $\beta = 1/\alpha$ we obtain

$$\frac{\log \Pi}{\log \theta} = \frac{1 + 1.6\,(n/C)^{\beta}}{0.6\,(n/C)^{\beta}},$$

or, with $C_1 = 1.67\,C^{\beta}$

$$\log \theta = \frac{\log \Pi}{1.67(C/n)^{\beta} + 2.67} = \frac{\log \Pi}{C_1/n^{\beta} + 2.67} \tag{9}$$

This is the required relation by which θ, and therefore T_4, can be calculated for every set of values of Π, n, and T_{em}, once the constants C_1 and β have been determined for a certain compressor. In this case $C_1 = 38.8$, $\beta = 0.667$.

TABLE V

$$f_1 = \frac{k-1}{\varkappa - k} \qquad f_2 = \frac{k-1}{\varkappa^* - k}$$

Test No.	1	2	3	4	5	6	7	8
log n	2.213	2.147	2.085	1.961	1.799	2.241	2.146	2.085
f_1	5.56	4.56	3.71	2.64	1.70	8.09	4.56	3.66
log f_1	0.745	0.659	0.569	0.422	0.231	0.908	0.659	0.564
f_2	1.30	1.21	1.11	0.936	0.724	1.46	1.21	1.10
log f_2	0.114	0.083	0.045	$\bar{1}$.971	$\bar{1}$.860	0.164	0.083	0.041

Test No.	9	10	11	12	13	14	15
log n	1.949	1.795	2.238	2.139	2.065	1.966	1.795
f_1	2.54	1.84	5.25	3.88	3.08	2.57	1.63
log f_1	0.405	0.265	0.720	0.589	0.489	0.410	0.212
f_2	0.916	0.760	1.27	1.13	1.01	0.923	0.705
log f_2	$\bar{1}$.962	$\bar{1}$.881	0.104	0.053	0.004	$\bar{1}$.965	$\bar{1}$.848

Test No.	16	17	18	19	20	21	22
log n	2.263	2.174	2.068	1.960	1.794	2.216	2.148
f_1	5.90	3.44	2.67	2.10	1.47	5.90	4.80
log f_1	0.771	0.537	0.427	0.322	0.167	0.771	0.681
f_2	1.33	1.07	0.948	0.824	0.658	1.33	1.23
log f_2	0.124	0.029	$\bar{1}$.977	$\bar{1}$.916	$\bar{1}$.818	0.124	0.090

Test No.	23	24	25	26	27	28	29
log n	2.074	1.966	1.791	2.212	2.211	2.211	2.214
f_1	3.45	2.42	1.61	8.53	7.00	7.00	7.00
log f_1	0.538	0.384	0.207	0.931	0.845	0.845	0.845
f_2	1.19	0.893	0.700	1.48	1.40	1.40	1.40
log f_2	0.076	$\bar{1}$.951	$\bar{1}$.845	0.170	0.146	0.146	0.146

THE WEIGHT OF AIR DELIVERED

As the indicator diagrams show, the pressure at the end of the suction-stroke (point 2) is very nearly equal to p_e. The weight of air in the cylinder at this moment is, therefore,

$$g_0 + g_v = \frac{(V_c + V_h)\, p_e}{R \cdot T_2} \tag{10}$$

where V_c denotes the clearance volume, V_h the piston displacement, and p_e the suction pressure (in m³ and kg/m² respectively).

As explained above, the weight of air remaining in the clearance space g_0 is determined (with the leakage of air through the closed valves assumed negligibly small)

not only by static factors such as p_2^*, V_c, and T_4, but also by the dynamic effect of the vibrations induced in the air and valves. It is, therefore, generally

$$g_0 = \lambda_0 \frac{p_2^* V_c}{R T_4} \tag{11}$$

where the factor λ_0 may be called the "volumetric efficiency" of the clearance space.

If the values given for the compressor

$V_c = 244$ cm³, $V_h = 2486$ cm³, and the relation

$$T_2 = T_{em} + \Delta t \tag{12}$$

are substituted in these equations, the following forms are obtained:

$$\Delta t = \frac{0.00273\, p_e}{29.27\,(g_0 + g_v)} - T_{em} = \frac{p_e}{10720\,(g_0 + g_v)} T_{em} \tag{10a}$$

where

$$g_0 = \frac{\lambda_0 p_2^*}{120000 \cdot T_4} \tag{11a}$$

For tests No. 21—25 it was put $\lambda_0 = 1.15$ for the reasons explained above; for all other tests no appreciable increase in weight by dynamic causes was assumed and it was put $\lambda_0 = 1$. The amount of air delivered per cycle was calculated from the values G_{DS} given by Kollmann:

$$g_v = \frac{G_{DS}}{60\, n} \tag{11b}$$

and thus the increase in temperature Δt during the suction phase, in relation to the ideal ambient temperature T_{em}, could be determined.

In this calculation there are several factors of uncertainty:

The calculation of g_0 is based on certain assumptions which seem to be fairly justified, but there may be slight deviations. The weight G_{DS}, on which g_v is based, was not actually measured but calculated, on the basis of the proportion of the indicated work of this side of the cylinder in the total indicated work, from the total amount of air delivered by both sides. This total amount, in turn, measured by different methods, showed differences of 1—2%. These uncertainties will necessarily be reflected in the calculation of Δt, and an accuracy in the calculation of T_2 of $\pm 1\%$ or ± 3°C will be the best we can expect. Table VI gives the calculated values and Figure 5 shows them plotted with $\log \Pi$ as abscissae. It is seen that all points (with the only exception of No. 10, for which some measurement seems to have been incorrect) lie inside a band, not more than 6—7°C in height, which rises in linear form with $\log \Pi$. A straight line drawn as the centre line of this band gives the temperature increase Δt as a function of $\log \Pi$, with the maximum accuracy that can be expected. The fact that this line also passes through the origin is purely accidental, since the basic temperature T_{em} was determined on arbitrary assumptions. It is shown here that, for this compressor at least, these assumptions are fairly justified.

The general relation

$$\Delta t = C_2 + C_3 \log \Pi \tag{13}$$

is therefore reduced to the form

$$\Delta t = 36.8 \log \Pi \tag{13a}$$

and, by substituting it in equation (10a), the weight of air delivered

$$g_v = \frac{p_e}{10720\,(T_{em} + 36.8 \log \Pi)} - \frac{\lambda_0 p_2^*}{120000\,T_4} =$$

$$= \frac{p_e}{120000\,T_{em}} \left(\frac{11.18}{1 + 36.8 \log \Pi / T_{em}} - \frac{\Pi \lambda_0}{\theta} \right) \tag{14}$$

and the volumetric efficiency

$$\lambda = \frac{g_v K T_{em}}{V_h p_e} = 0.098 \left(\frac{11.18}{1 + 36.8 \log \Pi / T_{em}} - \frac{\Pi \lambda_0}{\theta} \right) \tag{15}$$

are given as functions of p_e, T_{em}, Π, and θ, which is itself a function of Π and n by equation (9).

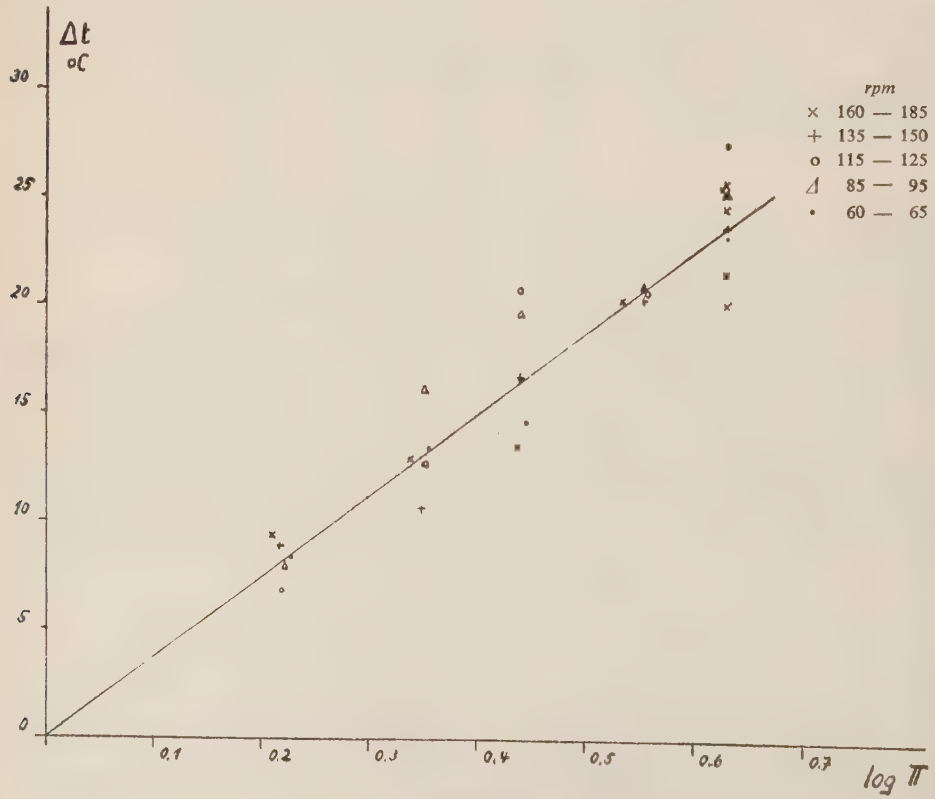

Figure 5

TABLE VI

Test No.	g_0 (kg)	g_v (kg)	Δt (°C)	Test No.	g_0 (kg)	g_v (kg)	Δt (°C)
1	0.00375	0.00939	25.2	16	0.00198	0.00988	12.9
2	0.00382	0.00930	23.5	17	0.00202	0.00972	10.6
3	0.00387	0.00915	27.3	18	0.00205	0.00962	12.6
4	0.00398	0.00922	25.1	19	0.00208	0.00954	16.0
5	0.00413	0.00920	23.0	20	0.00213	0.00955	13.3
6	0.00312	0.00982	20.2	21	0.00173	0.00960	9.4
7	0.00316	0.00935	20.1	22	0.00174	0.00952	8.9
8	0.00318	0.00935	20.4	23	0.00175	0.00956	6.8
9	0.00328	0.00942	20.8	24	0.00178	0.00951	8.0
10	0.00340	0.00931	30.8	25	0.00181	0.00935	8.4
11	0.00243	0.00978	13.4	26	0.00358	0.00919	21.3
12	0.00248	0.00964	16.6	27	0.00365	0.00926	19.9
13	0.00251	0.00943	20.6	28	0.00366	0.00921	24.4
14	0.00255	0.00952	19.6	29	0.00370	0.00917	25.5
15	0.00262	0.00954	14.5				

THE INDICATED WORK

According to definition,

$$F = F_2 - F_1, \text{ or}$$

$$g_v L_{ind} = (g_0 + g_v) L_{c\ ind} - g_0 L_{e\ ind}, \tag{16}$$

and, if $L_{c\ ind}$ and $L_{e\ ind}$ can be determined analytically, L_{ind} will be known, too.

1) The reexpansion of the air left in the clearance space begins at point 4, where we have a considerable tempera ure difference between air and cylinder walls. Heat is given up to the walls, the line representing the actual expansion in the T—S diagram tends to the left until the temperature of the air equals that of the walls, and at that point the direction of heat-transfer, and with it that of the curve of expansion, is reversed, and the fall of the temperature becomes slower and slower. Therefore, the upper part of the expansion curve always lies below the polytropic (between T_4 and T_{em}) and so may do the lower part, but its slope may also decrease sufficiently so that it would cut the polytropic at point 8 and continue its course above it.

It may therefore be

$$\eta_{e\ ind} = \frac{L_{pol}}{L_{e\ ind}} \gtreqless 1. \tag{17}$$

Measurements with a large number of indicator diagrams taken from compressors with normal water-cooled cylinder heads and walls show that the difference of L_{pol} and $L_{e\ ind}$ is very small, and, taking into account that in order to calculate $L_{e\ ind} = F_1/g_0$ the very small area F_1 must be measured, it is found that this difference is usually smaller than the necessary error entailed in the use of the planimeter on such a small area[2].

For example, the areas F_1 were measured for the diagrams given at the end of Kollmann's paper for tests No. 1, 5, and 21. The minimum error introduced by the planimeter was assumed to be $\pm$ 10 mm², and this error, expressed as percentage of F_1, was compared with the difference of $L_{e\,ind}$ and L_{pol} (in % of $L_{e\,ind}$). The values are given in Table 7.

TABLE VII

Test No.	F_1		*Error in measurement of F_1*	g_0	$L_{e\,ind}$	L_{pol}	*Deviation**
	cm²	*mkg*	*%*	*kg*	*mkg/kg*	*mkg/kg*	*%*
1	3.0	57.24	±3.3%	0.00375	15250	14910	+2.3%
5	2.9	56.10	±3.4%	0.00413	13600	14130	—3.9%
21	1.1	7.49	±9.1%	0.00173	4320	4440	—2.8%

* $[(L_{e\,ind} - L_{pol})/L_{e\,ind}] \times 100$

We may, therefore, also in this case put $\eta_{e\,ind} \sim 1$, or

$$L_{e\,ind} = L_{pol} \quad . \tag{17a}$$

2) The relation between $L_{c\,ind}$ and L_{pol} is not quite as simple. The compression always begins at a temperature $T_2 > T_{em}$, and at first the actual compression curve is steeper than the polytropic. With increasing temperature differences between air and walls the slope decreases, but it always remains $T_3 > T_4$. This causes the additional work of compression between the pressures p_e and p_2^*, represented in the P—V diagram (Figure 1) by the area $(2' - 2 - 3 - 3')$, $(2' - 3')$ being the polytropic determined by the relation

$$\frac{(3' - 5)}{(4 - 5)} = \frac{(2' - 0)}{(1' - 0)} = \frac{g_0 + g_v}{g_0} \quad .$$

To this work is to be added the loss caused by the resistance of the valves, represented by areas $(1 - 6 - 2 - 2' - 1)$ and $(3 - 7 - 4 - 3' - 3)$. It is, therefore, in every case $L_{c\,ind} > L_{pol}$, or

$$\eta_{c\,ind} = \frac{L_{pol}}{L_{c\,ind}} < 1 \tag{18}$$

By equations (3) and (16) it follows:

$$\frac{1}{\eta_{c\,ind}} = \frac{F_2}{(g_0 + g_v)L_{pol}} = \frac{g_0 L_{pol} + g_v L_{ind}}{(g_0 + g_v)L_{pol}} =$$

$$= \frac{1}{g_0 + g_v}\left(g_0 + g_v \frac{1}{\eta_{ind}}\right) \tag{19}$$

where

$$\eta_{ind} = \frac{L_{pol}}{L_{ind}} \tag{19a}$$

The values of L_{ind} were calculated from those of AL_{ind} given by Kollmann by dividing by $A = 1/427$; L_{pol} was calculated from equation (4a), and from the values of g_0 and g_v in Table VI; those of $\eta_{c\ ind}$ were obtained as given in Table VIII.

TABLE VIII

Test No.	L_{ind} *mkg/kg*	L_{pol} *mkg/kg*	$\frac{1}{\eta_{ind}}$	$\frac{1}{\eta_{c\ ind}}$	$\eta_{c\ ind}$
1	16800	14910	1.127	1.091	0.917
2	16600	14850	1.118	1.085	0.921
3	16650	14750	1.129	1.088	0.920
4	16600	14500	1.145	1.101	0.909
5	16400	14130	1.160	1.111	0.900
6	13700	12510	1.095	1.072	0.932
7	14140	12720	1.111	1.082	0.923
8	14190	12680	1.119	1.088	0.920
9	13860	12400	1.118	1.088	0.922
10	13800	11870	1.163	1.120	0.894
11	10540	9830	1.071	1.059	0.944
12	10630	9640	1.103	1.082	0.924
13	10580	9700	1.089	1.070	0.935
14	10400	9600	1.082	1.067	0.938
15	10320	9550	1.082	1.067	0.938
16	8160	7400	1.102	1.088	0.920
17	8100	7530	1.077	1.063	0.939
18	8180	7540	1.085	1.070	0.935
19	8050	7410	1.086	1.071	0.934
20	8050	7430	1.084	1.072	0.933
21	5680	4440	1.280	1.239	0.807
22	5620	4530	1.241	1.205	0.829
23	5710	4560	1.252	1.213	0.823
24	5470	4570	1.198	1.167	0.857
25	5490	4650	1.180	1.152	0.868
26	17600	15620	1.126	1.092	0.915
27	17410	15420	1.129	1.091	0.917
28	17410	15300	1.139	1.101	0.908
29	17200	15300	1.124	1.091	0.917

Figure 6 shows $\eta_{c\ ind}$ plotted against Π, and it is seen that here, too, the points fall very closely on a continuous line, i.e. that $\eta_{c\ ind}$ is a function of Π only. Larger deviations (apart from test No. 10) occur only at the lowest pressure-ratio $\Pi = 1.65$, and as a result the graph curves downwards in the right direction, to reach zero at $\Pi = 1$. From the form of the graph, the two factors which tend to increase the work can be determined: the valve losses are the determining factor at small pressure-ratios, whereas the non-polytropic character of the compression, due to the varying

temperature differences between air and cylinder walls, becomes more and more pronounced with increased pressure-ratios, at which the percentage of the valve losses grows smaller and smaller. A maximum of $\eta_{c\,ind}$ is reached, therefore, at an intermediate value of $\Pi \sim 2.4$, with $(\eta_{c\,ind})_{max} \sim 93.5\%$.

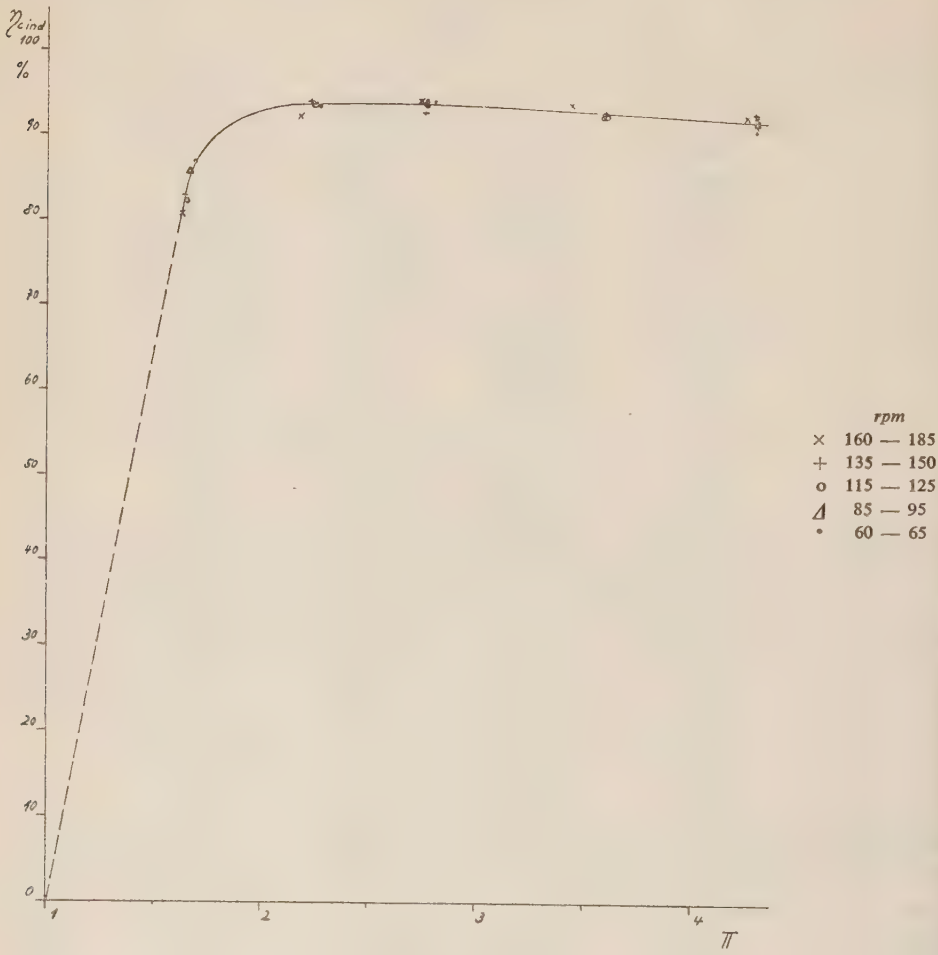

Figure 6

CONCLUSIONS

The polytropic work required to compress air from the pressure p_e and temperature T_{em}, as given by eq. (1) and (1a), to the pressure p_2^* and temperature T_4 is given by eq. (4a). A clearer picture of the factors affecting it can be obtained by writing

$$L_{pol} = R \ln \Pi \frac{\Delta T}{\ln \theta} \sim 2.303\, R \log \Pi \frac{T_{em} + T_4}{2} = 1.151\, R \log \Pi \left(T_{em} + T_4 \right) \quad (4b)$$

By substituting the arithmetic mean for the logarithmic, an error of less than 1% is introduced with the relevant values of θ. This can also be written:

$$L_{pol} \sim 1.151\, R\, T_{em} \log \Pi (1 + \theta) = 33.7\, T_{em} \log \Pi (1 + \theta) \qquad (4c)$$

so that the variables are separated. T_{em} is given by T_e and T_e'[eqs. (1) and (1a)], whereas θ is a function of Π and n only and can be calculated by eq. (9) once the constants C_1 and β have been determined for the compressor. Further experiments are required in order to show the values of these constants for different compressors and to determine whether certain types of compressors may be found for which equal values can be assumed. Since θ will be greater with smaller values o C_1 and of $\alpha = 1/\beta$ and vice versa, these constants will characterize the efficiency of cooling during compression, and equality of constants for different compressors would mean equal cooling-efficiency. Further tests will be required at higher speeds, in order to determine whether the value of $\varkappa^* = 1.6$, on which eq. (9) is based, will also hold under these conditions, or whether another (probably higher) value should be substituted instead. With all this additional information obtained, eq. (4c) will give a very complete and clear idea of the increase of L_{pol} caused by higher T_e (e.g. as a result of incomplete intercooling before the stage in question), by higher T_e' and n, or by poorer design resulting in limited heat transfer during compression.

Not quite as simple and clear are the relations between the variables and the indicated work which is given, by eq. (19) and (19a), as:

$$L_{ind} = L_{pol} \frac{1}{\eta_{ind}} = L_{pol} \frac{g_0/g_v(1 - \eta_{c\ ind}) + 1}{\eta_{c\ ind}} \qquad (20)$$

Here, g_0 is given by eq. (11a), where the factor λ_0 is put equal to 1 if the pressure-difference $p_2^* - p_e$ is greater than some critical value (2.7 at. in this case, but not necessarily the same for other compressors, in view of its dependence on the mass of the valves etc.), and greater than 1 below this critical value. g_v is found from $g_0 + g_v$, which, for given values of p_e and T_{em}, is determined by equation (10a). The temperature-increase Δt was found to be a function o Π only, and can be calculated by equation (13), once the constants of this equation have been found by tests with the compressor under consideration. Here again, the question to be answered by further tests is whether, and to what extent, the design of different compressors will affect the value of these constants. Also, the last factor in the determination of L_{ind} and $\eta_{c\ ind}$ was found to be dependent on Π only. This complex relation, determined by the combined effect of two entirely different factors, was not formulated analytically, but only graphically. Here, too, further tests must show the course of this curve for different compressors. It seems, however, quite possible that, since the differences in design and cooling-efficiency were already taken into account in the determination of L_{pol} and Δt one common curve of $\eta_{c\ ind}$ will be applicable with sufficient accuracy to compressors of any type.

In order to show with which degree of accuracy the performance of an air-compressor can be predicted for different working conditions with its characteristic constants determined by experiment, Table IX was prepared. It gives, for the three tests for which the indicator diagrams are given at the end of Kollmann's paper, the calculated values of T_4, g_v, and L_{ind}, their measured values, and the percentage deviation of the measured values. It is seen that the agreement is very close indeed.

TABLE IX

Test No.	1			5			21			
T_e	295.3			285.8			292.6			°K
T'_e	281.8			281.8			282.8			°K
p_e	4.45			4.40			3.67			ata
p_2^*	18.98			18.98			5.97			ata
n	163.2			62.91			164.6			rpm
	calcd.	measrd.	dev.	calcd.	measrd.	dev.	calcd.	measrd.	dev.	
Π	4.27			4.31			1.627			
T_{em}	290.2			284.5			292.6 (corr)			°K
θ	1.442			1.330			1.311			
T_4	418.5	420.2		378.4	382.3		330.9	331.3		°K
			—0.4			—1.0			—0.1	%
Δt	23.2			23.4			7.8			°C
λ_0	1.0			1.0			1.15			
$1000\, g_0$	3.78			4.17			1.73			kg
$1000\, g_v$	9.47	9.39		9.15	9.20		9.65	9.60		kg
			+0.9			—0.5			+0.5	%
$\eta_{c\ ind}$	0.912			0.911			0.806			
L_{pol}	14920			14080			4440			mkg/kg
η_{ind}	0.881			0.875			0.870			
L_{ind}	16950	16800		161	16400		5690	5680		mkg/kg
			+0.9			—1.8			+0.2	%

APPLICATION TO OTHER TYPES OF COMPRESSORS

As explained above, it was of interest to find out whether the results obtained for a compressor of conventional design were also applicable to other types of compressors.

For this purpose, tests were carried out at the Mechanical Engineering Laboratory of the Israel Institute of Technology, Haifa, with a Unicylinder Two-Stage Monobloc Compressor, manufactured by Messrs. Browett-Lindley Ltd., Letchworth, Herts., England. This compressor differs from the conventional design of two-stage compressors in several respects.

Although the two stages are in the same cylinder, the first one below the piston and the second above it, the same piston area is used for both, instead of the differential piston design usually found in such cases. With the piston displacement equal in both stages (or even smaller in the first one, due to the piston-rod), other means have to be applied to reduce the effective stroke volume of the second stage in accordance with the reduced air volume at the intermediate pressure; this is achieved by enlarging the clearance space of the second stage to about twice that of the first stage.

Into this enlarged clearance space, cooling fins protrude from the water-jacketed cylinder head, thus providing a larger cooling surface than usual in the second stage,

whereas the cylinder head of the first stage is formed by the thick castings of the body and the stuffing box assembly, and not water-cooled at all.

It is to be expected that these differences in design, clearance volume, etc., will directly affect the performance of both stages and, therefore, be reflected in the results of calculations similar to those made above.

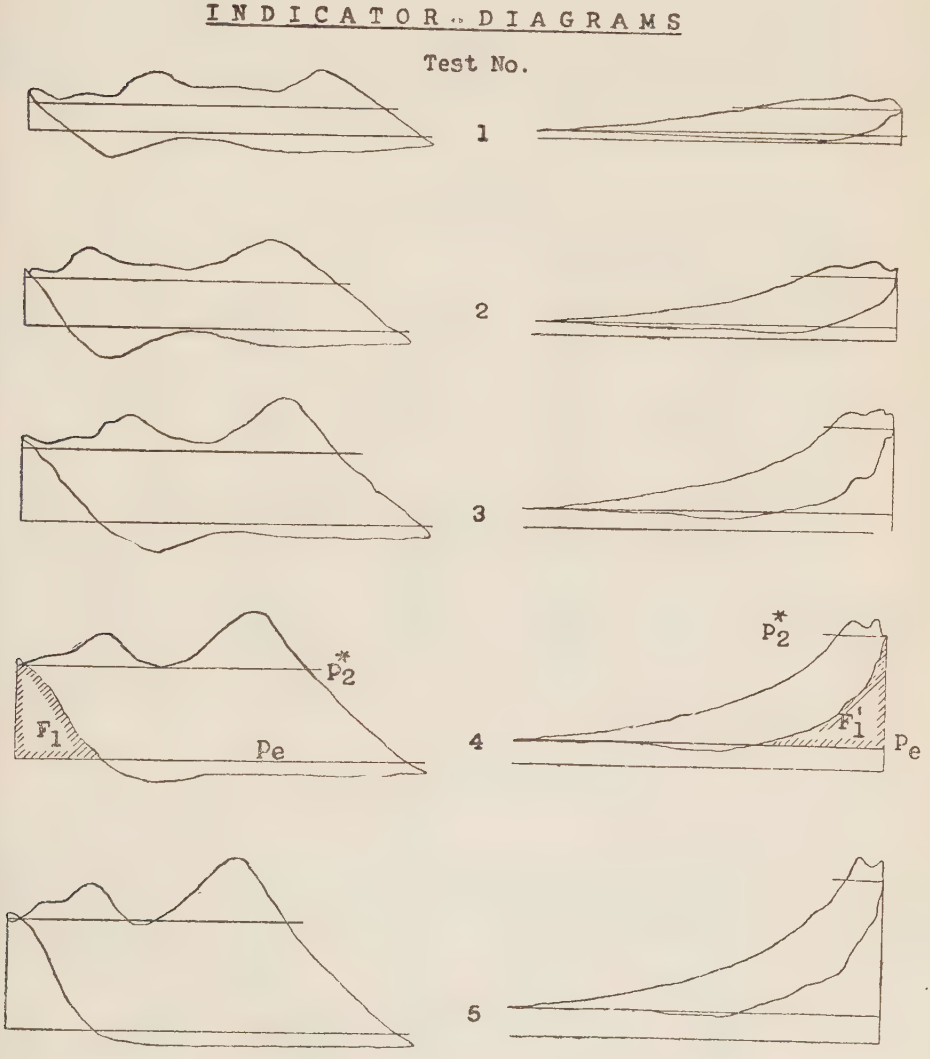

Figure 7

The tests for these calculations were carried out on January 5th, 1953. The compressor was driven by a three-phase induction motor, with very slight variation of speed. Measurements of temperatures and pressures were carried out by means of five different openings of the throttle-valve connecting the air-receiver with the atmosphere, with several readings taken at each load and the arithmetic mean used for the calculations. Indicator diagrams were taken for both stages with ordinary drum- and pencil-type engine indicators with outside springs. Average diagrams for each pressure are shown in Figure 7.

Tables X and XI give the calculations of k for the two stages. The same notation as above was used to denote the different temperatures and pressures.

TABLE X

First stage

Test No.	1	2	3	4	5	
n	472	470	466	463	459	rpm
p^*	1.30	1.50	1.77	1.98	2.17	ata
p_e	1.03	1.03	1.03	1.03	1.03	ata
log p^*	0.1139	0.1761	0.2480	0.2967	0.3365	
log p_e	0.0128	0.0128	0.0128	0.0128	0.0128	
log Π	0.1011	0.1633	0.2352	0.2839	0.3237	
T_4	332.3	345.0	359.3	372.6	383.3	°K
T_e	296.3	297.3	299.3	300.7	302.3	°K
T_e'	293.0	294.0	294.0	294.0	295.0	°K
T_{em}	295.2	296.2	297.5	298.5	299.9	°K
log T_4	2.5215	2.5378	2.5555	2.5712	2.5835	
log T_{em}	2.4701	2.4716	2.4735	2.4749	2.4770	
log θ	0.0514	0.0662	0.0820	0.0963	0.1065	
log Π / log θ	1.96	2.47	2.86	2.95	3.04	
k	2.04	1.68	1.54	1.51	1.49	

TABLE XI

Second stage (speeds as above)

Test No.	1	2	3	4	5	
p_2^*	2.49	3.63	5.33	6.73	7.83	ata
p_e	1.30	1.50	1.77	1.98	2.17	ata
log p^*	0.3962	0.5599	0.7267	0.8280	0.8938	
log p_e	0.1139	0.1761	0.2480	0.2967	0.3365	
log Π	0.2823	0.3838	0.4787	0.5313	0.5573	
T_4	351	370	392	408	422	°K
T_e	312	319	329	337	344	°K
T_e'	293	294	294	294	295	°K
T_{em}	305.7	310.7	317.3	322.7	327.7	°K
log T_4	2.5453	2.5682	2.5933	2.6107	2.6253	
log T_{em}	2.4853	2.4923	2.5015	2.5088	2.5155	
log θ	0.0600	0.0759	0.0918	0.1019	0.1098	
k	1.27	1.25	1.24	1.24	1.25	

a) *Second stage* (*Table* XI). Here, as before, the values of k are fairly constant, as should have been expected for nearly constant speed. This is true even at pressure-differences $p_2^*-p_e$ as low as 2.13 at. (test 2), and also in test 1, for which $p_2^*-p_e = 1.19$ at., the increase of k is much less than in the previous example. This shows that in this case the dynamic conditions at air discharge result in a lower critical pressure-difference, below which after-vibrations are induced; when they ensue and lead to the reentrance of a certain amount of air into the cylinder, the effect is reduced by the relatively larger volume of the clearance space. While earlier it has been assumed that the increased weight of expanding air would completely counteract the effect of the water-temperature on T_{em}, and, therefore, $T_{em} = T_e$, in this case the difference will be far smaller. For instance, in order to obtain a value of $k = 1.25$ also for test 1, $T_{em\ corr}$ is to be assumed 307.8 °K, or higher than T_{em} by only one third of (T_e-T_{em}).

With an average value of $k = 1.245$ it follows from equation (9):

$$\frac{C_1}{n^\beta} = \frac{k}{k-1} - 2.67 = 2.40,$$

whereas for the compressor tested by Kollmann it would be, for an average speed of 466 rpm:

$$\frac{C_1}{n^\beta} = \frac{38.8}{466^{0.667}} = 0.644, \quad \text{or} \quad k = 1.430.$$

Although the practically constant speed does not permit the separate determination of the constants C_1 and β in this case, the improved cooling by the enlarged surface is also clearly demonstrated by the increase of the whole expression C_1 / n^β.

It shall now be ascertained whether the use of the equations will give a clearance space of approximately the right volume, which should, of course, be the same for all five tests.

By eq. (3a): $L_{e\ ind} = F_1 / g_0$, which, by combining it with eq. (11), gives

$$V_c = \frac{R T_4}{\lambda_0 p_2^*} \frac{F_1}{L_{e\ ind}} = \frac{\eta_{e\ ind}}{\lambda_0} \frac{R T_4}{p_2^*} \frac{F_1}{L_{pol}} \tag{21}$$

Since F_1 is not known as long as the clearance volume V_c is not given, it has to be replaced by $F_1' = F_1 - V_c(p_2^* - p_e)$, which is the diagram area between the vertical through the dead centre, the expansion curve, and the pressures p_2^* and p_e. It follows:

$$V_c = \frac{F_1'}{p_e + p_2^* \left(\frac{\lambda_0}{\eta_{e\ ind}} \frac{L_{pol}}{R T_4} - 1\right)} \quad (\mathrm{m}^3) \tag{22}$$

and the percentage clearance

$$\varepsilon_0 = \frac{V_c}{V_h} 100 \quad (\%) \tag{22a}$$

in which the piston displacement V_h is given by the dimensions of the compressor:

Piston diameter 10.5 ″

Piston-rod diameter: 1.75 ″

Piston stroke: 5.5 ″

$V_h = 0.00762$ m³ for the first stage

$V_h = 0.00783$ m³ for the second stage.

The values were calculated and collected in Table XII, by putting again $\lambda_0 = 1$ and $\eta_{e\,ind} = 1$. It is seen that the values are of approximately the right magnitude to be expected for a clearance space of about twice the normal volume, and that they are fairly constant, with the exception of test 1. It is shown in the table that, if in accordance with the correction made in T_{em} for this test the increase in air weight is also taken as only one-third of that assumed in the former case (5% instead of 15%), or $\lambda_0 = 1.05$, the clearance will be about the same for this test as for the others. It should not, however, be forgotten, that the calculated value of V_c is proportional to the very small area F_1' which, for test 1, was found to be 20 mm². The planimeter was used with the shortest length of the tracer arm, for which one unit of the vernier represents 4 mm². Since again an error of ±1 vernier-unit must be allowed for, it is seen that in this case

TABLE XII

Second stage

Test No.	1	2	3	4	5	
F_1'	0.20	0.40	0.94	1.28	1.74	cm²
	5.04	10.08	23.2	32.3	43.0	mkg
T_4	351	370	392	408	422	°K
T_{em}	305.7	310.7	317.3	322.7	327.7	°K
ΔT	45.3	59.3	74.7	85.3	94.3	°C
$\log \Pi / \log \theta$	4.71	5.05	5.21	5.23	5.09	
L_{pol}/RT_4	0.609	0.809	0.990	1.093	1.138	
$p_e + p_2^*(L_{pol}/RT_4 - 1)$	3220	8070	16947	26060	32500	kg/m²
$1000\ V_c$	1.57	1.25	1.37	1.24	1.32	m³
ε_0	20.0	16.0	17.5	15.9	16.9	%
$T_{em\,corr}$	307.8					°K
$\log T_{em\,corr}$	2.4883					
$\log \theta_{corr}$	0.0570					
$\log \Pi / \log \theta_{corr}$	4.96					
k_{corr}	1.25					
$(\Delta T)_{corr}$	43.2					
$1.05\ (L_{pol}/RT_4)$	0.641					
Denominator	$4030 = p_e + p_2^*\left(1.05\ (L_{pol}/RT_4) - 1\right)$					kg/m²
$1000\ V_c$	1.25					m³
ε_0	16.0					%

the calculated value of V_c may be inaccurate by as much as $\pm 20\%$. The correction by introducing $\lambda_0 = 1.05$ has, therefore, to be regarded as merely tentative, to show that the corrections for equal values of k and of V_c, to be applied to tests below the critical pressure-difference, point in the same direction, rather than as an exact calculation of the weight of the air which returns to the cylinder during the after-vibrations of the discharge valve.

b) *First stage.* Table X shows that the values of k are far from constant if based on values of T_{em} calculated from eq. (1a). This is partly due to the fact that here, for all tests, the pressure-difference $p_2^* - p_e$ is below the critical value, but in addition the thick metal mass of the uncooled cylinder head tends to accumulate and store some heat from the entire surroundings, and thus forms an additional factor bearing on T_{em}.

In order to estimate this effect, we have to abandon in this case the previous definition of T_{em} as determined by the temperatures of air and cooling-water alone, and start from the assumption that here, too, k should be constant if based on the right values of $T_{em\ corr}$.

The approximation represented by eq. (4b) gives an easy means of finding the values of $T_{em\ corr}$ satisfying this requirement, provided it is assumed in addition that the difference $T_{em\ corr} - T_{em}$ will be the same for all tests. For this approximation means that the logarithmic curves of the isobars and polytropics are replaced by straight lines in the T—S diagram, and thus for constant k the straight lines connecting T_4 and $T_{em\ corr}$ for each test should be parallel and form, with the negative direction of the abscissae, the angle φ given by the relation

$$\tan \varphi = -\frac{\Delta T_4 - \Delta T_{em}}{\Delta S_4 - \Delta S_{em}} \tag{23}$$

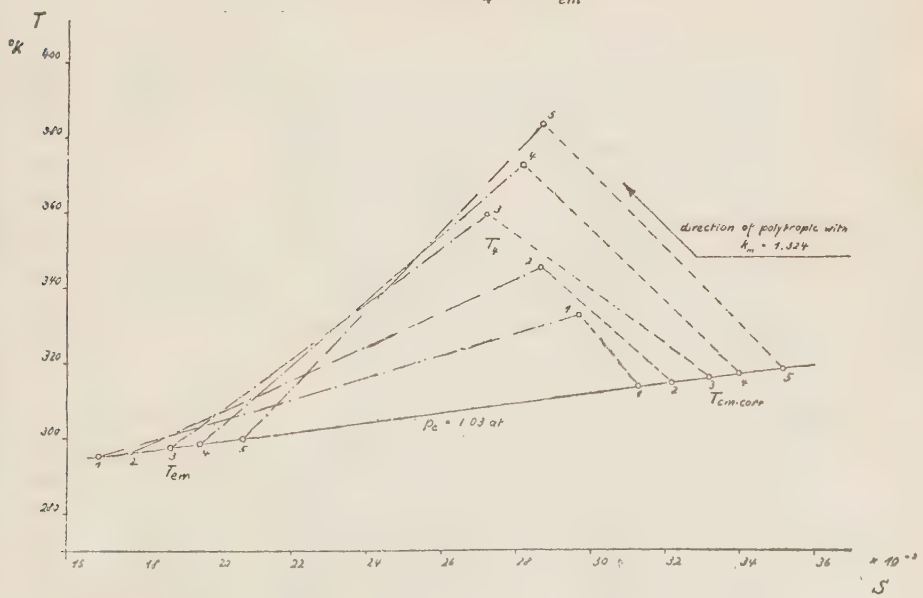

Figure 8

in which ΔT and ΔS are the respective differences of temperatures and entropies for corresponding points of any two tests. The results of these calculations are given in Table XIII. The entropies were taken with 1 at. and 273°K as basis, tan φ calculated for the four differences between any two consecutive tests, and the arithmetic mean taken of the four angles thus determined; its tangent gives the required direction (φ_m).

Figure 8 shows a graphical representation of these relations, but, since the scale of the abscissae was enlarged a thousand times, the angles φ, which are in reality very close to 90°, do not appear in this diagram in their true size.

$T_{em\ corr}$ can now be found for any one of the tests, either graphically, by finding the intersection of a line of the right direction through point T_4 with the isobar p_e, or analytically, from the relation

$$\frac{T_4 - T_{em\ corr}}{\tan \varphi_m} = A R \ln \Pi - c_p \ln \theta_{corr} \sim AR \ln \Pi - 2c_p \frac{T_4 - T_{em\ corr}}{T_4 + T_{em\ corr}}$$

which results in the quadratic equation:

$$T_{em\ corr} = -\frac{X}{2} \tan \varphi_m \pm \sqrt{\frac{X^2}{4} \tan^2 \varphi_m + T_4 (T_4 + Y) \tan \varphi_m} \qquad (24)$$

where $X = 2c_p + A R \ln \Pi$ and $Y = 2 c_p - A R \ln \Pi$, with only the positive sign before the root valid.

TABLE XIII

First stage

Test No.	1	2	3	4	5	
S_4	0.02956	0.02860	0.02719	0.02812	0.02867	kcal/kg °C
S_{em}	0.01683	0.01769	0.01873	0.01951	0.02069	"
ΔS_4	—0.00096	—0.00141	+0.00093	+0.00055		"
ΔS_{em}	+0.00086	+0.00104	+0.00078	+0.00118		"
ΔT_4	12.7	14.3	13.3	10.7		°C
ΔT_{em}	1.0	1.3	1.0	1.4		°C
tan φ	6420	5300	82000	14750		
φ—90°	—32.1	—38.9	+2.5	—14.0		sec
$[\varphi$—90°$]_m$			—20.6			sec
tan φ_m			10013			
$T_{em\ corr}$	313.7	314.7	316.0	317.0	318.4	°K
$S_{em\ corr}$	0.03125	0.03211	0.03315	0.03393	0.03511	kcal/kg °C
log $T_{em\ corr}$	2.4965	2.4979	2.4997	2.5011	2.5030	
log θ_{corr}	0.0250	0.0399	0.0558	0.0701	0.0805	
log Π/log θ_{corr}	4.00	4.10	4.20	4.04	4.02	
k	1.33	1.32	1.31	1.33	1.33	

This equation was applied to test 5 and gave $T_{em\ corr} = 318.4°K$ for this test, or $T_{em\ corr} - T_{em} = 18.5°K$, from which $T_{em\ corr}$ was found for the other tests. They are given, together with the values of k resulting from them, in Table XIII. k is fairly constant, as was to be expected, with an average value of 1.324, corresponding to $C_1/n^\beta = 1.41$, which is somewhat higher than the value 0.644 previously found for the compressor with normal water-cooling of walls and head. It can, therefore, be concluded that owing to the massive uncooled cylinder head the temperature T_{em} is raised as it would be by higher temperatures of the incoming air and/or cooling-water. Since, however, this heat accumulator tends at the same time to equalize temperatures and thereby decrease the last factor of eq. (4c), its effect on the polytropic work is far less unfavourable than it would be for a similar increase of T_{em} caused by one of the other factors.

If in this case, too, the clearance volume V_c and the percentage clearance ε_0 are calculated with the assumption of $\lambda_0 = 1$ and $\eta_{e\ ind} = 1$ (Table XIV), values are obtained which are not constant and several times the correct magnitude. Other values must, therefore, be substituted for λ_0, and probably also for $\eta_{e\ ind}$, since the equality of $L_{e\ ind}$ and L_{pol}, which was shown to hold for compressor-stages with water-cooled walls and heads, must not necessarily hold also in this case of different design.

As the indicator diagrams of this stage show, the pressure falls more slowly than usual with beginning reexpansion, with or without the formation of loops above the discharge-pressure curve. This would seem to indicate a considerable time-lag in the closing of the discharge-valve, resulting in a high percentage of reentering air. Before drawing such conclusions it was, however, considered advisable to ascertain whether the expansion curve represents the actual pressures inside the cylinder, and to what extent the indicator, working at elevated speed and with a relatively weak spring, might be responsible for distortions.

For test 5, therefore, the pressure-time diagram was plotted, and the velocities and accelerations of the indicator-piston found by repeated graphical differentiation. The maximum velocity $v_{max} = 46.3$ mm/sec was found at a pressure of about 1.5 ata, the maximum acceleration $a_{max} = 7.12$ m/sec^2 at approximately 2 ata and the maximum deceleration $d_{max} = 8.9$ m/sec^2 at a pressure of about 1.25 ata. The weight of the vibrating masses, assumed to be concentrated in the piston, was estimated to be 0.05 kg, and from it the inertia forces were calculated, reaching the respective maxima of 0.036 kg upward and 0.045 kg downward at the points of maximum acceleration and deceleration. To these inertia-forces the frictional resistance determined by static tests (0.036 kg) was algebraically added, giving a maximum of 0.072 kg at the point of maximum acceleration. Divided by the piston area (0.5 sq.in.) and multiplied by the scale of the spring (18 mm/at.), these algebraic sums give, neglecting the molecular damping of the system for this purpose, the vertical distances by which the curve drawn by the indicator deviates from the real cylinder pressures at every moment. The maximum of these deviations was accordingly found to be 0.4 mm upward, or about 2.2% of the gauge pressure at this point, and also the total area F_1' was found too large by about the same percentage. This value alone is below the limit of inaccuracy entailed in the measurement of this area by planimeter; besides, the inertia effects of the drum which must be accelerated from rest at dead centre will tend to decrease the size of the recorded area, and thereby counteract the inertia effect of the piston system on the diagram.

It can therefore be concluded that the error introduced by the inertia effects of the indicator is, even at this speed, smaller than the unavoidable inaccuracy in measuring the area.

Since, on the other hand, nothing is known about the values which should reasonably be assumed for λ_0 and $\eta_{e\ ind}$ in this case, the values of $\lambda_0 / \eta_{e\ ind}$ were calculated (see Table XV) which would correspond to a clearance of 8%, showing them to be between 1.6 and 2, i.e. considerably higher than the values found so far.

As long as these two factors cannot be separated, it cannot be stated with certainty which of them contributes more to this increase. Theoretically it is possible to find an expression for λ_0 alone from the shape of the expansion curve, and it is now being ascertained whether this method can provide practical results with sufficient accuracy.

It should be expected that in this case λ_0 will be obtained somewhat smaller than $\lambda_0 / \eta_{e\ ind}$, or $\eta_{e\ ind} < 1$.

TABLE XIV

First stage

Test No.	1	2	3	4	5	
F_1'	0.22	0.40	1.04	1.54	1.96	cm²
	1.24	2.36	5.78	8.55	10.91	mkg
ΔT	18.6	30.3	43.3	55.6	64.9	°C
$L_{pol} / R T_4$	0.224	0.360	0.506	0.604	0.680	
$p_e + p_2^* (L_{pol}/RT_4 - 1)$	250	680	1580	2460	3360	kg/m²
$1000\ V_c$	4.95	3.47	3.66	3.48	3.25	m³
ε_0	65.0	45.5	48.1	45.7	42.7	%

TABLE XV

First stage

$$\frac{\lambda_0}{\eta_{e\ ind}} = \frac{F_1' / V_c + (p_2^* - p_e)}{p_2^* L_{pol} / RT_4}$$ for an estimated value of $V_c = 0.08$, $V_h = 0.00061$ m³

Test No.	1	2	3	4	5	
F_1'/V_c	2040	3870	9480	14010	17900	kg/m²
$p_2^* - p_e$	2670	4710	7380	9500	11400	kg/m²
$p_2^* (L_{pol} / R T_4)$	2910	5400	8950	11960	14760	kg/m²
$\lambda_0 / \eta_{e\ ind}$	1.63	1.59	1.89	1.97	1.99	

ACKNOWLEDGMENT

The author wishes to express his thanks to Professor S. Frank, A.M.I.Mech.E., Chairman of the Division of Power and Heat Engineering, Israel Institute of Technology, Haifa, for his kind interest and the valuable suggestions given for the completion of this paper.

REFERENCES

1. Kollmann, K., 1931, Der Wärmeübergang im Luftkompressor, *Ver. dtsch. Ing., Forschungsh.*, **348.**
2. Carpenter and Diedfrichs, 1911, *Experimental Engineering*, John Wiley & Sons, New York, 7th ed., p. 41.

SYMBOLS AND UNITS USED

C, C_1, C_2, C_3	Design constants of compressor	
F, F_1, F_2	Areas in P—V diagram	mm² or mkg/cycle
G	Weight of air	kg
g_0	Weight of air in clearance	kg/cycle
g_v	Weight of air delivered	kg/cycle
k	Exponent of polytropic	
L_{ind}	Indicated work	mkg/kg
L_{pol}	Polytropic work	mkg/kg
n	Speed of rotation	rpm
P	Pressure	kg/m² (abs.)
p_e	Air inlet pressure	kg/cm² (abs.)
p_2^*	Air discharge pressure	kg/cm² (abs.)
R	Gas constant of air	m/°C
S	Entropy	kcal/kg °C
t	Temperature	°C
T_e	Inlet remperature of air	°K
T_e'	Inlet temperature of water	°K
T_4	Discharge temperature of air	°K
V_c	Clearance volume	m³
V_h	Piston displacement	m³
α, β	Design constants of compressor	
η_{ind}	Indicated efficiency based on polytropic	
$\eta_{c\ ind}$	do., for compression alone	
$\eta_{e\ ind}$	do., for reexpansion alone	
θ	Temperature ratio of polytropic process	
$\varkappa$	Exponent of reversible adiabatic compression	
$\varkappa^*$	Exponent of real (irreversible) adiabatic compression	
λ	Volumetric efficiency	
Π	Pressure ratio of polytropic process	

SYMPOSIUM
ON MAGNESIUM COMPOUNDS

Held at Jerusalem, March 31, 1955

OPENING REMARKS

S. A. Abrahams

Consulting Engineer, Berkeley, California

It is a deep personal pleasure and privilege for me to participate with you in this Symposium on Magnesia Compounds in Israel. I am particularly grateful to the Minister of Development, the Honourable Dov Joseph, for both his invitation and his full cooperation and assistance in the work connected with my survey.

Not only was I impressed with the excellent facilities available for both fundamental and applied research, but also with the wealth of work and knowledge in the chemistry of magnesium compounds. The warmth of my reception and the wide inrerest in this field were most gratifying. As I continued my inspection tour I became increasingly convinced of the necessity of mutually sharing this knowledge and experience in the field of magnesium compounds.

If I may be permitted to digress for a moment, it must be apparent that the continued development and growth of the State of Israel will depend primarily on its indigenous human resources. Granted that special skills, knowledge and "know-how" may be occasionally imported for specific problems, the eventual outcome will be dependent on local talent. It is my hope that I shall be able to serve as a catalyst to bring together the knowledge, experience and skills which I have found in great abundance here and to help you formulate a sound and constructive policy for the exploitation of the magnesium resources of Israel.

That is the principal reason for this meeting. In several instances I found that some workers in this field were unaware of the prior investigations that had been made. Furthermore, there were sharp divisions as to methods, processes and the best means of developing these resources. Since the need is urgent and the country's resources limited decisions must be made quickly on methods and processes for maximum development of mineral resources. We hope that, following this meeting, those who have further knowledge in this field will come forth and assist in the program.

The courage, energy and devotion to the ideal that founded this dynamic state will, I am sure, also contribute to the full development of all of its resources.

Now to return to the development of processes for the recovery of magnesium values from the Dead Sea, which was my original assignment. It became increasingly evident following my tour of the country that not only were there other important sources, but also several interesting processes for the extraction of commercial products from these sources were possible.

Magnesium, as you all know, is one of the most abundant of the elements of the earth's surface. The most important ores are dolomite, of which whole mountain chains are composed, magnesite, brucite and carnallite. In addition, sea water has become in the last 15 years an important source for magnesium metal and compounds.

Bull. Res. Counc. of Israel, Vol. 5C, 1955.

In the United States, five major companies are extracting upwards of 800 tons of magnesia per day from the sea. The sea water process has become the principal source for magnesium metal as well as for many special compounds of magnesium, aside from a minor production from magnesium brine wells. Dolomite is also still widely used as a source for magnesium compounds. It is also the primary reactant in the sea water process for the precipitation of magnesium hydroxide. The Pattison process using dolomite, which was developed in England nearly a century ago, is still basically employed for the preparation of magnesium compounds in the United States and Great Britain.

Israel particularly abounds in magnesium resources. There are a number of factors that will influence the decision to exploit any given raw material source. Availability of low cost power, fuel, water, transportation, markets, not to mention political considerations, all must be properly evaluated.

You are all familiar with the great potential mineral wealth of the Dead Sea. The uniqueness of its composition definitely offers a challenge to our ingenuity and resourcefulness. The pioneer work and achievements of Dr. Novomeysky and his associates in the exploitation of the potash values can well serve as an inspiration for the development of new recovery processes.

In connection with the growth and development of the magnesia industry in the United States, I should like to offer a few personal comments and observations from my association with this industry for almost thirty years. For some inexplicable reason we have not witnessed either the intensive research or growth that other industries have had in the last quarter century.

Last year, together with an associate, we conducted a market survey for the higher priced magnesia chemicals. We excluded the refractory and agricultural grades from our analysis. In the heavy calcined magnesia field we estimated a production of 50,000 tons valued at approximately $ 5,000,000. We believe it reasonable to state that, if one third as much effort had been expended on the development of products and uses of heavy calcined magnesia as has been expended for products such as calcium carbonate, this figure would have increased three-fold to 150,000 tons.

In the light magnesia field approximately 4,000 tons were consumed at an average selling price of around $ 500 a ton, or 25 cents a lb. Here again there exists an opportunity for expanding the use of this highly reactive magnesia.

Take again the field of normal and basic magnesium carbonates. Fifteen years ago we discovered the self-setting properties of a normal magnesium carbonate and developed the precision molded process for the production of 85% magnesia, which is the world's leading heat insulating material in the temperature range from 40° to 325°C. It represents a $ 50,000,000 industry annually in the United States. Today 4 of the 6 major heat insulating manufacturers are using the precision self-set process.

Basically this process involves the preparation of needle-like crystals of normal magnesium carbonate, setting the carbonate mixed with asbestos fibres in a machined mold, extruding the set product and then drying in conventional ovens. Remarkably, the set product which contains over 85% water dries substantially without shrinkage. This process permitted for the first time the production of magnesia insulations

without final milling or machining to precise dimensions. In addition it was possible to control the density to approximately 11 lbs/ft^2, thus producing a more efficient and uniform insulating product.

I wish to emphasize that even this property of normal magnesium carbonate has not been fully exploited in the United States or elsewhere in the world, to the best of my knowledge.

In discussing this reaction with some of your chemists I learned that many years ago in Germany an interesting process had been developed using carnallite and normal magnesium carbonate and carbon dioxide gas. This process will produce potassium carbonate, an important chemical. Difficulties were encountered due to the variation in activity of the magnesium carbonate. It is possible that the techniques we had developed in the United States could be instrumental in solving the technical difficulties of this process. The need for converting the magnesium chloride of the Dead Sea to a hydroxide or oxide led to the study of the process of decomposing the chloride directly into magnesium oxide and chlorine or hydrochloric acid.

In searching for a cheap and conveniently located source of either limestone or dolomite, as a precipitant for the magnesium chloride in the Dead Sea, I learned of the work on bituminous limestone shale. Dr. Feilchenfeld has studied this problem and Mr. Clark is directing further pilot plant investigations. There is a possibility we could use the calcined product as a means of recovering magnesium hydroxide from the Dead Sea.

While inspecting the laboratory facilities of the Israel Mining Industries, I observed the work of Dr. Schächter in producing bromine directly from Dead Sea brines and from magnesium hydroxide. This offers another possibility of producing a high purity magnesium oxide suitable for special uses.

An exciting visit next door to the Chemicals and Fertilizers laboratories and engineering division further enhanced my appreciation of the growth and development of the research and engineering facilities of Israel. Later I was conducted by Mr. Molleson through the present and future production facilities which were in the process of construction. To my pleasant surprise I learned that he had worked on the engineering of the sea water magnesium extraction plant in England. Mr. Goldberg had directed the operations of this plant as well as visited most of the sea water plants in the United States.

From Dr. Ben-Tor and his staff at the Geological Institute we sought the location of suitable deposits of dolomite and limestone.

From Dr. Bloch, whose mind is a veritable storehouse of information and ideas, I learned much of the early developments for the extraction of chemicals from the Dead Sea. He has been most helpful in my investigations.

As you now can well see, there are definite interlinkages in the whole study of the magnesium resources of the State of Israel. This conference should serve as a springboard for a more intense investigation to determine the most practical course to pursue.

Dr. Markowicz will discuss the present and potential use of magnesium compounds as well as export markets that may be available for these products.

We have not included the production of salt, either from the brines of the Dead Sea, or the ocean waters of the Mediterranean on the Gulf of Eilat, since further investigations are still in progress. However, it has become clearly evident that it would be desirable to enlarge the solar salt producing facilities in the Haifa area. Low cost salt in this area would be a boon to the budding electrochemical industries as well as provide the economic basis for a future soda ash plant.

The bitterns from these solar salt works would then become an important source of magnesium compounds. Availability of low cost soda ash or tronas from alkali lakes in the Middle East could lead to interesting processes for the production of magnesium compounds from bitterns.

The wide variety of available processes coupled with the wide range of suitable material resources make it mandatory that a thorough study be made of all the factors involved.

WATER SOLUBLE MAGNESIUM COMPOUNDS IN ISRAEL

M. R. Bloch

Mifalei Yam Hamelach, B. M., Beersheba

Sources for water soluble magnesium compounds in Israel are 1) ocean water (Mediterranean Sea and Gulf of Eilat), 2) Dead Sea water, 3) Tiberias hot springs and possibly other wells.

Ocean water

Ocean water contains 4.6 g/lit $MgCl_2$ and 2.6 g/lit $MgSO_4$. When treated with $Ca(OH)_2$, $Mg(OH)_2$ is precipitated. The washing process of the adhering brine is rather difficult. If the $Mg(OH)_2$ is to be converted into carbonate by CO_2, this washing is required to prevent formation — by any remaining Ca ions — of $CaCO_3$ which is considerably less soluble than $MgCO_3.3H_2O$. Any admixture of $CaCO_3$ and $MgCO_3$ compounds is undesirable for use as a heat insulator or filler because the product is heavier, and for use in refractories because of reduced fusion quality.

In addition to ocean water there are available "bitterns" produced through the solar evaporation process at 'Atlit. These bitterns (sp.g. 1.236), which comprise about 60,000m^3 per annum, contain 45 g/lit $MgSO_4$ and 65 g/lit $MgCl_2$, equivalent to 42 g/lit MgO or to 2500 tons MgO per annum. The $MgSO_4$ in the bitterns can be precipitated by further evaporation together with Glauber's salt, but none of these possibilities is at present exploited.

If new salt pans for ocean water evaporation were constructed, for instance at Eilat and at Acre, the quantity of magnesium available might reach the considerable amount of about 12,000 tons per annum.

Dead Sea water

Raw Dead Sea brine contains 135 g/lit $MgCl_2$ and 35 g/lit $CaCl_2$. SO_4^{--} content of 0.8 g/lit is determined by the solubility of the gypsum in the brine. Before the Israel War of Liberation in 1948, Mg^{++} from the Dead Sea brine was used in 3 forms:

a) As $MgCl_2.6H_2O$ crystallized from the end brine of the solar pan system in crystals and fused.
Analysis (%): $MgCl_2$ 45, NaCl 2.5, KCl 1.5. This is satisfactory for use in Sorel cement. The U.K. bought several thousands of tons per annum. Today the price is about $ 50 per ton, but the market seems very limited.

b) As fused anhydrous carnallite ($MgCl_2.KCl$) as flux in light metal casting. During and after World War II several thousand tons were sold for this purpose.
Analysis (%): KCl 46, $MgCl_2$ 47, NaCl 1.5, MgO 3.0. A process for fusion has been evolved which makes an oxide-free product and which could be put into operation quickly, but the competition of anhydrous $MgCl_2$ which is a by-product of titanium production in the Kroll process is at present too great.

c) As brine mixed with $CaCl_2$ for dust laying on dirt roads and for heat transfer in refrigerators. Both these uses are of considerable interest, since almost no manipulation is required except for concentration in the solar pans and solidification for export in directly fired cast iron vessels. Before the war the Mg^{++} was not exploited commercially for production of carbonates, oxides or Mg-metal, although preliminary investigations were carried out. Besides the raw brine, the starting materials available for these purposes are as follows:

1. Carnallite brine

   Analysis (g/lit): $MgCl_2$ 300, $CaCl_2$ 85, KCl 26, NaCl 18, $CaSO_4$ 0.1. Of this brine some 15 million m^3 per annum will be produced, but, since it is the intermediate product for KCl production, only a small fraction will be available for other uses.

2. End brine, after carnallite decomposition (sp.g. 1.350)

   Analysis (g/lit): $MgCl_2$ 400, $CaCl_2$ 100, KCl 6, NaCl 2, SO_4^{--} traces. Some 8 million m^3 per annum will be available. This brine is almost always warmer than 25°C, in summer warmer than 40°C; a factor possibly of interest in connection with $Mg(OH)_2$ precipitation.

3. Factory waste brine (so-called Filtrate No. 1)

   Analysis (g/lit): $MgCl_2$ 320, $CaCl_2$ 15, KCl 40, NaCl 30, SO_4^{--} 0.2. About 1 million m^3 per annum will be available. About 15% might be made almost free of Ca^{++} and of SO_4^{--}. The brine is returned to the solar evaporation pans for further evaporation and additional carnallite production for the potash factory.

4. The evaporation of Filtrate No. 1 leaves another kind of mother liquor (sp.g. 1.350) poor in $CaCl_2$ (500,000 tons per annum).

   Analysis (in g/lit): $MgCl_2$ 480, KCl 4, NaCl 5, $CaCl_2$ 50, SO_4^{--} traces.

5. The mother liquor after further evaporation of Filtrate No. 1 would lead to about 100,000 tons per annum of a very good $MgCl_2.6H_2O$.

   Probable analysis (%): $MgCl_2$ 45, NaCl 2.5, KCl 1.5, $CaCl_2$ traces.

6. Carnallite as a solid might provide great interest for Mg^{++} reactions of all kinds. Of the more than one million tons of carnallite a fraction could be spared, if profitable uses like "flux" could be found.

   Analysis (%): $MgCl_2$ 29, $CaCl_2$ 1, NaCl 12, KCl 20, SO_4^{--} traces.

Tiberias hot springs and other wells

The Tiberias hot springs contain some 1.5 g/lit $MgCl_2$ and about 500,000 m^3 per annum of this solution are available.

In oil drilling operations magnesium containing brines are quite often found. The New Mexico potash deposits, for instance, were a by-product of oil drilling. Measures must be taken here to investigate properly any brines discovered in oil drilling.

J. Aman: Could Dr. Bloch indicate the most economical choice from the various possible brines available for the production of $MgCl_2.6H_2O$, taking into consideration the purity of the final material, especially its Ca content?

M. R. Bloch: The cheapest source of $Mg++$ besides raw Dead Sea brine is end brine (sp.g. 1.350). The next cheap source is factory brine. It is a much better source and nearly as cheap as the other. As long as we do not have to evaporate the brine we can deliver it very cheaply. To make solid magnesium chloride is quite expensive. If it is done by solar evaporation, one has to reckon with large areas, supervision, etc. Whether it is cheaper to evaporate with sun energy than with oil is not quite certain for $MgCl_2.6H_2O$. Carnallite, which contains magnesium chloride in solid form, is much cheaper than magnesium chloride. It is easily available, since we make it anyhow for our potash production.

H. E. Heimann: With regard to magnesium compounds from the Tiberias hot springs, it is of interest to consider as a sideline the possibility of making strontium compounds. The springs contain something like 170 g/m³ of strontium. Furthermore, some dolomites from Gilboa' slopes (Bet Alpha) close to the Jordan Valley also contain a definite percentage of strontium. A survey on that point should be undertaken.

A. Braunfeld: The analysis of the Gilboa' dolomites you mention is fairly complete, but there seems to be no strontium, although traces of barium and titanium are shown. The layer is 4 to 5 m thick and would not be suitable for conversion of magnesium metal. It would be difficult to quarry economically because of the overburden.

H. E. Heimann: It seems to me that more than traces of strontium have been found.

MAGNESIUM HYDROXIDE PRODUCTION BY ELECTROLYSIS OF DEAD SEA BRINES

O. SCHÄCHTER

Israel Mining Industries, Ltd., Haifa

In our work on a method for electrolysis of various brines, attention has been almost exclusively devoted to the anodic part of the process, i.e. to the production of bromine. This has been successfully concluded on a laboratory scale by Dr. Reznik and the author. At present the cathodic part of the reaction is being studied to a limited extent.

In order to describe briefly the principle of our invention, I shall refer to a simple model of an electrolytic cell.

The cell is U-shaped with a tube attached at the lowest point for the entry of the feed, and with overflows at both legs for the discharge of anolyte and catholyte. The anode is a graphite rod, the cathode a cylindrical piece of iron sheet. The cell has no diaphragm and works continuously. Its principal feature is that the feed enters into the electrochemically neutral zone between the anode and the cathode compartment and flows upwards.

Thus various effects which render the electrolysis of halides in diaphragmless cells impractical are eliminated. They are: mixing of anolyte and catholyte, penetration of bromine into the neutral zone, instability of the neutral zone due to difference in the migration velocity of H^+ and OH^- ions.

Magnesium ions help establish a stable neutral zone by their buffering action at *p*H values corresponding to the solubility product of magnesium hydroxide.

As a matter of fact, if brines in which the prevalent ions are alkali metals, or even calcium, are electrolysed, a much smaller current yield is obtained. Fortunately, most brines which come into consideration as sources for bromine are also very rich in magnesium.

Magnesium ions are also a source for pure magnesium hydroxide which it is hoped to obtain as a marketable by-product of the manufacture of bromine.

In part of our experiments we worked with brines from the Dead Sea, in particular:

a) Dead Sea water

Analysis (in g/lit): $MgCl_2$ 130, $CaCl_2$ 38, NaCl 80, KCl 11, $MgBr_2$ 4.

b) End brine

Analysis (in g/lit): $MgCl_2$ 330, $CaCl_2$ 110, NaCl 10, KCl 10, $MgBr_2$ 12.

We also worked with end brine from the 'Atlit salt pans. Different samples had somewhat different compositions, but the following is an approximation:

Analysis (in g/lit): SO_4^{--} 46, total halogen (as Cl^-) 169, Br^- 1.8—2.1, Mg^{++} 36, Ca^{++} <0.2, Na^+ 58, K^+ 11.

With all these brines, magnesium hydroxide formed without any difficulty. This is remarkable, since earth alkali ions present in salt solutions in very small amounts, are known to be detrimental in chlorine-alkali electrolysis. In fact, a preliminary purification step is usually required to eliminate earth alkali metals from the electrolyte.

Magnesium hydroxide is formed in a flocculent state and settles, filters and washes with very great difficulty. In fact, the conditions under which these properties can be improved will form one of the main subjects of further study.

Our experiments so far have not dealt with this problem, but have touched, in a preliminary way, on the following aspects:

A. Current density

Eleven experiments were made with Dead Sea water, changing the current density from 0.33 to 1.1 amp/dm²*. No appreciable variation in results was obtained.

The current efficiency was 65—75%. As at the same time bromine was produced with a yield of over 95%, it seems that the losses were incurred during manipulation rather than as true current losses.

B. Chemical purity

Magnesium hydroxide was analysed repeatedly in our analytical department. It was found to be practically pure, in particular entirely free from calcium. What impurities were found were due to imperfect washing and to absorption of carbon dioxide from the air**.

C. Slurry density

As the equivalent ratio of magnesium to bromine in Dead Sea brines is about 200 to one, the withdrawal of catholyte can be regulated at a much lower rate than that of the anolyte. In the above experiments, the volume ratio of anolyte to catholyte was between 5—12 to one. In the best case the amount of magnesium hydroxide was 20 g/lit catholyte. In experiments made some time ago we tried to reach extreme values and produced finally a paste at the cathode. Even at this stage we had no difficulty in conducting electrical current. It may however be that this material will be still more difficult to work than the more dilute slurry.

In conclusion it may be added that the source of magnesia just described must be looked upon as a minor potentiality. Assuming equal current yields, the quantity of magnesium hydroxide produced would be a little over one third that of bromine. Even if our most optimistic hopes with respect to the latter materialize this would still not mean much in terms of magnesia. However, looking at the prices for magnesia and magnesium hydroxide, one is startled by the fact that the ratio of prices for different qualities is as much as 1 : 15. If it were possible to produce one of these highly valued modifications this source could then assume economic importance.

* Current density was calculated on the entire surface of the cathode. The values given are significant only for comparison among themselves, since the current is carried only by a fraction of the total area.

** Impurities were halides of the order of 0.2—0.3 % expressed as chloride, hypohalogenites of the order of a few hundredths of one percent, and about 1 % carbonate.

A. E. SIMCHEN: As to the bromine production by electrolysis, I wish to know whether the magnesium hydroxide did adhere to the cathode, or give a slurry. Moreover, I wish to mention some experiments I did at the Palestine Potash Laboratories back in 1943 by electrolysis of magnesium chloride without diaphragm, and obtaining a chloride or oxychloride of magnesium ($MgOCl_2$?) (= mixed chloride and hypochlorite of magnesium, analogous to chloride of lime, $CaOCl_2$), which may be used as a disinfectant. The product was solid, fairly insoluble at room temperature, smelled strongly of chlorine. A German patent (Siemens?) of the early 30's exists on a similar subject.

O. SCHÄCHTER: No scaling of the cathode by magnesium hydroxide has been observed. Even after many hours of operation no rise in resistivity of the electrolyte was observed.

J. AMAN: I would like to know a little more about the economics of the brine electrolysis for the winning of the bromine compared to the normal process using chlorine. Will the difference in the costs of production offset the fact that no cathodic material is produced? Obviously the cost of $Mg(OH)_2$ might affect the whole picture.

S. A. ABRAHAMS: What are the economics of the direct electrolysis process for bromine compared to the standard chlorine process for recovery of bromine?

O. SCHÄCHTER: In our economic calculations we diregarded the value of the magnesium hydroxide. Even under this assumption, production costs for bromine turn out to be only part of the world market price. Obviously, we would be very much interested in any possibility of producing magnesium hydroxide, in particular of a Neoprene-grade or similar.

P. GOLDSCHMIDT: I would like to know if Dr. Schächter has worked with higher temperatures, i.e. 54—56°C. In my work together with the late Dr. Haene many years ago in Stassfurt on that problem, we found out that we could get bromine with a very low chlorine content (ca. 0.15% Cl_2), and the scaling of the electrode was diminished. Furthermore the filtration of magnesium hydroxide could be improved.

O. SCHÄCHTER: We worked at room temperature. We aimed at a brine containing 90—95% of the original bromine in elementary form. We would prefer to win the bromine by solvent extraction rather than by distillation. As for scaling, we never experienced a rise in voltage or in resistance, as already mentioned.

MINERAL MAGNESIUM DEPOSITS IN ISRAEL

A. S. Braunfeld

Geological Survey, Ministry of Development

DEFINITIONS AND PETROGENESIS

Much confusion exists about the right use of the term *dolomite*. Ideally the term denotes a mineral containing equimolecular proportions of the carbonates of lime and magnesia, $MgCO_3$. $CaCO_3$. In practice the name is applied to a carbonate rock which contains predominantly the mineral dolomite. A limestone containing dolomite but consisting chiefly of calcium carbonate is called a *dolomitic limestone*. A *magnesian limestone* is, petrologically, a limestone containing about 5 to 15% of magnesium carbonate but no dolomite. But generally none of these terms are applied with any attempt at precision. In the field dolomite generally shows better formed rhombohedral crystalline forms than calcite. It effervesces only feebly with cold hydrochloric acid but freely when the acid is boiling. In cases of insufficient evidence one is tempted to call the rock a dolomitic limestone.

Dolomitic limestone is one of two main categories which form calcareous rocks, the other being calcitic limestone. Dolomitic rocks can be of primary or secondary deposits. Secondary dolomitic rock is produced by metasomatic alteration of limestone.

As a primary deposit dolomite is precipitated directly, the latter state is obtained by the addition of $MgCO_3$ to the $CaCO_3$ or by the leaching of $CaCO_3$ from fossil shells in the limestone, with replacement by $MgCO_3$. An example of primary deposition is the Keuper marl in the British Isles where small rhombs can be seen and the rock may have been laid in the Keuper lake.

There is no visible difference between the rhombohedral carbonate dolomite and calcite. In secondary deposits dolomite tends to crystallize into small rhombs obstructing most of the previous structure. Dolomitization usually affects the least crystallized part of the limestone.

STRATIGRAPHY AND DISTRIBUTION

The magnesium-containing rocks in Israel occur in all major systems present and are spread all over the country. We have black and pink carboniferous dolomites north of Beer Ora, in Nahal T mna'. Further north, in Makhtesh Ramon, we have dark grey Triassic dolomite, some of it oolitic, and the Jurassic dolomite marls apparently of fresh water origin. In the Cretaceous, especially in the Cenomanian series, we have dolomite, in thicknesses reaching several hundred metres. In the Sdom area dolomitic rocks have been ascribed to the Miocene. In the same district we have the Samra series which is classified as lower Pleistocene and which has an upper member containing dolomitic gravel with a calcareous matrix.

Bull. Res. Counc. of Israel, Vol. 5C, 1955.

The largest exposed division in Israel is the Cenomanian of the Cretaceous period. This division consists mainly of limestone and dolomitic rocks, the latter being predominant. From this one can conclude that dolomitic rocks form the most extensive outcrop of any pre-Pleistocene rocks in Israel. It can be seen from the geological map of Israel that there are few areas in Israel which are not within easy reach of the Cenomanian and thus of magnesium-containing limestone. It should be stated that one of the peculiarities of the Israel calcareous rocks is that they vary laterally and the limestone may pass gradually into a dolomite, and vice versa, with all the intermediate stages. And it happens in one and the same stratigraphical horizon.

PRESENT POSITION IN ISRAEL

There has never been a proper survey of the quantities of dolomites in the country. For this reason I made a reconnaisance survey along the coastal plain and in the Galilee.

A most central locality to supply a magnesium industry would be Binyamina where a dolomite quarry exists, connected to the main Tel Aviv—Haifa railway line by a side line. This quarry can be considered the most suitable one to supply any locality in the coastal plain. The part of the hill at present being quarried contains some 2.5 million tons of dolomite. A number of samples were taken from various layers and the results are as follows (average results of 9 samples):

Insoluble residue	0.48%
R_2O_3	0.28
CaO	33.02
MgO	18.90

Another dolomite quarry at present in operation is the so-called "4½ kilometre quarry" near Haifa. Although the quality is very similar to the dolomite in the Binyamina quarry, town planning considerations strongly advise against starting any large scale quarrying here.

There are a great number of other localities which might prove to be suitable, and should the Binyamina quarry not suit the purpose a number of other places in the Carmel could be explored.

It cannot be overemphasized that one of the greatest drawbacks of the limestone deposits of Israel hills is that the strata change laterally from limestone into dolomite and vice versa. This makes it difficult to assess the various dolomite occurrences, even if they are known to be of great thickness. Channel samples have to be taken at frequent intervals before one is able to assess quantities properly.

Although the Usdum series contain certain dolomitic strata no quantitative or qualitative determinations are known. The dolomitic rocks in the Eilat area are in most cases covered by overburdens which may make quarrying uneconomical; also any larger deposits are rather inaccessible at present. Here again a proper survey would have to be made.

The only economic use hitherto made of the Israel dolomitic rocks has been in building, besides sporadic use for ceramic and fluxing purposes. Dolomites are usually more crystallized than limestones and close grained. In Wadi Rushmia and in the Haifa district a fine grey and crystalline stone containing 91% of dolomitic molecules has been quarried. There is the Iskander dolomite which is a soft chalky stone and is

popular because of its lightness and ease in dressing. The most important building stone at present in use in Jerusalem is a fine grey dolomite from Qastel. Dolomite is also very popular as a road metal. The grey and buff so-called marbles from Har Tuv and Beit Safafa are half-crystallized dolomites.

Since dolomitic limestones are porous due to molecular contraction — when the calcium is converted into calcium magnesium carbonate — they form better reservoir rocks than limestone.

Any survey of magnesium-containing rock would be incomplete without mentioning the black olivine basalts in the Galilee and to a smaller extent of the Carmel. An analysis of a dyke rich in olivine at Jebel Asfar, typical of the late flows of basaltic lava of the Hauran and Tiberias area, gives us not less than 47% of MgO.

A. MARKOWITZ: What is known today about further outcrops and geological findings of bituminous limestones besides that at Um Barek? Prof. Picard once stated that bituminous limestones can be found not only in Um Barek but in many other parts of the country.

A. S. BRAUNFELD: Oil shales in Israel have been investigated at various times in the last 30 years and numerous reports have appeared. Bituminous rocks occur in the Galilee in the Tarshiha (according to Blake) and Safad areas, and outcrops can be seen at a number of localities south of Beersheba as far south as Wadi Jiraffi. It seems that research should be conducted first on the Dead Sea area shales, as these are the richest known to us. Oil and other drilling may reveal new localities but as far as I know bituminous material and oil shales can be quarried economically only from surface deposits.

BITUMINOUS LIMESTONE: FUEL AND CHEMICAL RAW MATERIAL

E. L. Clark

Israel Mining Industries, Ltd., Haifa

The pilot plant laboratories of Israel Mining Industries have been working for the past year on methods of utilizing the deposits of oil shale or bituminous limestone available in Israel. The largest deposit of this material thus far discovered occurs at Um Barek on the shore of the Dead Sea approximately 20 kilometres north of Sdom. Our primary interest has been in the organic material contained in the stone and its use as a source of fuel. Recent discussions with Mr. Abrahams have brought out the possibilities of utilizing also the inorganic portion of the stone as a raw material in the production of magnesium compounds. Both these possibilities are of direct interest to this Symposium. The possibility of a supply of cheap fuel and low-cost power in the Sdom—Um Barek area will obviously affect the economics of chemical processing in that area. If the ash or inorganic portion of this fuel can be utilized as a raw material for chemical processing, an additional important advantage may be gained.

Pilot plant tests have indicated that Israel oil shale can be efficiently utilized as a solid fuel. These tests have been performed in a shaft furnace with shale fed at the top and ash removed at the bottom. Combustion air enters at the bottom, is preheated by the out-going ashes, and the flue gases leave at the top. Better than 90% of the organic matter is consumed when 20 to 40% excess air (based on that required for complete combustion of organic matter) is used. The shaft furnace has an internal diameter of 28 cm and the fuel bed is about 50 cm deep. It has been possible to burn over 100 kg shale per hour in this furnace. This represents a combustion rate of over 1600 kg/m^2/hr based on cross-sectional or "grate" area. This may be compared with industrial data on Swedish shale-coke of 700 kg/m^2/hr. In our tests shale particles of 3 to 14 mm diameter were used. No difficulties were encountered in sintering, clinker formation or swelling.

As a result of these encouraging tests exploration was started in the Um Barek area to prove definitely sufficient reserves of material for feeding a power plant of at least 20,000 kW. Preliminary estimates of the costs of generating electric power from shale were made. The explorations thus far completed have definitely proven 2,500,000 tons of oil shale containing 500,000 tons of organic matter. Approximately 1,000,000 tons of organic matter would be required to justify the construction of a 20,000 kW power plant. Estimates indicate that the costs of electric power, using oil shale as fuel, would be less than those now obtained in any generating station in the country provided the oil shale could be mined for IL. 3 per ton and that the organic content continues to average 20 percent of the shale. Since this material occurs in very thick beds with

a reasonable ratio of overburden to oil shale, the open quarry mine visualized should produce the material at considerably less than our conservative estimate. We feel that, without being unduly optimistic, we can confidently predict a plentiful supply of power at low cost and at a large saving in foreign currency for industries based on chemicals from the Dead Sea.

Mr. Abrahams has pointed out that the ash obtained from the combustion of shale might be an important raw material for a future magnesium compounds industry. It must be realized that our interest has been primarily in the organic portion of this material. We do not have complete data on the inorganic portion but tests at our pilot plant on raw material have indicated that before combustion the shale contains 60 to 70% magnesium plus calcium carbonate. During combustion these carbonates are partially decomposed. If the decomposition could be made complete, and the resulting oxides of magnesium and calcium hydrated and separated from the silica, alumina and other oxides, the milk obtained could be utilized to recover magnesium compounds from brines. We are planning to start preliminary laboratory tests to investigate this possibility. The main attraction is, that these ashes will be available at no cost and that the carbonates will be already partly decomposed. Native limestone or dolomite would otherwise have to be quarried, crushed, and calcined. Both the economics of power production and magnesium recovery could benefit.

A. E. Simchen: Mr. Clark indicated the importance of bituminous limestone for power generation which may be very great indeed for electrolysis in the Dead Sea region — for bromine production and other purposes (chlorine, caustics, magnesium metal etc.). Its importance may be less as a raw material for magnesium compounds because of the carbon content of the ashes.

E. L. Clark: The utilization of any mineral requires at least two stages in exploration.

1) The geological exploration;

2) The determination of proven mineable reserves. The second step is very expensive and must be preceded by the careful development of a process for utilization of the mineral. We are now conducting this second type of exploration at Um Barek. The reason for not emphasizing the use of the bituminous limestone ash as a raw material is that we have not done any experimental work. The amount of carbon in the ash is extremely small (less than 1%). How to handle this ash is a problem for research.

M. Lewin: At what temperature is this ash obtained?

E. L. Clark: The temperature of the combustion bed was from 600—800°C. The degree of calcination does not vary: 55 to 70% calcine. The calories required to decompose carbonates in combustion of bituminous limestone represent only 10—15% of the energy available.

H. E. Heimann: What is the yield in useful calories and in energy expected when burning bituminous limestones? The burning of the carbonates to oxides consumes to my rough estimation half of the calories developed and only the other half is left for steam production.

E. L. Clark: With an organic material content of 15%, less than 15% of the calories developed by combustion are consumed in carbonate decomposition. Naturally with higher organic contents, a smaller percentage will be consumed for carbonate decomposition.

DECOMPOSITION OF MAGNESIUM CHLORIDE

J. AMAN

The Hebrew University of Jerusalem

DATA AND CONSIDERATIONS

It is known that $MgCl_2.6H_2O$ undergoes dehydration and hydrolysis when heated to high temperatures. Work on various aspects of these reactions has been done here mostly at the Hebrew University and at the Dead Sea Works. The energy requirements and equilibria of the various steps involved have been summarized by Kelly[1].

Partial pressure of HCl

The reactions of interest are:

$$MgCl_2.H_2O \rightarrow MgOHCl + HCl \rightarrow MgO + 2HCl$$

and the direct action of water vapour on $MgCl_2$:

$$MgCl_2 + H_2O \rightarrow MgO + 2HCl,$$

all three reactions taking place concurrently.

Kelly gives the following decomposition pressure for reaction 2 which requires higher temperatures than reaction 1:

Temperature (°C)	*Pressure HCl (mm Hg)*
326.8	3.2
426.8	56.0
526.8	465.0

and the equilibrium constants for reaction 3:

Temperature (°C)	$K\ p'^2_{HCl} / p_{H_2O}$
426.8	1.17×10^{-2}
526.8	8.49×10^{-1}
626.8	3.87

It can be shown from these figures that a complete decomposition of the $MgCl_2$ can be achieved within the temperature range 500 to 700 °C depending on the partial water vapour pressure of the heating gases and the partial pressure of HCl required.

Energy requirements

For our purpose the heat of the overall reaction should be considered:

$$MgCl_2.6H_2O \rightarrow MgO + 2HCl + 5H_2O - Q$$

Q equals 120 Kcal per mol $MgCl_2.6H_2O$ decomposed to 1650 Kcal per kg HCl formed.

Rate of hydrolysis

No direct data are available, but it can be assumed that the reaction proper is very rapid and that the actual rate is determined by the diffusion rate of the water vapour and HCl gas (when dehydration and hydrolysis are considered respectively) from the inner part of the liquid or solid to the outside atmosphere. This rate will be characteristic of the system and will increase with rising temperature (giving a higher dehydration and decomposition pressure of H_2O and HCl) and with the decrease of the thickness of the layer through which the gas must diffuse.

TECHNICAL CONSIDERATIONS

The technical problem consists of bringing the magnesium chloride crystals to the reaction temperature, of supplying the required heat of reaction with good thermal efficiency and of finding the proper materials of construction for handling such a corrosive system. In considering the possible equipment, one must also take into account the phase transitions of the $MgCl_2$ crystals when heated to high temperatures. The technical studies on this reaction were carried out previously by Talmi and Yaron[2] and by Cohen[3].

Based on work done by the author[4], we came to the conclusion that the use of a reactor similar to a spray dryer would be the best way to carry out the decomposition reaction. The heat efficiency in such a spray tower can be very high, the duration of contact can be varied by varying the size distribution of the particles which determine the physical properties of the magnesium oxide produced. Lastly, the problem of materials of construction can be solved rather easily.

Work on a laboratory scale gave encouraging results, and a pilot plant now under construction in the U.K. should soon provide data necessary for setting up the full scale plant. A commercial plant has been in operation since the beginning of 1954 in the U.S., but no technical information has been available.

ECONOMIC CONSIDERATIONS

The cost of production depends mainly on the cost of $MgCl_2$ crystals, of transport and of fuel. The following table gives cost estimates of HCl produced at 2 potential localities for the commercial plant.

TABLE I

Estimated cost of 1 ton HCl as a function of the cost credited to MgO for potential plants at Timna' and at Oron

Cost MgO ($/*ton*)	*Cost HCl at Timna' plant* IL. *plus* $	*Cost HCl at Oron plant* IL. *plus* $
0	43.080 23.05	20.580 14.60
10	16.55	8.10
15	13.30	4.85
20	10.05	1.60
25	6.80	
30	3.55	

Since the physical properties of the raw magnesium oxide are still unknown, we assumed meanwhile that we should compete on the world market with the cheapest of the MgO products: that used for refractories costing about $ 40/ton in the U.S. and £ 16 in the U.K. If we, therefore, estimate a value of $ 15/ton at the production site in order to allow for cost of inland transport and shipment, the cost of 1 ton HCl will be IL. 43 plus $13 or about $ 37/ton at Timna' and L. 20.500 plus $ 4.85 or about $ 16/ton at Oron.

The availability of cheap HCl based on abundant local material will have far reaching repercussions on the industrial development of the country and on the development of local mineral resources, but this discussion is outside the scope of this paper.

REFERENCES

1. Kelly, K. K., 1945, Bureau of Mines Tech. Paper 676.
2. Talmi, A. and Yaron, F., 1955, *Bull. Res. Counc. of Israel*, **5C**, 111.
3. Cohen, A., unpublished results.
4. Aman, J., unpublished results.

HYDROCHLORIC ACID FROM MAGNESIUM OXYCHLORIDE CEMENT

A. Talmi

Fertilizers and Chemicals, Ltd., Haifa

The experiments I am going to describe were carried out by Dr. U. Garbatski, Dr. F. Yaron and myself under the direction of the late Professor L. Farkas and of Dr. M. R. Bloch. Dr. Garbatski carried out his experiments in 1940. Dr. Yaron and I began our work in 1942, gradually increasing the scale of the experiments until we reached a production of 5 kg HCl per hour in a pilot plant at the Dead Sea. The greater part of this work was done by Dr. Yaron.

When MgO is mixed with a concentrated solution of $MgCl_2$ a mass is obtained which sets to a hard solid. If this solid is heated to 500—600°C by the gases obtained from the combustion of oil, it gives up a large part of its chlorine in the form of HCl. At the same time a considerable amount of moisture evaporates from the cement. The calcine is very friable and this makes it possible to separate it from the non-calcined cement. If the calcine is mixed with a $MgCl_2$ solution of appropriate strength a new batch of cement is obtained which can be used for further HCl production.

In pilot plant experiments at the Hebrew University and at the Dead Sea the following data were obtained:

For the production of 1 ton of HCl some 10 tons of oxychloride cement have to be calcined, 3 to 4 tons of water have to be evaporated and about 1 ton of fuel oil has to be burnt. The quantity of water could probably be reduced, and future research work should deal with this point. The fuel consumption is considerably in excess of the theoretical one, and may be somewhat reduced by applying even better heat insulation around the furnace and by using the hot calcine to heat the incoming air. The heat of the gases leaving the furnace may be utilized.

Regarding the furnace it has been calculated from pilot plant data that a production of 1 ton HCl per day requires a grate area of 2 m^2. A furnace height of 2—3 m has been proposed but seems somewhat excessive.

A grate consisting of spiked rods, which could be revolved, proved very useful in separating calcine from non-calcined cement. The grate must of course be made to resist the temperatures involved.

The calcine is far from being pure MgO. It is rich in $MgCl_2$, and a very important question is whether this salt can be washed away.

In pilot plant experiments 50 to 60% of the chlorine originally present in the cement escaped in the form of HCl, but in laboratory experiments higher "chlorine yields" of up to 80%, were obtained. Dr. Garbatski reports even higher yields. In laboratory experiments steam was found to accelerate the liberation of HCl but not to alter the final yield.

When the cement was heated electrically, in a current of air, a considerable part of the HCl was oxidized to elementary chlorine. From the equation

$$\frac{p^2_{Cl_2} \times p^2_{H_2O}}{p^4_{HCl} \times p_{O_2}} = K_p$$

it follows that the percentage of chlorine is very much affected by the percentage of HCl, and that for a given percentage of HCl the oxidation can be reduced by the presence of water vapour or by lowering the partial pressure of the oxygen. Both these effects are obtained when combustion gases are used.

The rate of setting of the cement can be controlled. If the $MgCl_2$ solution used is concentrated or hot or if much MgO is used a rapid setting results. If the $MgCl_2$ solution contains some $CaCl_2$, the setting is slowed down and the cement is somewhat deliquescent.

The chlorine content of the cement should not exceed 20%; otherwise the cement tends to fuse in the furnace.

PRODUCTION OF POTASSIUM CARBONATE THROUGH ENGEL'S SALT

H. H. Heimann

Technion—Israel Institute of Technology, Haifa

My own work in this field dates back to 1922 and was done on behalf of the German Potash Industry at the Institute of Physical Chemistry at Karlsruhe (T. H.). Since no records are left at my disposal, I shall limit myself to remarks of a more general character.

NEU-STASSFURT PROCESS

Main reactions

1. $3(MgCO_3.3H_2O) + 2KCl + CO_2 \rightleftharpoons 2(MgCO_3.KHCO_3.4H_2O) + MgCl_2$
2. $2(MgCO_3.KHCO_3.4H_2O) + MgO \rightleftharpoons 3(MgCO_3.3H_2O) + K_2CO_3$

Side reactions

3. $MgCl_2 + Ca(OH)_2 \rightleftharpoons Mg(OH)_2 + CaCl_2$
4. $Mg(OH)_2 + CO_2 + 2H_2O \rightleftharpoons MgCO_3.3H_2O$

Reactions 1 to 4 may be added up algebraically:

$$2KCl + CaO + CO_2 \rightleftharpoons K_2CO_3 + CaCl_2$$

The process was given up in Germany for technical and economic reasons. The technical obstacles seem to have been the low reactivity of the magnesium carbonate used in the process and the bad filtrability of the double salt obtained as intermediate. The main economic drawback is the simplicity of making potassium carbonate by carbonating the potassium hydroxide obtained by electrolysis of potassium chloride. Where low-priced electrical energy is available, the Neu-Stassfurt process seems, therefore, not economical.

What are the reasons that could induce us to take up this process and to adapt it to our special conditions and needs?

1. We have an ample supply of potassium chloride of a rather high degree of purity. The same material will be processed in Haifa into potassium sulphate and kept in store anyway.

2. At present a cheap source of electricity is not available, and there are no indications that this situation may change in the near future.

3. We are well supplied with potential sources of magnesium oxide or carbonate as specified in other lectures of this symposium.

4. Limestone of high quality is within easy reach of the plant of Fertilizers and Chemicals, Ltd.

5. Carbon dioxide of highest concentration is cheaply available as a by-product of ammonia synthesis.

6. The disposal of the final solutions of calcium chloride and other products may easily be arranged for.

7. The work of S. A. Abrahams and others has provided more information on the conditions needed for preparing magnesium carbonate of high reactivity.

8. Much progress has been made in the engineering of processes involving solid-liquid separations (Dow units, Landskrona filters, etc.).

PRELIMINARY ESTIMATION OF RAW MATERIALS INVOLVED IN THE PRODUCTION OF 1000 TONS OF PURE K_2CO_3

Raw material	*Assumed yield*	*Tons for production*
KCl	75%	1450
Burnt lime	75%	750
MgO	For making up losses in recirculation	100
CO_2	40%	800 (400,000m³)

Since any calculation of the economic feasibility is premature before determining the volume of the production intended, a market analysis should first be made.

The quotations for the potassium compounds involved are today as follows:

Potassium chloride (99.9%): $ 27.50 per ton.

Potassium carbonate (calcined): $ 200.00 per ton.

SUGGESTED RESEARCH PROBLEMS

1) The reactivity of magnesium carbonate and its dependence on the starting material and method of preparation.

2) The kinetics of the reaction between magnesium carbonate and potassium chloride as influenced by various factors, such as particle size, stirring conditions, presence of surface active agents, etc.

3) The most appropriate method for decomposing the double salt.

PRODUCTION OF POTASSIUM CARBONATE BY THE ENGEL-PRECHT PROCESS

I. SCHNERB
Research Council of Israel

It was in 1940, during World War II, that, at the suggestion of Dr. Bloch, we started in the laboratories of the Palestine Potash Company a series of experiments to produce potassium carbonate from potassium chloride according to the Engel-Precht process. There are many problems connected with this process. This can be seen also from the large number of patents which in the first decades of this century were granted in Germany where this process was developed and carried out on a big scale.

The Engel process consists of two main reactions: first, the formation of the so-called Engel salt, and second, the decomposition of Engel salt and the simultaneous formation of potassium bicarbonate or carbonate:

1) $3MgCO_3.3H_2O + 2KCl + CO_2 \rightleftharpoons 2(MgCO_3.KHCO_3.4H_2O) + MgCl_2$

2a) $MgCO_3.KHCO_3.4H_2O \rightleftharpoons MgCO_3.3H_2O + KHCO_3 + H_2O$

or 2b) $2(MgCO_3.KHCO_3.4H_2O) + Mg(OH)_2 \rightleftharpoons 3MgCO_3.3H_2O + K_2CO_3 + H_2O$

We have also the following auxiliary reactions:

$CaCO_3 \rightleftharpoons CaO + CO_2$
$CaO + H_2O \rightleftharpoons Ca(OH)_2$
$MgCl_2 + Ca(OH)_2 \rightleftharpoons CaCl_2 + Mg(OH)_2$
$Mg(OH)_2 + CO_2 + 2H_2O \rightleftharpoons MgCO_3.3H_2O$

or, alternatively,

$MgCl_2.6H_2O \rightleftharpoons MgO + 2HCl + 5H_2O$
$MgO + H_2O \rightleftharpoons Mg(OH)_2$
$Mg(OH)_2 + CO_2 + 2H_2O \rightleftharpoons MgCO_3.3H_2O$

We approached this process since all raw materials necessary for it are found in the Dead Sea or in its surroundings: KCl, $MgCl_2$ and $CaCO_3$, the latter in the form of dolomite or bitumen shale.

Attention will be drawn here only to the main problem in the Engel process, which is to get a magnesium carbonate suitable for the formation of Engel salt. There exist different kinds of magnesium carbonate, and not every kind suits the process.

Basic carbonates give no reaction at all. The carbonate must be a well-defined material; it must be the trihydrate, and even this trihydrate is not always well reactive. The magnesium carbonate should be crystalline, and it seems that large crystals are preferable for the reaction.

The source of the magnesium carbonate trihydrate is really not a decisive factor. We worked with magnesium carbonate obtained from $Mg(OH)_2 + CO_2$, from $MgCl_2 + K_2CO_3$ (or Na_2CO_3), or from $Mg(OH)_2 + NaHCO_3$. MgO obtained by hydrolysis from $MgCl_2.6H_2O$ also gave with CO_2 a well reactive trihydrate. Moreover, the suitability of a MgO originating from $MgCl_2$ decomposition opens the possibility of a completely new aspect of the process, since we can obtain a suitable MgO directly from $MgCl_2$, avoiding the need of making $Mg(OH)_2$ from lime, which is a very inconvenient process.

But regardless of how the magnesium carbonate trihydrate was produced, we sometimes had difficulties in bringing this trihydrate into reaction with KCl and CO_2.

One of our most important findings was that magnesium carbonate, independent of its origin, could be activated by adding a small amount of potassium carbonate or potassium or sodium bicarbonate. In this way, carbonate, which did not react by the usual method, began to react, and the whole process consumed less time.

This observation led us to attempt to omit CO_2 in the first stage of the process. Instead of CO_2 we used sodium bicarbonate, so that the reaction was now:

$$MgCO_3.3H_2O + KCl + NaHCO_3 + H_2O \rightleftharpoons MgCO_3.KHCO_3.4H_2O + NaCl$$

The great advantage of this reaction is that we use up the whole amount of $MgCO_3$. In the Engel process, using CO_2, we always lose one third of the $MgCO_3$ in the form of $MgCl_2$; here we obtain NaCl instead of $MgCl_2$.

Moreover, the carbonate regained after thedecomposition of the Engel salt is reactive again; all products — the carbonate and the Engel salt — are in this case well formed crystals, and disturbing sludges, as observed in the normal Engel process, were not encountered here. A further advantage of this method is that the mother-liquor of the Engel salt, always containing a surplus of KCl, can be used once more by adding the missing quantities of KCl and $NaHCO_3$. This can be repeated until the brine is saturated with NaCl. In the normal Engel process, the filtrate of the Engel salt cannot be used again, in spite of the excess of KCl, because of the presence of $MgCl_2$, which does not allow the reaction to go in the direction of the Engel salt formation.

The method using $NaHCO_3$ instead of CO_2, has, of course, only a theoretical value as long as we have no natural source or any other cheap source of sodium bicarbonate. However, at the time the experiments were made, we saw a possibility for a cheap soda from the Egyptian "Trona".

As a matter of fact, we tried to work with a sample of Trona-Soda. This sample contained 20% Na_2CO_3 and 27% $NaHCO_3$, the remainder was NaCl, Na_2SO_4 and H_2O. We enriched this product in $NaHCO_3$ by treating the dry product with CO_2, and it was then well reactive. Almost two parts of Trona-Soda had to be used for one part of final potassium carbonate.

But even today sodium carbonate may be considered as a possible starting material for the Engel process. Magnesium carbonate can be obtained from sodium carbonate and magnesium chloride, and the sodium bicarbonate (for the Engel salt formation) can be obtained from sodium carbonate by carbonizing it with CO_2. In this way, we

do not need lime for making $Mg(OH)_2$ and all the inconvenient manipulations with $Mg(OH)_2$ can be omitted, so that the layout of such a factory could be most simple. The quantity of sodium carbonate required would be 2.6 tons Na_2CO_3 for every ton of potassium carbonate.

As to the second stage of the process (the decomposition of the Engel salt), this stage is most decisive for the economic aspect of the whole process. The re-use of the magnesium carbonate obtained in this stage and the amount of water used for decomposition, which must afterwards be evaporated, are two important points in this respect. But these two decisive points depend one on the other and, as a matter of fact, counteract each other. If we want to get a re-usable magnesium carbonate, we have to decompose with a considerable amount of water at a low temperature (45°C); we get in this way a rather diluted solution (about 9%) of $KHCO_3$, which means that we have to evaporate a large amount of water. If, on the other hand, we aim at a concentrated solution of $KHCO_3$ in order to reduce the amount of water to be evaporated, then we have to decompose at a high temperature (100°C) using a K_2CO_3 solution or we have to decompose under pressure, but in this case, the magnesium carbonate is transformed into a basic carbonate and is no more reactive and usable for the Engel process. But this is not necessarily a disadvantage, and it need not impair the value of the process, because the basic carbonate can be successfully used for other purposes. We know that magnesium carbonate is today a product of great value, used in a great number of industries. We know, for example, that magnesium carbonate is used as an anticaking ingredient for table salt. The same is true for potash, which tends to cake still more than table salt. Thus the Potash Works alone could, when carrying out the Engel process, most probably use about 700 tons of magnesium carbonate per annum in their own Works as an anticaking material.

As to the quantities of materials in the process, we bring three examples. The first, according to the usual Engel process, provides for re-using of a part of the magnesium carbonate for further batches.

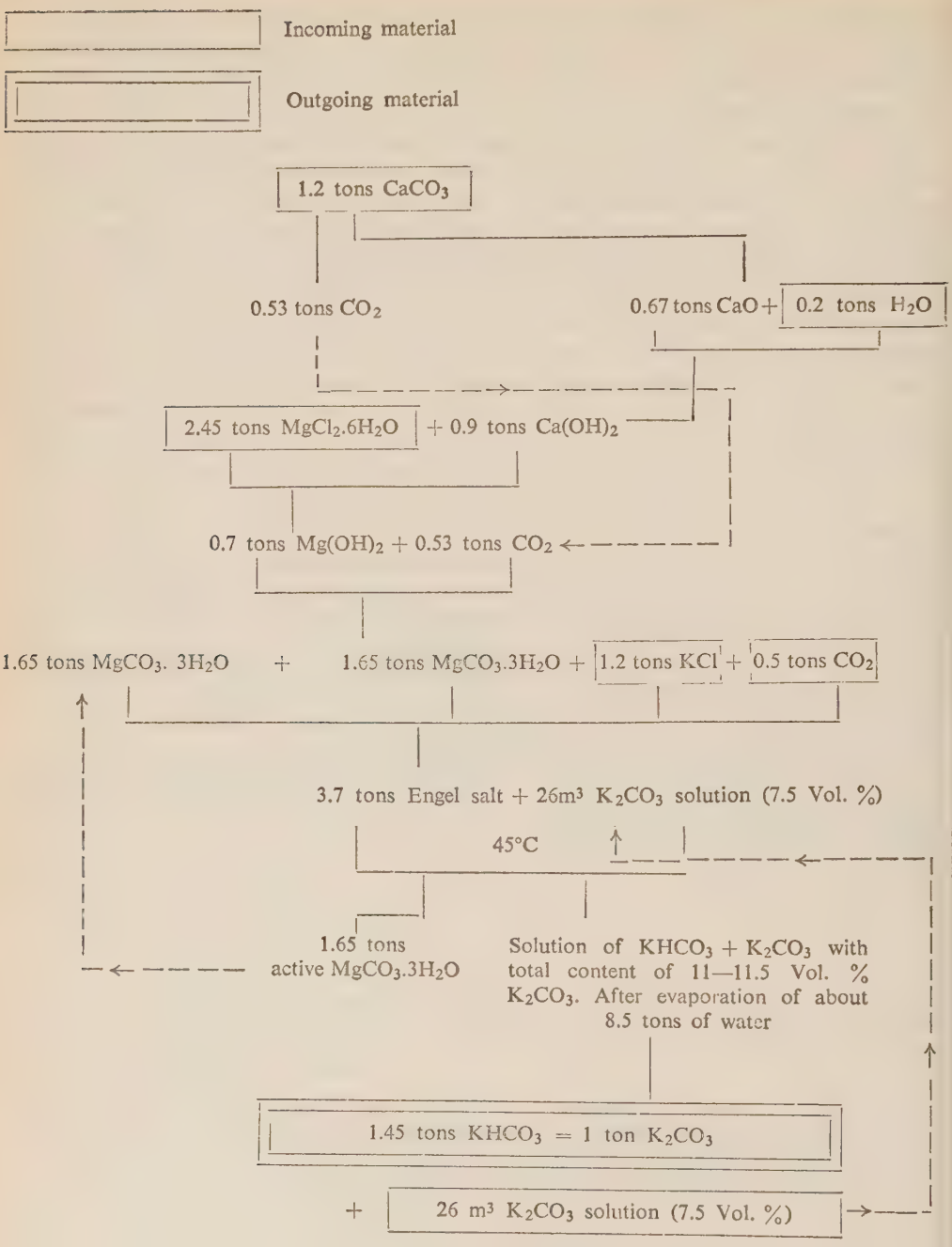
Incoming material
Outgoing material
1.2 tons $CaCO_3$
0.53 tons CO_2
0.67 tons CaO + 0.2 tons H_2O
2.45 tons $MgCl_2.6H_2O$ + 0.9 tons $Ca(OH)_2$
0.7 tons $Mg(OH)_2$ + 0.53 tons CO_2
1.65 tons $MgCO_3.3H_2O$ + 1.65 tons $MgCO_3.3H_2O$ + 1.2 tons KCl + 0.5 tons CO_2
3.7 tons Engel salt + 26m³ K_2CO_3 solution (7.5 Vol. %)
45°C
1.65 tons active $MgCO_3.3H_2O$
Solution of $KHCO_3$ + K_2CO_3 with total content of 11—11.5 Vol. % K_2CO_3. After evaporation of about 8.5 tons of water
1.45 tons $KHCO_3$ = 1 ton K_2CO_3
+ 26 m³ K_2CO_3 solution (7.5 Vol. %)

The second example, also according to the normal Engel process, provides for the use of fresh magnesium carbonate for every batch.

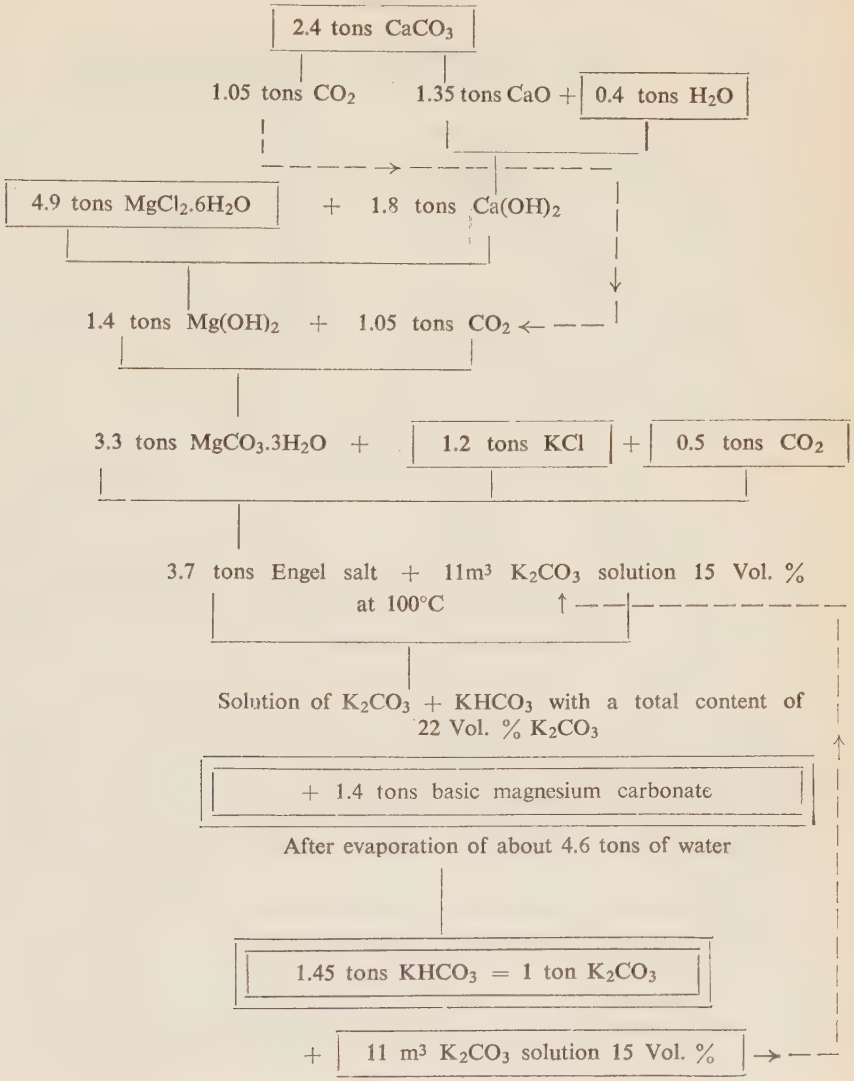

The third example represents the process using sodium carbonate as starting material both for magnesium carbonate and for the Engel salt formation. (The decomposition of Engel salt is the same as in the second example).

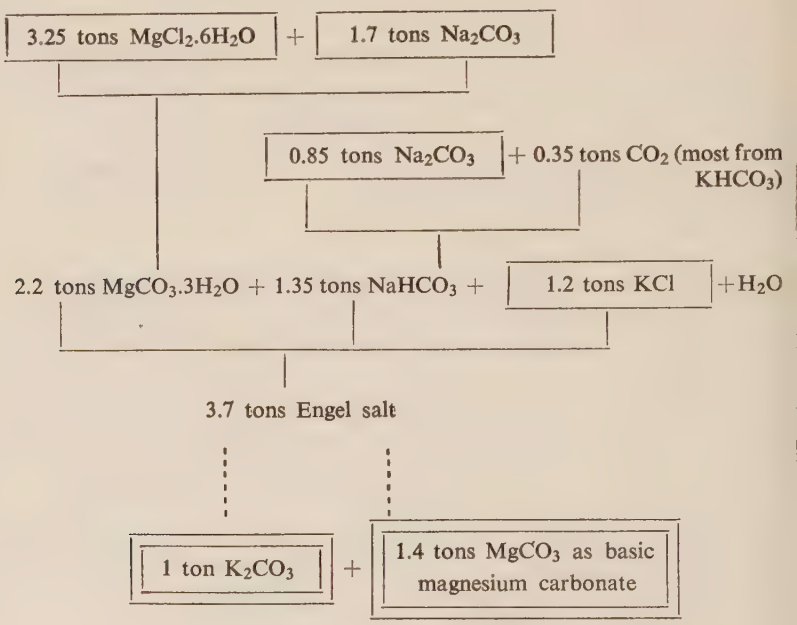

I have not touched on the economic aspects of the Engel process for the production of K_2CO_3, and it may be that, when comparing the Engel process with the process of K_2CO_3 production from electrolytically made caustic potash, the Engel process will perhaps prove less economical and not competitive with the electrolytic process.

However, by using sodium carbonate as a starting material, the Engel process becomes extremely attractive because of its low investment costs as compared with the electrolytic process. Furthermore, if the process is conducted in the manner already mentioned, using the magnesium carbonate which one gets in the decomposition reaction of Engel's salt for other purposes, then the Engel process opens quite interesting aspects. It offers the possibility to produce a magnesium carbonate of high value together with potassium carbonate which, compared with potassium chloride and soda ash, the two starting materials, is a highly valued material as well.

If you also consider that the potassium carbonate, according to the Engel process, can be made practically free of chloride (which cannot be done when produced electrolytically), then one can see quite clearly that the Engel process has great advantages.

H. E. HEIMANN: 1. The proper location for a potash carbonate plant seems to be Fertilizers and Chemicals, Haifa, owing to the availability of carbon dioxide of 100% purity in unlimited quantities.

2. Use of soda ash in making potash means introducing into the process a chemical that has to be imported. Furthermore it means an overall conversion: $Na_2CO_3 + 2KCl \rightarrow K_2CO_3 + 2NaCl$. Such a conversion could be achieved by other means cheaper than the Engel-Precht process.

3. The claim that larger crystals of magnesium carbonate proved to be more reactive than smaller ones needs to be rechecked. As the formation of the double salt is a reaction between a solid and a liquid it seems more convincing that a large surface reacting area, i. e. small crystals, should give a more intensive reaction.

M. FORT: Engel salts have an apparent industrial potential. On the theoretical side for process control I suggest that an investigation be made of crystal forces in solution, because of apparent phase changes. It seems that a soda ash plant of 10,000 tons per year might prove to be economical, and that, since there is an immediate need for that much in Israel now, soda ash might be available for the Engel salt process sooner than now contemplated.

P. GOLDSCHMIDT: The practical work in big scale productions according to the Engel-Precht process is, according to my own experience, very difficult. That is why a process was worked out by my firm to produce potassium carbonate in a straightforward process from calcium cyanamide and potassium sulphate. I propose that the economics of both processes be compared. As this is not within the scope of this symposium, I will discuss this question later. This is a matter of great importance as we will now have a potassium sulphate plant.

J. SCHNERB (*reply to Heimann*):

1. We need for the formation of magnesium carbonate a gas containing only 10—15% CO_2 and for Engel salt formation a gas containing about 30% CO_2.

2. The use of Na_2CO_3 for the Engel process gives the possibility to obtain from two relatively cheap materials (KCl and Na_2CO_3) two highly valued materials (K_2CO_3 and $MgCO_3$); moreover, I do not know of another reaction to convert the Na_2CO_3 to K_2CO_3 other than via the Engel salt.

3. It may be that the big magnesium carbonate crystals react better than the small ones because of their shape. But, as a matter of fact, we succeeded in bringing also small (needle) crystals to react by adding them to an already formed Engel salt. The same small crystals had previously given no reaction after being treated for 48 hours in the absence of Engel's salt.

H. E. HEIMANN (*Reply to J. Schnerb's answer*):

1. From a technical point of view it makes quite a difference if you have to put through a reacting slurry a reacting gas of 100% or of 16% purity. In the latter case you have to blow through the mixture six times more of gas volume. That means more expenses in mechanical energy and a slower rate of reaction.

2. Dolomite quarries with high quality stone are close to the Haifa plant.

3. There should be simpler ways for the double conversion $NaHCO_3 + KCl \rightarrow KHCO_3 + NaCl$ than that proposed by Dr. Schnerb, going through Engel's salt, for instance an ion-exchange system.

THE PRODUCTION OF MAGNESIA FROM SEA WATER

A. GOLDBERG

Fertilizers and Chemicals, Ltd., Haifa

GENERAL

Sea water contains approximately 0.1% of the Mg ion mostly in the form of $MgCl_2$ and $MgSO_4$. When reacted with milk of lime $Mg(OH)_2$ is formed which can be collected in the form of a slurry. The flow sheet of the process is shown in Figure 1. Instead of milk of lime slaked burnt dolomite can be used. Dolomite increases the throughput of the equipment, thus reducing the capital cost of the process, but has certain disadvantages which will be described later. As far as the writer knows (his information is four years out of date) the total quantity of MgO produced by the sea water process is about 450,000 tons per year, apart from Russia, for which figures are not available. Of this amount about 100,000 tons are produced in Europe and 350,000 tons in U.S.A., mostly in the warmer waters of the Gulf or California.

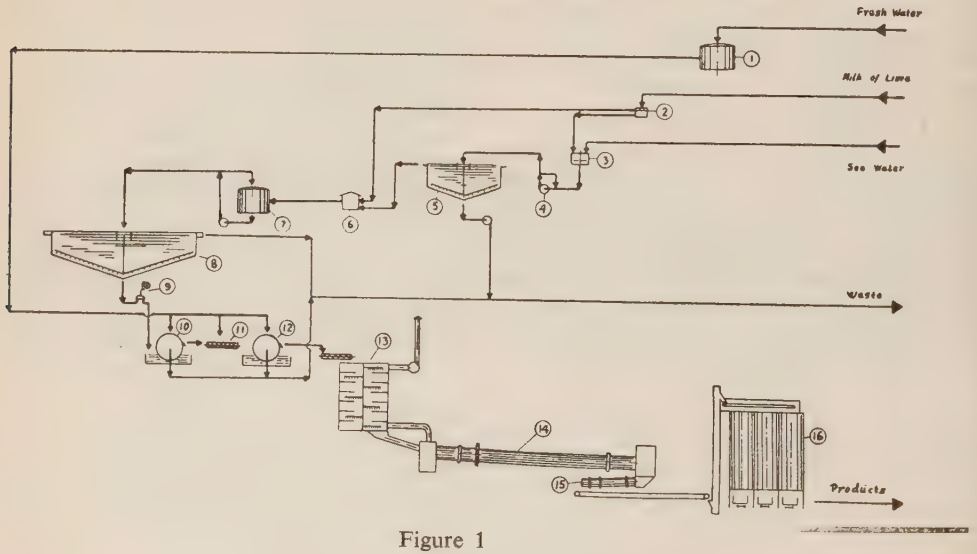

Figure 1

DETAILS OF THE PROCESS

Pretreatment

The purity of the end product is dependent, to a substantial extent, upon elimination of any soluble non-magnesium salts in the sea water which will precipitate with addition of the calcium hydroxide. The most common impurity is calcium bicarbonate, which

tends to precipitate with the addition of $Ca(OH)_2$. Those plants aiming at a pure product eliminate the bicarbonate by a careful predosing of sufficient milk of lime to remove the bicarbonates. This pretreatment is best carried out in an agitated tank or by the addition of the milk of lime in a centrifugal pump before the pretreatment thickener. Some plants use a back washing filter at this stage in order to remove the carbonates and other mechanical impurities which may come in with the sea water—including fauna and flora.

Preparation of milk of lime or dolomite

It is essential to have very pure milk of lime or dolomite. Since it is easier to burn lime rather than dolomite to a reactive state, those plants aiming at high purity use burnt lime and not dolomite. The reason is that all dolomites are, in nature, mixtures to some extent of limestone and dolomite. Limestone and dolomite require different temperatures for their calcination and a kiln set for the burning of dolomite will underburn limestone. Any unslaked material remaining in suspension in the hydrate slurry will go right through the process to the end product.

The most satisfactory product is produced in the rotary kiln, in which burning control is easier than in the vertical kiln. On the other hand, rotary kilns use 20% more fuel than vertical kilns. The real raw material of magnesia production is the burnt lime or dolomite and the success of the process depends, to a large extent, upon the successful calcination of the raw material. Really reactive and chemically pure lime is obtained by Dow by the calcination of crushed oyster shells — a very pure source of calcium carbonate. Most other plants use a high grade dolomite and put up with a poorer end product. As far as I know, only one plant uses vertical shaft kilns and 16 plants use rotary calciners, the biggest being 3.70 m in diameter and 110 m long. The feed to the kilns is invariably closely sized in order to improve calcination. After calcination the burnt stone is cooled and then slaked, normally in wet tumbling barrel slakers which produce a thin slurry (12% solids). This slurry is classified in bowl and rake classifiers and the grits rejected. The slurry is further thinned either with stripped sea water or fresh water to about 4% solids.

$Mg(OH)_2$ slurry production

The milk of lime and sea water are usually premixed in agitated tanks or in tanks with pump circulation and then the mixture is discharged into thickeners of large diameters. The free settling rate of pure $Mg(OH)_2$ in sea water is about 12—20 inches per hour. Very large thickeners are, therefore, required and most plants operate with 100 to 150 ft diameter thickeners. Some 250 ft diameter thickeners have been installed. The slurry is usually thickened to about 5% solids. The height of the thickener is usually about 5 m. The plants operating on dolomite have better settling rates, as the nuclei of burnt MgO obtained from dolomite calcination have a greater settling rate (but this is usually at the cost of purity).

The slurry which is formed is very gelatinous and it is advisable to place the slurry pumps at the base of the thickener. Centrifugal pumps are not recommended for the pumping operation as the material is thixotropic and the filtration rate is seriously

affected by the action of centrifugal pumps. This is particularly the case with high purity magnesium hydroxide.

The slurry is pumped to the filters and the spent sea water sent back to the sea. Control of the operation by *p*H meters on a by-pass of the main stream is utilized.

The overflow of the thickeners is returned to the sea at a distance from the intake channel.

Filtration

A number of different filtration methods are in use. The slurry is very difficult to filter. Most plants use a series of rotary vacuum filters with displacement washing between filtration steps. Since reslurrying is inadvisable, a very satisfactory method of washing is the production of filter cake slugs in an extrusion pump and the dropping of these slugs through a vertical tower. These towers are up to 10 m high and have an upward flow of fresh water.

Dow use enormous Moore filters and Sweatland pressure filters have also been employed. The slurry is difficult to de-water and recirculation of dried material is used as a filter aid. The filter cake usually contains up to 50% water.

Drying and calcination

The cake is preformed in special feeders and dried in rotary driers, as well as calcined. By varying the speed and temperature of the rotary driers various degrees of dehydration can be obtained.

Where magnesia is needed the material is calcined in rotary kilns. Normal calcination temperatures for reactive material are about 800°C. Pure magnesia will convert into periclase at a temperature of 1700°C. Since such a temperature is not feasible for normal rotary kiln operation, the cake can be adulterated with iron in order to drop the periclase formation temperature (up to 2% of red mud from alumina production can be introduced in order to drop the temperature to 1400°C).

For high purity materials the cake is calcined up to 1400°C and is then further burnt in beehive kilns. Natural gas or producer gas are essential for calcining high purity materials, in order not to introduce contamination by ash.

Costs

Sea water magnesia plants have an investment of about $ 50—70 per annual ton of production dependent upon size and location and including the facilities for lime production. This represents a charge of $ 3 to 4 per ton for *depreciation. Manpower* is small, being of the order of two man hours per ton of product including supervision.

Raw materials

Limestone — 2.2 tons per ton of magnesia, fuel — 0.45 tons per ton magnesia, fresh water — 12 m^3 per ton magnesia, power — 120 KWH per ton magnesia.

ENGINEERING ASPECTS OF THE PRODUCTION OF MAGNESIA FROM SEA WATER

A. V. I. Molleson
Fertilizers and Chemicals, Ltd., Haifa

The previous paper described the process of producing magnesium oxide from sea water and the various chemical steps involved, and other papers have also referred to the chemical aspects of the problem rather than the engineering ones. The process people have the advantage of knowing that the process will remain substantially the same wherever the plant is located, whereas any attempt at describing the engineering involved must be confined, to some extent, to generalities, because neither the location nor the size of the plant are yet known. I will, therefore, confine my comments to bringing out general design points in each of the major steps of the process.

SEA WATER INTAKE

The economics of pumping large quantities of water dictate that the entire magnesia plant must be low lying to avoid having to overcome excessive pumping heads. A settling basin must usually be provided at the intake, to allow solids which are in suspension due to the inevitable turbulence of coastal waters, to settle out. The better this settling basin performs its functions, the less the filter plant in the pretreatment stage will have to do, and even if this does not necessarily decrease the investment in the filter plant, it will certainly contribute to its satisfactory operation. Where a large plant has to be located some little distance from the coast, it is worth considering providing a concrete feeder channel going into the plant, rather than a large pipeline. In that case the pumping station would normally be at the plant end of the channel, thus easing its supervision and maintenance. Since the pumps will be large, electrically or diesel driven centrifugals, the concentration of the power supply at the plant is also a point in favour of the installation of the pumping station at this end of the feeder channel. I would select double entry horizontal pumps, with a flat capacity-head characteristic, and low specific speed. It is true they require priming where a vertical pump would not, but the maintenance is so much easier.

PRETREATMENT

The usual method of carrying out the pretreatment of the sea water is to use large mixer tanks, similar to thickeners, but much deeper in proportion. These are followed by sandbed filters consisting of a number of cells with the usual cycling and backwash arrangement. Since the levels at this point in the plant tend to be quite high, say 8 m or more because it is usually desired to continue the process by gravity flow, welded steel tanks are preferable for this pretreatment. This is, in fact, the highest point of the hydraulic system.

MILK OF LIME PREPARATION

Not very much further comment is required on the standard type of lime burning, slaking and classifying plant for the production of milk of lime, except perhaps to say that the fuel economy reported as being achieved in fluidized bed calciners sounds very attractive, and I think it will merit careful consideration in the design of any new plant. Unfortunately, this fuel economy is, to some extent, offset by the power consumption of the blowers, but these may be gas turbine driven.

The location of the milk of lime plant does not necessarily have to be immediately adjacent to the magnesia plant, for it is a matter for economic study whether it is cheaper to pump the milk of lime to the magnesia plant, always provided that this does not involve the two-way pumping of water for making the milk of lime, rather than to transport the limestone to the magnesia plant. It is always difficult to avoid some degree of double handling of solids in these conditions.

The milk of lime is metered into the plant through open Venturi flumes, as, indeed, is the main seawater feed stream.

MAGNESIUM HYDROXIDE THICKENERS

These thickeners are large and very costly tanks, some 45 to 50 m in diameter, and about 6 m deep. They may be constructed either in steel or concrete, or one may build the conical bottom in reinforced concrete and use welded steel plates for the vertical sides, and also design the top overflow launder in steel. Some weight of steel can be saved by using prestressed reinforced concrete construction, but this should not be undertaken lightly when dealing with jobs of this size and circular in shape. In exceptional locations the bottom may be just consolidated earth. In any case, because the thickeners are inevitably low lying, the difficulties involved and the cost of these structures must not be underestimated. Piling is generally quite out of the question because of the cost and the difficulties of satisfactory distribution of the pile reactions, so the site must be most carefully surveyed and probed with boreholes before deciding on the final position of the thickeners. The subsoil should preferably be of uniform consistency so that, should settlement take place, the thickener will remain on an even keel.

The plant may comprise two or three thickeners, and since these may be operated in series, they will be at slightly different levels which, in turn, will usually mean that trouble with ground water will be encountered in building any pipe tunnels required under the lower thickeners. These tunnels are also used for access to the slurry withdrawal points and the slurry pumps are sometimes positioned right under the centre of the thickener. Now, large thickeners are often constructed with a concrete central pillar around which the raker arms revolve at about $1\frac{1}{2}$ m/min at the tip and which also supports one end of the access bridge and the drive unit. The difficulties with tunnels in water-logged ground may be mitigated if the fixed pillar is made hollow, leading down into an enlarged chamber designed as a caisson which can accommodate the slurry pumps. In this case the slurry lines would, of course, lead upwards through the hollow pillar and along the access bridge. But since they eventually have to terminate at a pretty high level in the filters, this is no disadvantage.

Triple throw solid plunger reciprocating pumps have been successfully used for the slurry, but enclosed diaphragm pumps should be equally satisfactory.

The effect of wind on the surface of the thickener leading to disturbance of the settling rates of magnesium hydroxide particles may be quite serious and has necessitated the building of curved wind shields extending at least partly around the circumference of the thickener and up to about 3 m in height. It is quite easy to overlook an item like this in estimating the plant and it will run away with thousands of pounds. The premixed sea water and milk of lime are introduced into the centre of the thickener through a perforated diffuser to get uniform distribution.

The spent sea water overflows into the top launder and is returned to the sea along concrete flumes or a suitable canal. Much trouble may be experienced in the link-up of the flume and the thickener launder, where the flume passes over the backfill around the thickener walls. It is better to make this section of the flume in steel to retain some flexibility. It is hardly necessary to add that the design of the hydraulic system from the pretreatment tanks down to this point must be carried out with great care, bearing in mind that, with the sizes involved, rectification after erection of the plant is not possible and the penalty for incorrect design may be a very large expenditure on additional pumping power or a reduced throughput.

The construction of the thickeners is undoubtedly the longest item in the plant and, if this is accurately estimated, it can be used as a yardstick for the overall construction because all the rest of the work can probably be fitted in in substantially the same period if manpower is available.

FILTERS

The slurry from the thickeners has to be filtered to extract the magnesium hydroxide particles and this can be done in practically all the usual forms of large-scale filter, both continuous and batch. However, the filter cake is exceptionally sticky and difficult to handle, and initial care in the detail design of this phase of the process will repay handsomely in reducing the troubles which will attend this operation.

The installation of horizontal filters of the Sweetland type is, in my opinion, not entirely satisfactory because it involves too much manual labour in disengaging the cake from the closely spaced leaves, and this, in turn, leads to frequent damage of the filter cloth, reduced effective filtration area, and requires constant maintenance of the leaves. This filter must also have expensive banks of air operated valves linked in sequence control. The heavy filters have to be installed high up and require an expensive building. Cake removal is a major problem and the shape of the filter does not help the designer to guide the cake satisfactorily on its way as it will stick even to the vertical sides of a chute. Large rotary vacuum filters are a better solution, but I think that the recently developed Prayon caroussel type filter for the vacuum filtration of difficult materials may be suitable for this use in that it gives great flexibility in continuous operation. The control of the washing stages is easy and the effects can be observed from the surrounding walkway. No complex sequence controls are required, as this arrangement is built into a single central rotary valve. In addition the filter brings the cake to a single discharge point. I believe that this filter could be built in very large outdoor units.

DRYING AND CALCINATION

The choice of the method of drying the filter cake prior to calcination will depend on the efficiency of the filtration stage. If the cake is dry enough to be pelletized in an inclined rotating pan, I would say that pelletization may be followed by a Lepol type drying grate and a short rotary kiln as is now being installed in a number of cement plants, using recirculation of the gases to gain heat economy.

If the drying and calcination stages are separated, as is sometimes done when using a shelf dryer with slowly rotating scrapers, followed by a rotary kiln, then the minimum of mechanical handling must be designed into the system between the dryer and the calciner because the cake leaving the dryer is still not the easiest material to handle and a brief spell of incorrect dryer operation may choke the whole works in a surprisingly short time, and to the point of forcing a shut-down.

The calcine leaving the process is very abrasive and I think that nowadays it would be best handled by means of vibratory trough conveyors which can take it still hot from the air preheater calcine cooler following the kiln.

The calcined material is free-flowing and stable. It can be satisfactorily packed in valved paper bags or in drums, or dispatched in bulk. Unless the dead burned quality is being produced, the material should not be exposed to too much moisture.

PRESENT AND PROSPECTIVE USE OF MAGNESIUM COMPOUNDS IN THE ISRAEL INDUSTRY

E. MARKOWICZ

Ministry of Commerce and Industry

In spite of the presence of enormous quantities of magnesia in the soils of Israel and in the Dead Sea, magnesium compounds have been mainly imported. The present use of magnesia compounds, therefore, is not a real measure of prospective uses which will surely be created when the local sources are developed and exploited.

RUBBER INDUSTRY

One of the main users of magnesium carbonate and magnesium oxide is the rubber industry which uses magnesium carbonate as a filler and a hardening agent, and magnesium oxide as a neutralizing agent and a vulcanization additive. Quantities used for the rubber industry, which is developing quickly especially with the growth of tyre production in the last years, reach about 100 tons per year. Special brands are, of course, required, as small differences in quality influence the brand of the rubber.

PAINTS, VARNISHES AND PRINTING INKS

These industries use regularly small quantities of magnesium carbonate as fillers, and as flatting agents. The use could be enlarged if prices were suitable and local supply sufficient.

AGRICULTURE

That the magnesium salts removed from the soil by agriculture must be replaced by magnesium fertilizer has been recognized only in the last decade. Even if sufficient magnesium is present in the soil, the balance of ions within the soil is maintained only if the magnesium ion taken out of the soils is replaced. Local agriculture uses magnesium sulphate especially in the citrus industry. Magnesium sulphate is also important for the veterinary aspect of agriculture, and quantities necessary for these purposes are presently produced by the local industry which prepares magnesium sulphate from magnesia imported mainly from Greece.

TANNING INDUSTRY

The tanning industry uses locally manufactured magnesium sulphate as an agent for loading the hides and preserving them from dehydration.

PHARMACEUTICAL AND COSMETIC INDUSTRIES

The use of a number of magnesium compounds by these industries could be increased still more in the future. Epsom salt is used as an anti-constipation agent, and magnesia usta as a neutralizing agent for gastric acid. Magnesium hydroxide, sometimes in various combinations with magnesium carbonate, is also used for these purposes. Magnesium peroxide is effective against gastric acid and can be used for years without harm.

Magnesium compounds have been used in this country, but there is a trend to use magnesium carbonates instead of precipitated calcium carbonate for toothpastes. Magnesium stearate is recommended, but at the moment is not used extensively for powder base, although it could be used as well as zinc stearate as an ingredient for face powder.

BUILDING INDUSTRY

One of the most important uses of magnesia and magnesium carbonate is as an insulating agent. Magnesia insulating preparations are now imported as ready made slabs or as half shells for pipes. Half pipes of magnesia are as far as I know the best means of heat insulation. One of the main uses of magnesia is in the form of refractory magnesia bricks. Their local use could be encouraged.

The question of magnesia cement (Sorel cement) and the production of Xylolith have been discussed and trials made by Palestine Potash Co. Ltd. At present no use is made of magnesia in the local building industry. With sufficient applied research in this direction the essential setback of this commodity, its lack of stability in presence of humidity, could be overcome and good cement and floor tiles made.

ADDITIONAL USES

There are still some other possibilities of utilizing magnesium compounds in already existing local industries: magnesium chloride and magnesium sulphate in fireproofing compounds; magnesium silicates as anti-oxidants in rancid oils, decolorizers for vegetable oils, and as stabilizers for hydrogen peroxide solutions.

The paper and plastics industry could use inexpensive magnesia and carbonate as fillers in rather large quantities.

Finally, if magnesia is available at reasonable prices, many other magnesium compounds would be prepared for local as well as for export purposes.

A. BANIEL: What are the quantities of magnesium compounds being consumed in this country?

E. MARKOWITZ: 400—500 tons per year.

W. BODENHEIMER: I should like to add to the list a use of magnesium carbonate which I saw in England. In the production of gelatine from chrome leather works, the material is treated with $MgCO_3$ which is sufficiently alkaline to precipitate the chrome but not sufficiently strong to destroy the gelatine. The gelatine produced is of the highest edible quality.

E. MARKOWITZ: In addition we are successfully investigating the possibility of magnesium bi-sulphite replacing calcium bi-sulphite in our paper industry.

S. A. ABRAHAMS: There is a substantial market in the United States and also world-wide markets exploited mainly by England. A market survey should be conducted.

NOTICE TO CONTRIBUTORS

Contributors to the *Bulletin of the Research Council of Israel* should conform to the following recommendations of the editors of this journal in preparing manuscripts for the press.

Contributions must be original and should not have been published previously. When a paper has been accepted for publication, the author(s) may not publish it elsewhere unless permission is received from the Editor of this journal.

Papers may be submitted in English, French and Russian.

MANUSCRIPT

General

Papers should be written as concisely as possible. MSS should be typewritten on one side only and double-spaced, with side margins not less than 2.5 cm wide. Pages, including those containing illustrations, references or tables, should be numbered.

The Editor reserves the right to return a MS to the author for retyping or any alterations. Authors should retain copies of their MS.

Spelling

Spelling should be based on the Oxford Dictionary and should be consistent throughout the paper. Geographic and proper names in particular should be checked for approved forms of spelling or transliteration.

Indications

Italics

All symbols and text to be italicized should be underlined.

Capitals

Capital letters should be capitalized in the MS.

Stopping

Words to be stopped should be s p a c e d out in the MS.

Other specifications

Any other variations in type size or character should be indicated clearly in a legend preceding the MS.

Special care should be taken to record clearly relative height of symbols to the line. This is often more easily achieved in legible handwriting than typing. Indices and subscripts should be accurately placed. As far as possible formulae should be confined to one line, e.g. $\frac{1}{x}$ should rather be written $1/x$.

Greek letters should be indicated in a legend preceding the MS, as well as by a pencil note in the margin on first appearance in the text.

When there is any room for confusion of symbols, they should be carefully differentiated, e.g. the letter "I" and the figure "1"; "O" and "0".

Thermodynamic notation

The following notation should be used:

Internal energy	U	Work function	A
Enthalpy	H	Gibbs' function	G
Entropy	S	Chemical potential	μ

Mathematical punctuation

Decimal division is indicated by use of a full stop on the line, e.g., 1.000 (one, accurate to the third place). Division of thousands is made by use of a comma, e.g., 1,000 (one thousand). Multiplication is indicated by a full stop centrally placed, e.g. $8 \cdot 10^{12}$.

Abbreviations

Titles of journals should be abbreviated according to the *World List of Scientific Periodicals.*

Units are used in the abbreviated form, in the singular, and are not followed by a full stop (only in. is followed by a full stop). The following is a list of the more common symbols: mm cm m km cm^3 m^3 g mg kg sec min hr °K °C.

Summary

Every paper must be accompanied by a brief but comprehensive summary. Although the length of the summary is left to the discretion of the author, 3% of the total length of the paper is suggested.

References

In Sections A and C, and in Letters to the Editor in all Sections, references are to be cited in the text by number, e. g., ... Taylor[3] ..., and are to be arranged in the order of appearance.

In Sections B and D, the references are to be cited in the text by the author's name and date of publication in parenthesis, e.g., ... (Taylor 1932).... If the author's name is already mentioned in the text, then the year only appears in the parenthesis, e. g., ... found by Taylor (1932).... The references in these Sections are to be arranged in alphabetical order.

The following form should be used ;

3. TAYLOR, G. I., 1932, *Proc. roy. Soc.*, A138, 41.

Book references should be prepared according to the following form:

4. JACKSON, F., 1930, *Thermodynamics*, 4th ed., Wiley, New York.

TYPOGRAPHY

In all matters of typography the form adopted in this issue should be followed. Particular attention should be given position (of symbols, headings, etc.) and type specification.

ILLUSTRATIONS

Illustrations should be sent in a state suitable for direct photographic reproduction. Line drawings should be drawn in large scale with India ink on white drawing paper, bristol board, tracing paper, blue linen, or blue-lined graph paper. If the lettering cannot be drawn neatly by the author, he should indicate it in pencil for the guidance of the draftsman. Possible photographic reduction should be carefully considered when lettering and in other details.

Half tone photographs should be on glossy contrast paper.

Illustrations should be mounted on separate sheets of paper on which the caption and figure number is typed. Each drawing and photograph should be identified on the back with the author's name and figure number.

The place in which the figure is to appear should be indicated in the margin of the MS.

PROOFS

Authors making revisions in proofs will be required to bear the costs thereof. Proofs should be returned to the Editor within 24 hours, otherwise no responsibility is assumed for the corrections of the author.

REPRINTS

Each author will receive 50 reprints free of charge, and additional reprints may be ordered at the time the first proof is returned. A table designating the cost of reprints may be obtained on request.

Orders in America should be addressed to Interscience Publishers Inc., New York, N. Y., and in England and Europe to Wm. Dawson & Sons, Ltd., Cannon House, Macklin Street, London, W. C. 2, directly or through booksellers.

Annual subscription per section (four issues): IL.4.000 ($5.50, £ 2)
Single copy IL.1.000 ($1.50, 12 s.)

BULLETIN OF THE RESEARCH COUNCIL OF ISRAEL
PUBLISHED BY THE WEIZMANN SCIENCE PRESS OF ISRAEL

PRINTED BY GOVERNMENT PRESS, JERUSALEM